MASTER (MA)

Specialised Fluorescent Polymers: Structure and Behaviour in Styrene Maleic Acid Lipid Particles

Neville, George

Award date:
2018

Awarding institution:
University of Bath

Department of
Chemistry

UNIVERSITY OF BATH

CH40167: Advanced Chemistry Research

Specialised Fluorescent Polymers:

Structure and Behaviour in Styrene Maleic Acid Lipid Particles

George M. Neville

Registration number: 149057880

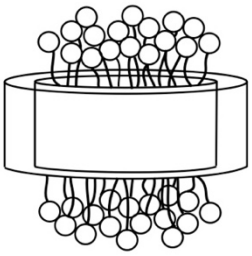

Abstract

Promising to rival detergents and revolutionise membrane protein extraction, the copolymer, styrene maleic acid (SMA), has been rapidly adopted by biologists and chemists alike. Recent attempts to optimise this system, however, have emphasised shortcomings in the underlying understanding of the technology. Here, novel, fluorescence-enabled SMA variants have been synthesised, with controlled molecular weights and compositions, that are hoped to further elucidate the currently abstract workings of styrene maleic acid lipid particles (SMALPs). Solvatochromism is evaluated as a possible method to monitor the dynamic structures of both SMA aggregates and SMALPs and Förster resonance energy transfer (FRET) is demonstrated as a feasible approach to probe polymer-protein interactions. Fully capable of both the formation of SMALPs and incorporation of proteins, these fluorescent polymers have the potential to benefit future SMALP and protein research.

Supervisors: Prof. K.J. Edler & Prof. G.J. Price

Plagiarism Declaration

Please complete the following declaration by adding your name and the date.

If handing in a printed copy, please sign this page. Submission of an electronic copy of this report through e.g. Moodle indicates that you agree with the statement

I certify that I have read and understood the entry in the Student Handbook for the Department of Chemistry on Cheating and Plagiarism and that all material in this assignment is my own work, except where I have indicated with appropriate references.

I agree that, in line with Regulation 15.3(e), if requested I will submit an electronic copy of this work for submission to a Plagiarism Detection Service for quality assurance purposes.

Student Name: George Neville

Student Signature: 

Date: 08/05/2018

Table of Contents

Specialised Fluorescent Polymers: Structure and Behaviour in Styrene Maleic Acid Lipid Particles

Abbreviations

2,2'-azobis(2-methylpropionitrile)	AIBN
Atom Transfer Radical Polymerisation	ATRP
Continually Stirring Tank Reactor	CSTR
2-(dodecylthiocarbonothioylthio)-2-methylpropionic acid	DDMAT
Dynamic Light Scattering	DLS
t-2-dimystoyl-glycero-3-phosphocholine	DMPC
Diffusion Ordered Spectroscopy	DOSY
Degree of Polymerisation	DP
Differential Scanning Calorimetry	DSC
Förster Resonance Energy Transfer	FRET
Fourier Transform Infrared Spectroscopy	FTIR
Gel Permeation Chromatography	GPC
G-Protein Coupled Receptor	GPRC
Lauroyl peroxide	LPO
Maleic Acid	MA
Maleic Anhydride	MAnh
Membrane Protein	MP
Membrane Scaffold Protein	MSP
Nitroxide-Mediated Polymerisation	NMP
Nuclear Magnetic Resonance Spectroscopy	NMR
Pyrene [SMA]	P [SMA]
Phosphate Buffer Solution	PBS
Polydisperisty Index	PDI
1-Pyrenemethyl Methacrylate	PmMA
Particle Size Distrobution	PSD
Reversible Addition Fragmentation Chain-Transfer	RAFT
Reversible Deactivation Radical Polymerisation	RDRP
Small Angle X-ray Scattering	SAXS
Small Angle Neutron Scattering	SANS
Size-Exclusion Chromatography	SEC
Scattering Length Density	SLD
Static Light Scattering	SLS
Styrene Maleic Acid	SMA
Styrene Maleic Anhydride	SMAnh
Styrene Maleic Acid Lipid Particle	SMALP
Styrene	Sty
Transmission Electron Microscopy	TEM
Transmembrane	TM
Vinylanthracene [SMA]	VA [SMA]

1.0 Introduction

Styrene maleic acid (SMA) copolymers promise to revolutionise the isolation and purification of membrane proteins. However, the use of poorly characterised commercial polymers has meant that the wide adoption of SMA has far outreached the fundamental understanding of the technology. While attentions have now turned to optimising SMA for protein research, this will require a detailed appreciation of both the structure and behaviour of SMALPs. Here, novel, fluorescence-enabled SMA variants, with a controlled molecular weight, composition and architecture, are synthesised in an attempt to both probe the SMALP system, as well as improve its subsequent application.

From cellular communication to the transportation of molecules, membrane proteins (MPs) are vital to the processes that enable life. In humans, over 30% of translated genes encode for MPs [1], and such proteins are the target for an estimated 50% of all therapeutics [2, 3]. Deciphering the structure and function of MPs is integral to the development of novel drugs to treat disease. Protein research has seen many advances in recent years, such as the discovery of G-protein coupled receptors (GPCRs) [4], as well as the advent of cryo-EM imaging techniques [5, 6]. However, surprisingly little progress has been made into elucidating the structure of MPs, with MPs constituting less than 2% of all high resolution structures in the Protein Data Bank [3, 7]. Much of this difficulty has been attributed to the poor methodologies surrounding protein isolation, which are heavily dependent on the inherently disadvantageous use of detergents.

Removing a protein from its natural lipid membrane will often cause it to unfold and denature, relieving it of both structure and function [8-10]. Therefore, a method is required which not only allows for the purification of MPs from the membrane, but which also sufficiently stabilises the protein so that its original structure and function are maintained. Traditionally, this is achieved with the use of various detergents which can act as a membrane mimetic environment, stabilising MPs inside micelles [7, 11]. However, due to the variety and complexity of cell membranes, this initially requires extensive empirical assessment to select a suitable detergent species. More importantly, by breaking the crucial interactions with the surrounding lipid environment and other weak protein-protein interactions, protein dynamics can be altered or lost [7]. Repeatedly, it has been shown that detergent micelles are a poor mimetic of a phospholipid bilayer and their differing physiochemical properties are not suitable for sustaining a protein's function [7, 11]. Lee *et al.* (2016, [10]) summarises the dilemma:

> *"A critical flaw with detergent approaches is the removal of the protein from the native lipid environment ... the choice of what membrane protein to study often being based not on importance but rather on which protein can be extracted from the membrane in the active, folded form."*

An established alternative to overcome this loss of the native lipid environment, is to reconstitute MPs, once extracted by detergent micelles, into fragments of foreign lipid bilayer, called lipid nanodiscs. This has previously been achieved by the use of membrane scaffold proteins (MSPs). Discovered in 2002, MSPs are amphiphilic proteins derived from human apolipoprotein A-1 [12]. Inside an MSP disc, the hydrophobic acyl chains of lipids can be shielded from solvents, and hence a segment of lipid bilayer can be solubilised in

water. These nanodiscs are then capable of extracting MPs from detergent micelles, incorporating and stabilising the MP in solution. Whilst much progress has been made in this domain, critically, detergents are still initially required to remove the protein from the cell membrane, thereby limiting the range of MPs that can be explored. Furthermore, as MSPs and MPs are both proteins, distinguishing the two causes difficulties during eventual MP analysis. Whilst the growing popularity of MSPs cannot be overlooked (*Figure 1*), a burgeoning, detergent-free technique using the copolymer *p*(styrene-c*o*-maleic acid) (SMA) has emerged over recent years.

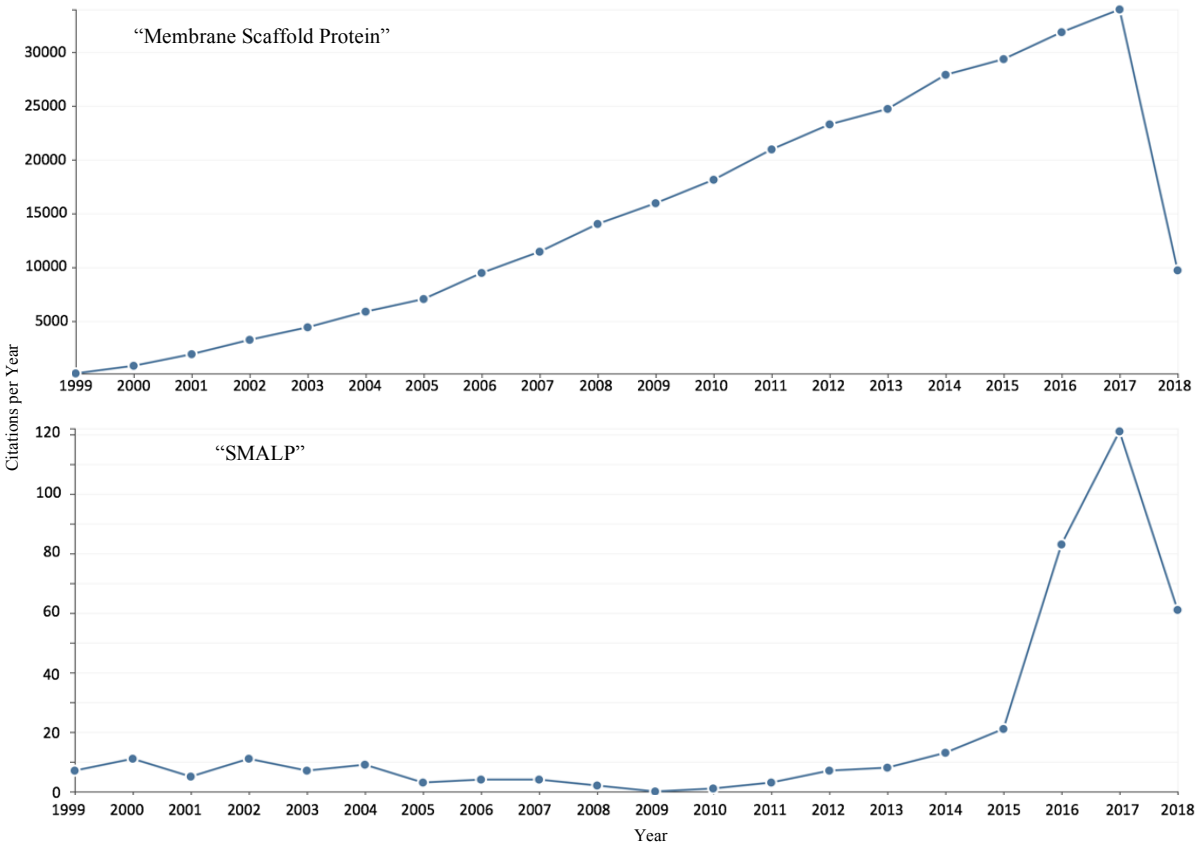

***Figure 1**: Web of Science citation reports for "Membrane Scaffold Protein" (Top) & "SMALP" (Bottom).*

SMA, like MSPs, can also form lipid nanodiscs, coined styrene maleic acid lipid particles, or SMALPs. SMA is an amphiphilic copolymer, where hydrophobic styrene moieties are capable of stabilising the hydrophobic acyl chains of phospholipids and the hydrophilic maleic acid units allow the nanodisc to be water soluble. The structure of both SMA and SMALPs can be found in *Figure 2*. When originally discovered, SMA nanodiscs were found to encapsulate hydrophobic molecules, and were initially considered for drug-delivery applications [13]. However, SMALPs have since found promise in membrane research [7, 10, 14, 15]. The greatest advantage of SMALPs is that not only can they solubilise MPs without any need for detergents, broadening the range of MPs that can be explored, but also that MPs can be directly incorporated from cell membranes, bringing their native lipid environment with them [7].

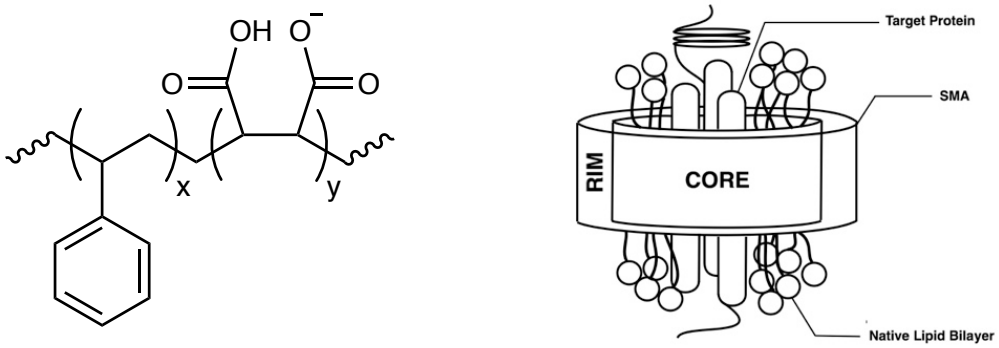

p(styrene-*co*-maleic acid) SMALP

***Figure 2**: Structure of p(styrene-co-maleic acid) (Left) & Schematic of SMALP with protein (Right).*

SMALPs have been widely successful, and reports of their benefits easy to find [6, 7, 14-16]. However, it is complacent to believe that the SMA variants currently in use represent the most optimised system. Since the conception of SMALPs for protein isolation by Knowles *et al.* (2009, [14]), the science surrounding them has rapidly advanced; perceptions of what a SMALP might look like and how it might be excepted to behave have been reshaped drastically from the few original studies. Although once heralded as potentially the ideal extraction method, with it being widely reported that protein dynamics remained unaltered [6, 15], it has come to light that this may not be the case. There is now strong evidence to suggest that not only are SMALPs comprised of multiple polymer chains [3, 17], but polymer chains, and more importantly, lipids will exchange between nanodiscs [17-20]. This means that SMALPs are no longer believed to be able to capture perfect, static snapshots of naturally behaving cell membranes. Instead, a new, more dynamic picture of the structure and behaviour of SMALPs is being developed.

SMALP research is now orientated towards diversifying and improving on the current SMALP system, where a refined understanding of SMALP behaviour has allowed for its targeted optimisation. This includes tackling pH dependency [21], SMALP resistant proteins [22], the design of alternative copolymers [23] and the functionalistion of nanodiscs to support protein research [17, 24, 25]. Here, SMA is copolymerised alongside the fluorescent compounds, anthracene and pyrene, which act as sensors to probe the structure and behaviour of SMALPs. It is hoped that by synthesising these polymers with controlled compositions and architectures this will facilitate the conclusive interpretation of results. Demonstrated in this proof-of-concept study is that, not only are these novel copolymers fully adequate for protein extraction applications, but may also enable new research avenues into the study of proteins and SMALPs alike.

1.1 The Structure of SMALPs

SMALP morphology has been recognised as offering many unique benefits to protein research. Both sides of a protein are solvent exposed, allowing for ligand binding studies, already seen to be comparable to those using natural membranes [26]. As SMALPs are relativity small, and, unlike MSPs, are free of secondary structures such as alpha helices, they do not scatter light [14, 26], simplifying the analysis of proteins. Knowles *et al*. (2009, [14]) have commented:

"SMALPs are nondenaturing and exhibit minimal scattering...rivalling the quality of spectra afforded by synchrotron radiation sources."

Currently, however, there is limited scope to adjust or tailor SMALP structures for different applications. For example, reduced SMALP diameters are required for effective NMR analysis [27] whereas larger ones are required when solubilising larger proteins [28]. Furthermore, from biomedical research it is well known that polymers and proteins form highly favourable interactions [34-36], and it remains to be seen if proteins avoid any interference from SMA. Despite the wide adoption of the SMALP system, still it is controversial whether a protein's structure and function are truly unperturbed. Therefore, imperative to the control and sophisticated application of SMALPs is the appreciation of how they are structured.

1.1.1 SMALP Morphology

Until 2015, the structure of the SMALP nanodisc was not yet known. Jamshad *et al.* (2015, [29]) were the first to attempt the extensive characterisation of SMALPs and were able to infer many structural properties. Small angle neutron scattering (SANS), transmission electron microscopy (TEM), as well as a range of other techniques were employed in this endeavour.

SANS data was fitted to a "*core shell cylinder*" model, found in *Figure 3*. It was found that the SMA copolymer formed a circular annulus around a fragment of lipid bilayer with an area between 41.7 and 50.2 nm^2, with a maximum radius of 9.8 nm. Both the thickness of the core and faces of these nanodiscs matched the dimensions expected of the hydrophobic tails and hydrophilic heads of the lipids, respectively.

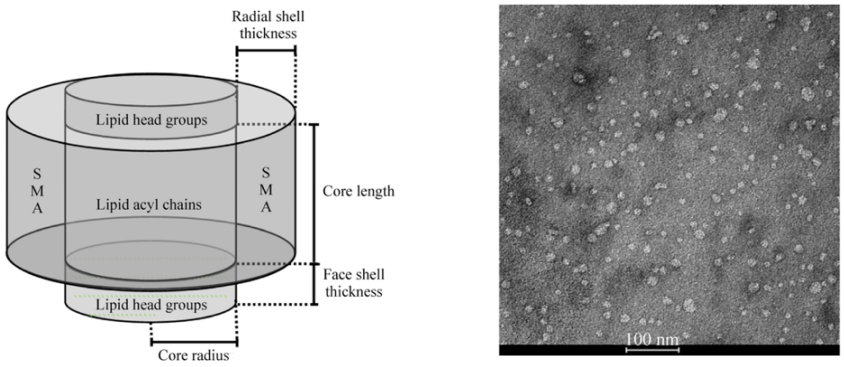

Figure 3: *(Jamshad et al., 2015, [29]), "Core Shell Cylinder" model (Left) used to fit SANS data & negative stain TEM image of SMALP nanodiscs (Right).*

Whilst confirming the disc-like shape of SMALPs, TEM, however, also suggested a bimodal distribution in their diameter: 11.1 and 16.0 nm. Whilst it is expected that TEM will overestimate these dimensions [14], later, Lee *et al*. (2016, [26]) highlighted that this difference was likely due to how individual particle had dried on the EM-grid, fluctuating in

orientation. This serves to highlight the inherent superiority of scattering experiments in comparison to other techniques, where particles can be free in solution.

Jamshad *et al.* also noted that the SMA annulus was 0.7 ± 0.2 nm thick, indicating that it was constructed of only a single layer of the copolymer. Whilst this is still may be true, in recent years, mounting evidence suggests that several chains are required to span the circumference. Fluorescent SMA, used for FRET experiments by Schmidt and Sturgis (2017, [17]) revealed that each nanodisc likely contained multiple polymer chains. Stroud *et al*. (2018, [3]) were able to corroborate this by reviewing reports of a polymer's length against the circumference of the SMALP it could form. This has consequences when considering possible mechanisms for SMALP self-assembly and demonstrates that complacency with the current model of SMALP morphology is unjustified. Therefore, where possible, it is critical that polymer characteristics be compared to SMALP structure to identify correlations that may allow for the more optimised application of SMA.

1.1.2 Scattering Techniques & SMALPs

By measuring the interaction of particles with radiation, it is possible to glean characteristics of their shape, size and structure. The following sections describe and discuss the scattering techniques used in this project, and how they might be applied in the study of SMALP nanodiscs.

1.1.2.1 Dynamic Light Scattering (DLS)

Now ubiquitous for the study of nanostructures, DLS, despite multiple drawbacks, is routinely used in SMALP research for the facile determination of nanodisc diameter [3, 37, 38]. In static light scattering (SLS), by measuring scattering intensity as a function of angle, θ, information on the size and structure of particles can be obtained, with scattering at a smaller angle relating to larger sized objects. Opposed to SLS, where the intensity at all angles is measured, DLS uses a fixed angle and measures the intensity change over time. In an infinite dilution regime, where particles cannot interact, particle size can be ascertained due to the fluctuations in scattering intensity arising from the changing distance between the scattering particles, or scatterers, and the detector. This causes interference between scattered waves and therefore the scattering intensity fluctuates characteristically over time in direct relation to the Brownian motion of the particles [30] *i.e.* smaller particles that diffuse faster, will cause faster fluctuations in intensity (*Figure 4*).

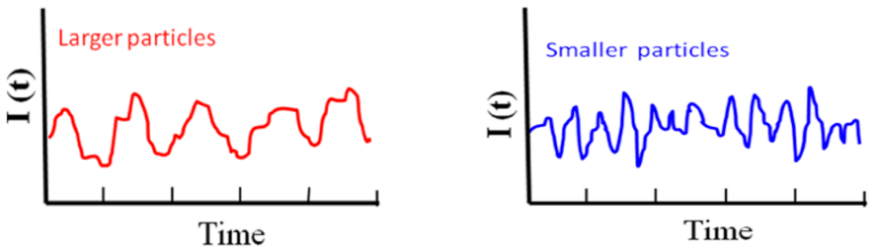

***Figure 4**: Variation to scattering intensity over time of large and small particles in solution [30].*

Due to the phenomena described above, particle size can be calculated mathematically through a correlation function (*Equation 1*) [30]:

$$g^2(\tau) = \frac{<I(t)I(t+\tau)>}{<I(t)>^2} \quad (1)$$

Where *I(t)* is the intensity at time *t*, and τ is an arbitrary time delay. At $\tau = 0$, the function should perfectly correlate, giving a value of 1, and at $\tau = \infty$ the function should be non-correlating. Perfect correlation, however, is unrealistic due to the discrepant time scales between measurement and diffusion, hence, a correlation value of approximately 0.8 at $\tau = 0$ is reasonable. An example of this can be found in *Figure 5*. The exponential decay of this correlation function can be described according to *Equations 2-3*:

$$g^1(\tau) = (g^2(\tau) - 1)^{0.5} \quad (2)$$

$$g^1(\tau) = A \times e^{-Dq^2\tau} + B \quad (3)$$

Where *A* is the amplitude of the correlation function, *D* is the translational diffusion coefficient, *B* is the baseline and *q* is the scattering vector described by *Equation 4*:

$$q = \frac{4\pi n}{\lambda} \sin\left(\frac{\theta}{2}\right) \quad (4)$$

Where *n* is the refractive index, λ is the wavelength of incident light and θ is the angle of scattered light. The data in *Figure 5* has been fitted to *Equation 2* in *Figure 6*.

From the diffusion coefficient, *D*, the hydrodynamic radius, R_h, representing the solvated, tumbling particle, may be calculated by the Stokes-Einstein equation (*Equation 5)*. Where k_B is the Boltzmann constant, *T* is temperature and η is viscosity.

$$D = \frac{k_B T}{6\pi\eta R_h} \quad (5)$$

Several assumptions are made in the equations described above, such as that scatterers are hard spheres, without fluorescence or colour, not met by the polymers or SMALPs that will be examined here. Therefore, in conjunction with DLS, another, more powerful scattering technique, small angle X-ray scattering (SAXS), will be used to quantify the error in DLS measurement, as well as provide a more detailed insight into SMALP morphology.

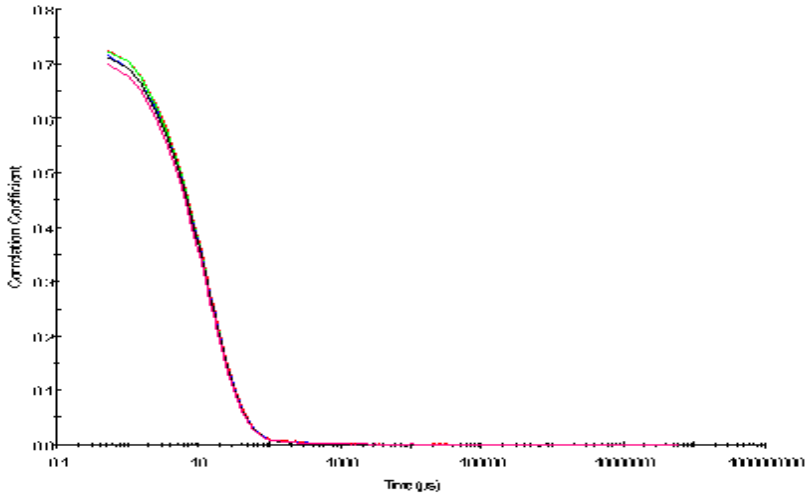

***Figure 5**: Example correlation function with time (Zetasizer software).*

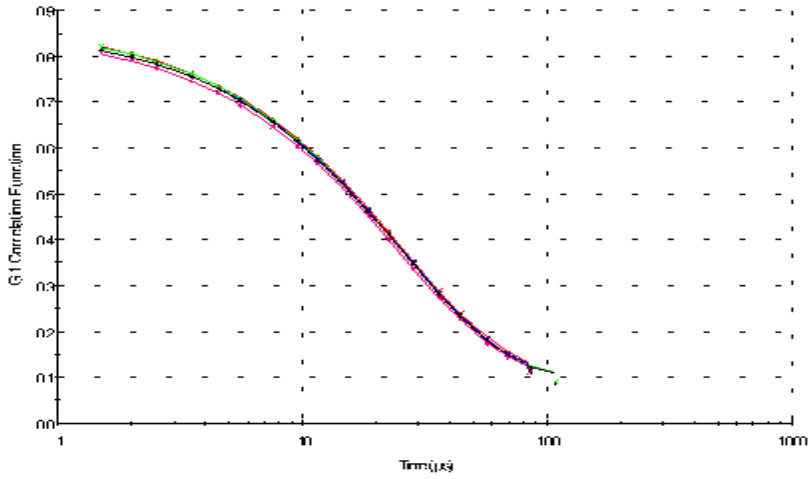

***Figure 6**: Fitted correlation function (Zetasizer software).*

1.1.2.2 Small Angle X-ray Scattering (SAXS)

Small angle X-ray scattering (SAXS) is used to interrogate the average size, structure and composition of particles. During this project, SAXS will be used as a reliable means of inferring the presence of SMALPs over unstructured aggregates, as well as to compare the structural properties of SMALPs formed by different SMA variants.

X-rays interact with electron density and may be scattered elastically or inelastically. Inelastic scattering occurs when incident X-rays lose energy, and hence scattered X-rays are incoherent and do not provide structural information. Elastic scattering, however, is coherent and scattered radiation interferes to create a pattern which may then be analysed. A general schematic of SAXS instrumentation can be found in *Figure 7*.

As all distances within the pattern are relative to the given wavelength, λ, of incident radiation used, rather than using angle, 2θ, the vector, q, is instead adopted to render the pattern wavelength independent (*Equation 6)*.

$$q = \frac{4\pi}{\lambda} \times \sin(\theta) \qquad \textbf{(6)}$$

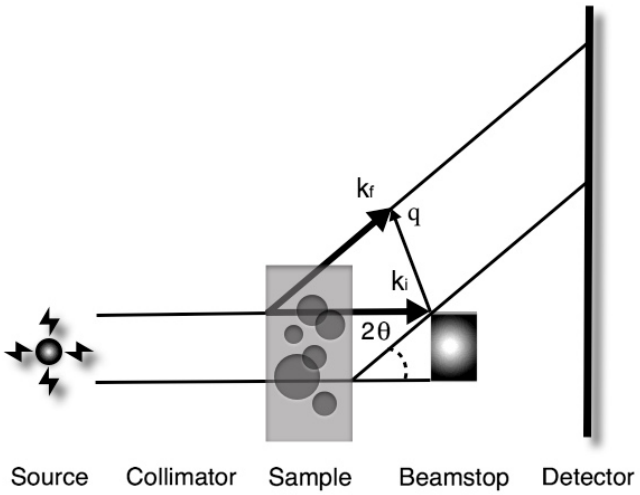

***Figure 7**: Schematic of SAXS experiment.*

In order for the structure of a particle to be observed, it must have a differing electron density, or contrast, to its surrounding environment. Consequentially, the signal arising from the solvent alone may be subtracted from that of the entire pattern, and so, unlike DLS, it is not the hydrodynamic radius but rather the absolute radius of the particle that is measured.

The overall scattered intensity (*Equation 7*) in a pattern can be described by a combination of constants, such as a material's scattering length density (SLD, ρ), or the strength of its interaction with X-rays, and a particle's volume (V), as well as the form factor, ($F(q)$), structure factor, ($S(q)$), and incoherent background intensity (B_{inc}) [31]. The form factor describes the shape of the structure. At low-q, the gradient of the form factor is predominantly the size of the particles, at mid-q, the cross-sectional structure (*i.e.* sphere, cylinder, disc *etc.*), and at high-q relates to the surface structure. The structure factor, arising from the interactions between individual particles, is further imposed over this. At low-q, the gradient relates to how particles are positioned relative to each other in solution. An increasing, or steep gradient at low-q indicates aggregation, whereas a decreasing, or shallow gradient at low-q indicates repulsive interactions. For systems sufficiently dilute, it can be assumed that $S(q) = 1$. Furthermore, the polydisperisty of samples must also be considered, as the overall pattern will be the sum average of the properties of each particle.

$$I(q) = N_p V_p^2 (\rho_p - \rho_s)^2 F(q) S(q) + B_{inc} \quad (7)$$

Whilst SAXS may only provide averaged results, the technique does allow for the detailed assessment of the composition and dimensions of different parts of the SMALP structure, and will therefore be used here for such advantages.

1.1.3 The Perfect Membrane Mimetic

Perhaps the most pressing controversy surrounding SMALP technology is the matter of whether protein, and by extension, lipid behaviours are sustained as they would be in the cell membrane. Containing carbohydrates and nucleic acids, as well as lipids and proteins, cell membranes can be incredibly complex, exacerbating this challenge. MPs can be classified

as either integral, where proteins are found to be closely associated with a membrane, including transmembrane proteins (TM) that span the entire width, or peripheral, whereby the protein is only loosely associated with the membrane or other integral proteins [32]. Furthermore, the levels of cholesterol within a membrane governs its rigidity and in turn mediates the freedom of a protein to move. Preserving the lipid environment of MPs is therefore imperative as their function is highly dependent on these subcellular differences.

When examining SMALP structure, Jamshad *et al.* (2015, [29]), using ATR-FTIR spectroscopy, further found that the styrene units of the copolymer are arranged perpendicular to the lipid chains. Here, the styrene component is closely associated with the hydrophobic acyl chains, interacting analogously to cholesterol in high density lipoproteins. It was also shown that due to this styrene-lipid interaction, some of the aliphatic chains in the lipids were forced to 'kink', inducing a gauche conformation of the C-C bonds. This caused the lipids to become more rigid, losing their mobility in comparison to a real cell membrane.

To quantify this effect, Jamshad *et al.* used differential scanning calorimetry (DSC) to assess how the gel to liquid transition of lipids may be altered by the presence of SMA. It was found that the lipid transition was reduced slightly from 24 °C to 23 °C, but, more importantly, the transition significantly broadened (*Figure 8*). This was due to the contact of 'boundary lipids' with the copolymer, causing them to loose cooperativity with the bulk. Therefore, certain membrane proteins, when incorporated in SMALPs, may not be able to make conformational changes.

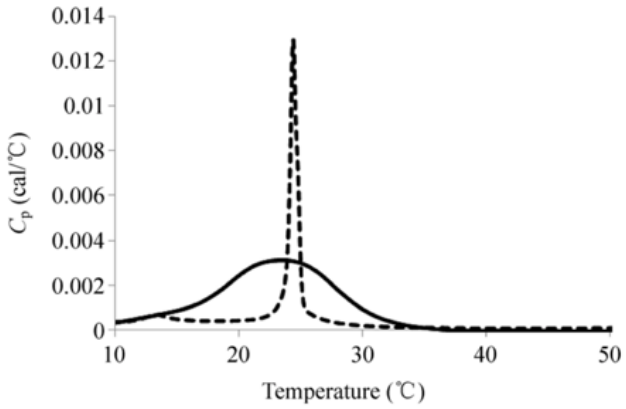

Figure 8: *(Jamshad et al., 2015, [29]), DSC data for DMPC vesicles (dotted line) & SMALPs (solid line).*

It is true that SMALPs have had wide success in isolating proteins thus far. All major systems used in the synthesis of recombinant MPs, including bacteria and yeast, as well as insect and human cells [7, 14, 15], have been extracted by SMALP techniques. Orwick-Rydmark *et al.* (2012, [15]) directly commented that, despite warnings that SMALPs may increase lipid ordering and restrict protein motion, the dynamic profile of a seven-transmembrane receptor protein was fully maintained. Despite these reports however, mainly due to the difficulty in conducting molecular dynamic simulations [26], the scientific community remains unsatisfied that SMALPs truly replicate the cell membrane without adulteration [3].

In addition to this, it has been recently found that the copolymer is likely to bury parts of itself inside the SMALP core [33]. Whilst the affect of this on protein function has not yet been examined, it is well known that polymers and proteins favourably interact [34, 35], with principle efforts in biomedical research attempting to mitigate these interactions [36]. It is hoped that by developing fluorescent SMA variants, the proximity of the polymer to the protein can be established by FRET techniques, and therefore the extent of these interactions may be inferred. Furthermore, by monitoring solvatochromic changes to fluorescent polymers, it may be established where the polymer exists within the SMALP structure and hence if this is potentially affecting lipid rigidity.

1.2 The Behaviour of SMALPs

Over time, many factors have been found to influence the outcome of SMALP self-assembly, including the ratio of lipids to polymer, the lipid identity, as well as the polymer composition and molecular weight [22, 37, 39-42]. Still, however, no clear axioms exist to guide biochemists as to which SMA variant is best to use or which method best to follow. Understanding this self-assembly process is important for both the easy and optimised application of SMALPs, but is also necessary if improved SMA variants are to be rationally designed. The following sections aim to set out what is currently understood about SMALP behaviours, as well as highlight the present gaps in the literature.

1.2.1 SMALP Self-Assembly

Scheidelaar *et al.* (2015, [37]) were the first to illustrate a possible mechanism of SMALP self-assembly (*Figure 9*). By a combination of turbidity experiments, TEM, DLS and size exclusion chromatography (SEC), Scheidelaar *et al.* devised and proposed a three stage model as follows:

1. Membrane Binding
2. Membrane Insertion and Destabilisation
3. Nanodisc Formation

The first step, membrane binding, was found to be mediated by two factors. Firstly, solubilisation occurred fastest when SMA was in excess. Secondly, it was found that the extent of anionic repulsion between the lipid head groups and maleic acid units of the copolymer controlled if binding could occur. By adding salt, increasing the ionic strength of the solvent, Debye charge screening effects allowed faster solubilisation to be observed [41]. These repulsions need to be balanced, however, with the necessity of their presence in allowing the eventual formation of water-soluble SMALPs.

Membrane insertion proved to be a more complicated process. Scheidelaar *et al*. postulated that defects in the membrane were a prerequisite for copolymer insertion. This was based on its dependency on temperature, or more specifically, the gel to liquid transition (T_m) of the target membrane. Below T_m, solubilisation was slow, where the rate of

solubilisation increased as T_m was approached, until plateau. As T_m is the point where both gel and liquid states coexist, it was thought this facilitated polymer insertion.

Scheidelaar *et al*. further suggested that the chemical structure of SMA was integral to SMALP formation. It was proposed that SMA achieves insertion due to its relatively small monomer units, and the insertion of rigid styrene was therefore possible due to this minimum loss of conformational entropy. This has since been corroborated by the thermodynamic analysis of SMALP formation between SMA and similar polymers [36]. As novel polymers begin to deviate from the original SMA variant, this will therefore be important for chemists to consider. For example, during this project when attempting to modify SMA with relatively larger fluorescent units, there is no guarantee that SMALPs will behave comparatively.

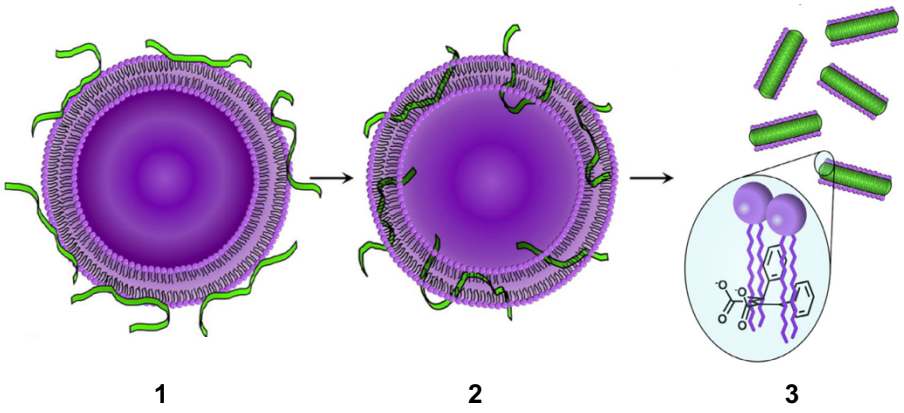

Figure 9: *SMALP self-assembly [3]: membrane binding (1), membrane insertion and destabilisation (2), nanodisc formation (3).*

1.2.2 The Dynamic SMALP

Perhaps rationalised by the findings presented in the previous section, it was quickly found that SMALPs preferably solubilised lipids from membranes with lower levels of cholesterol. For more than 30 years, cell membranes have been visualised using the fluid mosaic model; that the lipids they are made from are in a fluid, disordered state, and the MPs they contain are free to diffuse [43]. But within cell membranes, discrete sub-domains of ordered lipids, 'lipid-rafts', exist, whereby the membrane contains higher amounts of cholesterol and glycosphingolipids [37]. The effect of lipid-rafts on SMALP self-assembly was first recognised by Dörr *et al*. (2017, [39]), when, counterintuitively, they observed that internal organelles of human HeLa cells were solubilised before the complete solubilisation of the external, more rigid, plasma membrane. This effect is now better understood, with some creating methods to tackle this issue [22], as well as taking advantage of it to target only specific proteins within a cell [16].

Whilst the preference of SMALPs for certain membrane types appears innocuous enough, it does bring into question whether a SMALP would solubilise lipids based on their proximity to a protein, or would rather select lipids based on identity and preferential interactions. In recent years, a more dynamic picture of SMALP behaviour has started to emerge. Evidence has been found to suggest that lipids may exchange between SMALPs and a lipid monolayer [26], as well as between individual SMALPs themselves [18, 19].

Further to this, the use of fluorescent variants of SMA have shown that individual polymer chains have a propensity to 'swap' between SMALP nanodiscs [17]. Whilst not yet fully understood, these phenomena of SMALP behaviour add further reason to design and develop sensing, fluorescent SMA copolymers. Fluorescent variants of lipids and proteins are commercially available, and hence the development of fluorescent SMA would allow for experiments to properly monitor this exchange behaviour and evaluate the more dynamic aspects of SMALPs.

1.2.3 SMA in Solution

Later, Scheidelaar *et al.* (2016, [41]) examined the dependency of SMALP self-assembly on pH. It was found that at too high a pH (above ~ pH 9), the charge density of the polymer was too high to engage in membrane binding. Whilst lowering the pH mitigated this effect, too low a pH (below ~ pH 6) meant the polymer was too hydrophobic to be water soluble, where instead aggregation occurred. The structure of SMA in solution was originally thought of in term of 'hyper-coils' [13], although this has since been disputed with speculations of structures from 'zips' [45] to 'rosettes' [46]. The implications of this on SMALP technology has been summarised by Stroud *et al*. (2018, [3]):

> "*[SMA] can form a collapsed higher order aggregate. The structure of this aggregate is unknown, but it is likely to involve the partition of hydrophobic moieties into the interior of the aggregate… The formation of SMALPs may be limited by the ability of polymer chains to dissociate from this aggregate before inserting into the target membrane*."

Revelations of both the exchange of polymer chains between SMALPs [17], as well as the presence of multiple polymer chains per SMALP [3, 17], bring to light the potential importance of these aggregates in mediating SMALP behaviour. Therefore, where possible, the novel polymers presented here will be used to study not only the self-assembly of SMALPs, but also the structures and conformations of the polymer in solution.

1.3 Improving the Synthesis of SMA

Until recently, SMA has been bought from one of two major suppliers, *Polyscope* or *TOTAL Cray Valley*, but now, smaller quantities are also available from *Sigma-Aldrich* [7]. Whilst offering several varieties of SMA, these industrial polymers are found to be exclusively synthesised by flow free-radical copolymerisation. This leads to products with widely distributed molecular weights, denoted by the polydisperisty index (PDI), defined as the ratio of the weight-average molecular weight (M_w) to he number-average molecular weight (M_n). These terms are mathematically described in *Equations 8-10*, where N_i is the number of molecules with molecular weight M_i.

$$M_w = \frac{\sum_{i=0}^{\infty} N_i M_i^2}{\sum_{i=0}^{\infty} N_i M_i} \quad (\mathbf{8})$$

$$M_n = \frac{\sum_{i=0}^{\infty} N_i M_i}{\sum_{i=0}^{\infty} N_i} \quad (\mathbf{9})$$

$$PDI = \frac{M_w}{M_n} \quad (\mathbf{10})$$

Pivotal to this project, both the molecular weight and PDI of polymers can be ascertained through gel permeation chromatography (GPC). GPC is a size-exclusion chromatography (SEC) technique whereby solutes of differing diameter, dissolved in a solvent (mobile phase), are separated by a gel (stationary phase) with pores of a defined distribution. As the pores within the gel are not accessible to them, larger analytes have shorter elution times, whereas smaller analytes will have a longer path length and therefore a longer elution time [47]. It is common to find the PDI of commercial SMA samples between 2.0-2.5 [7], meaning the polymer chains are highly varied in length. Once styrene and maleic anhydride have been copolymerised, the maleic anhydride units are then hydrolysed by elevated temperatures or the addition of a base to form water-soluble SMA.

Further to a broad distribution of molecular weights, commercial SMA suffers from heterogeneous monomer sequences. In free-radical polymerisation, homogenous monomer distributions can be encouraged though the use of a continually stirring tank reactor (CSTR). As monomers are continually introduced in the desired ratio, and the product continuously extracted, this enables steady-state conditions [25]. The feed is typically maintained at approximately 97% styrene and 3% maleic anhydride to achieve a 2:1 SMA copolymer. However, the PDI of the product is still larger than desired, and the exact sequence of monomers along the chain remains uncontrolled.

Copolymer composition and PDI has been seen to affect the size distributions of nanodiscs, as well as their protein extraction efficiencies [41]. It is also apparent that the use of undefined copolymers has made it difficult to establish trends between polymer characteristics and their behaviour in SMALPs. Across the literature, demand has arisen for SMA to take advantage of controlled polymerisation techniques. Smith *et al.* (2017, [25]), in a paper detailing such a living polymerisation for SMA, highlighted:

> "*[SMA's] highly disperse composition is likely to influence the dispersity of the discs as well as the extraction efficiency...the field has yet to take advantage of modern polymerization techniques.*"

As well as this, the chemistry of SMA makes it susceptible to chemical modification [7, 48], particularly to amines [24, 28]. Dörr *et al.* (2016, [7]) envisioned an outlook for SMA nanodiscs where:

> "*...the structure of SMA should provide plenty of opportunities for chemical modification to tune its properties...thus an extensive toolbox of different SMAs and their derivatives may be generated for various applications*"

It is therefore clear that SMALP technology stands to benefit, firstly, by being synthesised in a controlled manner to ease the analysis of SMALPs, but also from the possibilities for functionalisation this affords.

1.3.1 RAFT Polymerisation

Copolymers between styrene (*Sty*) and maleic anhydride (*MAnh*) have a long history, and it is only recently that efforts have shifted towards controlled polymerisation, namely reversible deactivation radical polymerisation (RDRPs) practices [48]. All RDRP relies on an equilibrium between polymer chains that can grow and those that are dormant. Dormant chains are where an agent has reversibly added to the growing chain, preventing the further addition of monomer. This equilibrium therefore slows the rate of monomer addition, where the RDRP agent has enforced a limiting factor which means all chains will grow at the same rate. This not only allows the molecular weight of polymers to be controlled, facilitating low PDI products, but also to be reliably predicted. RDRP techniques include nitroxide-mediated polymerisation (NMP) [49] and reversible addition fragmentation chain-transfer (RAFT) polymerisation [49-51], a general mechanism for which can be found in *Scheme 1*. A further category of RDRP is atom transfer radical polymerisation (ATRP), however this seems inapplicable to SMA due to how *MAnh* interacts with the transition metals used.

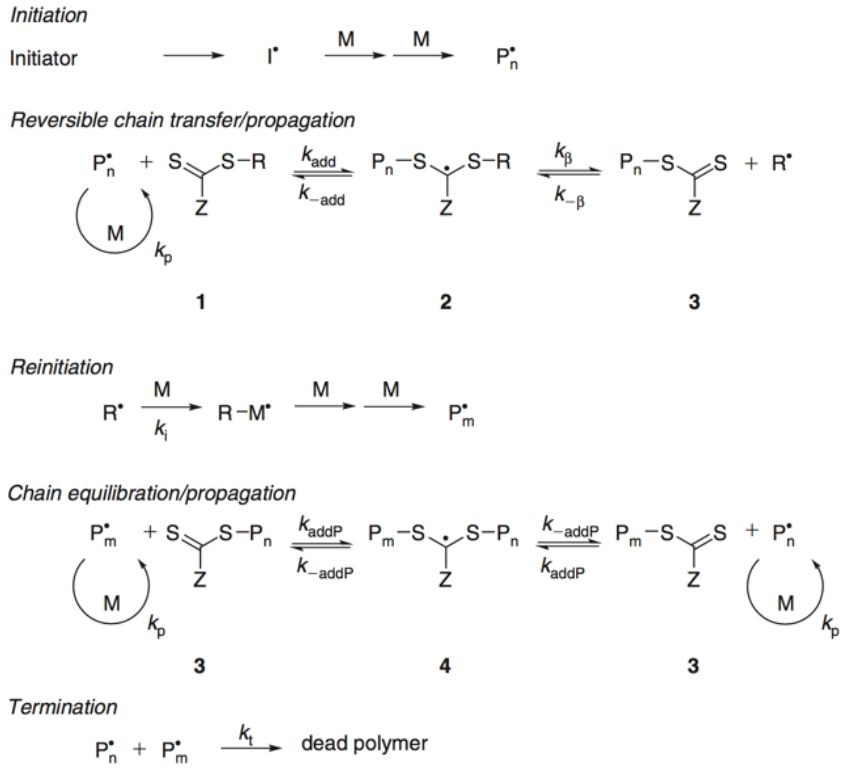

Scheme 1

Klumperman (2010, [48]) has worked with SMA since 1995, and has rationalised the behaviour of RDRP SMA. Reactivity ratios are defined as the likelihood that a monomer will preferentially add to itself over the other comonomer. The reactivity ratios of *MAnh* and *Sty* are nearly zero [38, 52]. As *MAnh* is electron withdrawing, and *Sty* electron donating, generally SMA will be synthesised with an alternating *Sty-MA-Sty-MA* architecture [7, 25, 41, 48]. As *Sty* has a slightly higher tendency to add to itself, styrene homoblocks of varying length are also present. Using this model, Klumperman showed that the reactivity ratio of *Sty-Sty* was constant as a function of the copolymer composition, and that of *MAnh-Sty* increased with the mole fraction of *MAnh* [42]. Therefore, in RDRP, the polymer propagates in a near perfect alternating fashion, but as the mole fraction of *MAnh* depletes, styrene begins to homopropogate. This is known as compositional drift, resulting in a gradiented polymer between the alternating *Sty-MAnh* and *Sty-Sty* homoblock [38]. Smith *et al*. (2017, [25]) simulated this compositional drift (*Figure 10)*, comparing SMA synthesised by RAFT versus CSTR methods.

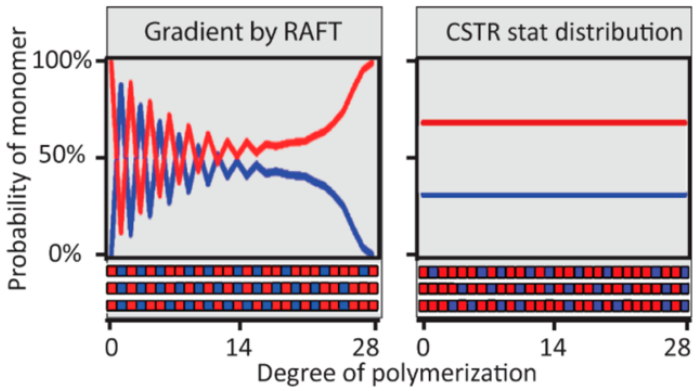

Figure 10: *(Smith et al., 2017, [25]) Simulated compositional drift in RAFT (Left) & CSTR (Right) synthesised SMA. Graph of probability of finding Sty (Red) or MAnh (Blue) in given monomer position. Rows (Bottom) show example distributions.*

The alternating character of the polymer is also somewhat dependent on temperature, where increased temperatures give rise to an increase in heterogeneity. For SMA, therefore, NMP has been superseded by RAFT, as RAFT can be conducted at lower temperatures (60 - 80 °C) than NMP due to the initiator species used [48, 49].

Craig *et al*. (2016, [38]) looked at how RAFT SMA formed SMALPs. It was found that irrespective of the molecular weight, the overall composition of the copolymers, the ratio of *Sty*:*MA*, is what determined the size of the nanodiscs. This suggests that smaller SMALPs can be formed by tailoring the surface tension between the nanodiscs and the solvent to be minimised. Furthermore, in a similar study, Smith *et al*. (2017, [25]) found that in most cases a large styrene homoblock was detrimental to nanodisc formation, however others have highlighted that the presence of at least a short styrene homoblock could be a driving force in this formation [33]. These effects remain largely unexplained, and therefore, by synthesising the fluorescent polymers here, with varying but controlled compositions and architectures, these effects may be probed.

1.3.2 Polymer End Group

With the adoption of controlled polymerisation techniques has come the inevitable question of how the polymer end group may be affecting SMALPs. The importance of end groups is well appreciated and several methods for polymer end group modification have been developed in this respect (see literature review: Lunn *et al*. (2017, [53])). SMALP technology, however, has yet to take advantage of this. A general mechanism for a radical end group modification processes is illustrated in *Scheme 2*.

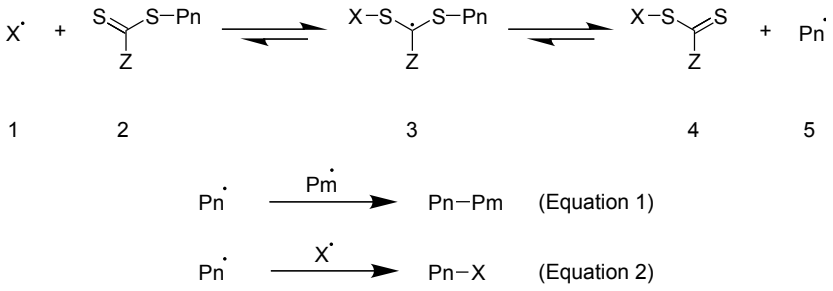

Scheme 2

Chen *et al.* (2009, [54]), key to the initial development of RAFT polymerisation, describe such a method. It is claimed that they have achieved the complete exchange of the thiocarbonylthio end groups, afforded by RAFT, for cyanoisopropyl end groups, with no resulting chain-combination. Previous to this, only part removal of the end group was possible in styrenic polymers as the polymeric $P_n^{\cdot}$ radicals (*5*) were a poorer leaving group compared to cyanoisopropyl radicals (*1*), produced by AIBN. By introducing lauroyl peroxide (LPO), an even poorer leaving group than $P_n^{\cdot}$, not only is this issue circumvented, but due to the increased available concentration of $X^{\cdot}$ (*1*), chain-combination (*Scheme 2*, *Equation 1*) is less likely to occur. A detailed mechanism for replacing the thiocarbonylthio end group with cyanoisopropyl can be found in *Scheme 3*.

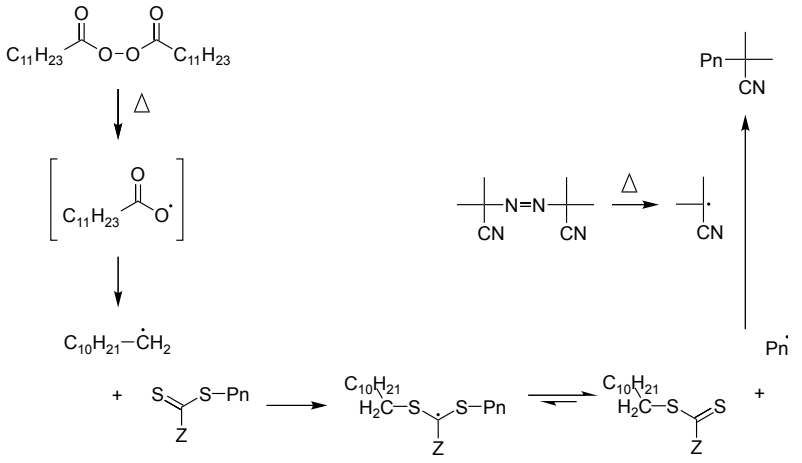

Scheme 3

This cyanoisopropyl group represents a significant physiochemical change from the thiocarbonylthio end group of RAFT polymers, primarily the shift from a hydrophobic to a hydrophilic end group. Therefore, this projects aims to use this reaction to compare polymer end groups and assess to what extent, if any, the effect polymer end group may have on SMALP behaviour.

1.3.2.1 Diffusion Ordered Spectroscopy (DOSY) ^{1}H NMR

DOSY is a 2D NMR technique which allows the comparison of chemical shift with the diffusion coefficient of molecules in solution, without the need for their separation. This is particularly useful for polymers, as it can give an indication of what is incorporated in the polymer chain, as well as the distribution of molecular weights within the sample [55]. In this project, DOSY will be used as means of assessing if the RAFT thiocarbonylthio end group is truly removed.

In general, to induce nuclear magnetic resonance, or transitions between magnetic energy levels, a magnetic field, B_1, oscillating at the Larmor frequency of nuclei, is applied alongside the static field. As magnetic energy levels are not highly separated, they are populated in an even distribution. Therefore, the similar magnetic moments of nuclei can be reduced to a bulk magnetisation vector, M_0 (*Figure 11*). To aid visualisation, the *rotating frame* can be employed [56], whereby the x, y and z axis rotate at the same rate as nuclear procession, and hence the same rate as the applied B_1 field. When the B_1 field is applied along the x axis, the M_0 vector is pushed into the x-y axis, where it is detected. The pulse-time, or the time that the B_1 field is applied for, determines how far the M_0 vector is pushed in this direction.

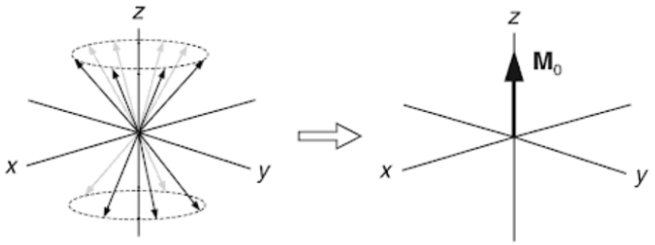

***Figure 11**: Visual representation of the bulk magnetisation vector and rotating frame, [56].*

DOSY operates by the acquisition of a series of spin-echos, a representation of which can be found in *Figure 12*. Each spin-echo uses a different gradient of magnetic field strength between the top and bottom of the sample. When this gradient is applied, due to the lack of a uniform magnetic field, it causes some nuclei to process faster, and some slower, than the rotating frame, resulting in the loss of signal. A 180° pulse is then applied. If nuclei were not diffusing through the sample, the magnetic field strength they experienced before the 180° pulse would be exactly the same after the pulse was applied, meaning all nuclei would again process at the same rate as the rotating frame, returning the signal strength (*Figure 12*). Therefore, nuclei that are diffusing are subjected to a different magnetic field strength before and after this pulse, resulting in their loss of signal. As the series progresses and the gradient steepened, those nuclei that diffuse faster will lose more signal than those that are diffusing

slower. *Figure 13* demonstrates this as the loss of signal of the peak at 1.30 ppm, at acquisition 4, is less than the loss of signal of the peak at 2.08 ppm (solvent).

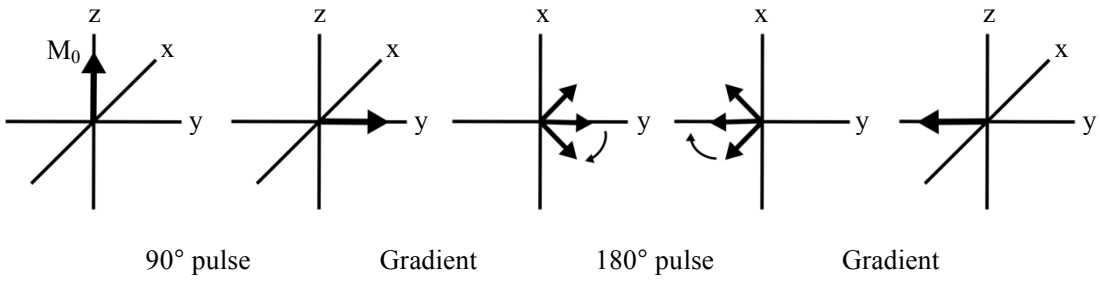

***Figure 12**: Vector model schematic for DOSY spin echo.*

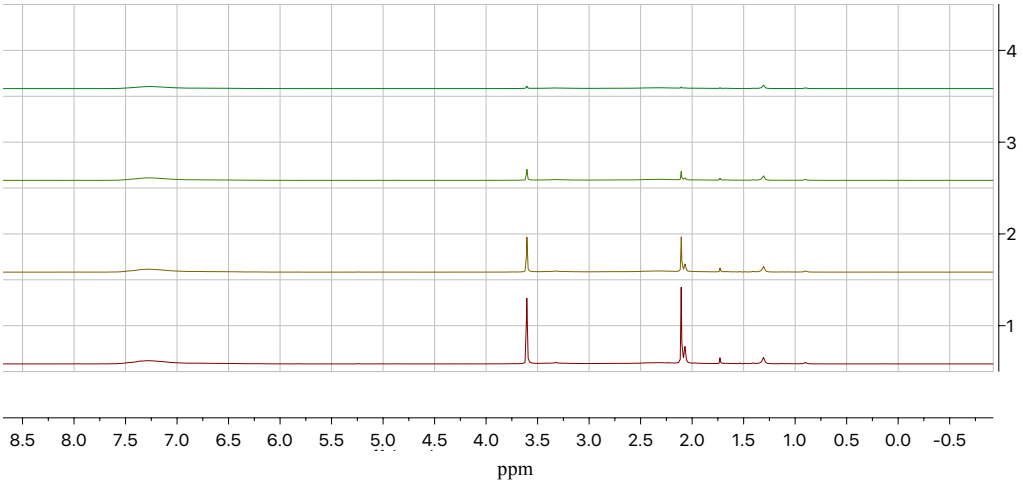

***Figure 13**: Loss of signal with increasing magnetic strength gradient (y-axis).*

This effect is described by *Equation 11*:

$$\boldsymbol{I = I_0 e^{-D\gamma^2 g^2 \delta^2 (\Delta - \frac{\delta}{3})}} \quad \textbf{(11)}$$

Where I is the signal intensity, I_0 is the signal intensity without a gradient applied, D is the diffusion coefficient, γ is the gyromagnetic ratio of the nuclei, g is the gradient strength, δ is the time the gradient is applied for and Δ is the time allowed for diffusion, or effectively, the length of the spin-echo. Therefore, a plot of ln (I) vs. g^2allows calculation of the diffusion coefficient. This will be used here to determine whether the end group, post the modification process, is attached to the polymer or free in solution.

1.3.3 Towards Functionalised SMALPs

The structure of SMA provides several opportunities for functionalisation, including the modification of anhydride moieties [24], end group adaption [25] and copolymerisation with additional monomers. This has implications for the applications of SMALPs in particular. Whether, immobilising MPs on a surface or probing MP dynamics with fluorescent labels, often the biological study of MPs requires difficult and complex preparation, exacerbated by their hydrophobic nature [24]. Therefore, developing strategies to overcome these issues by SMA functionalisation is highly desirable. The following sections present the case for developing fluorescent SMA variants for both protein and SMALP research.

1.3.3.1 Fluorescent Techniques and Fluorescent Polymers

The basis of all fluorescence is that a molecule, capable of absorbing a photon of light, is excited to a higher electronic energy level which then spontaneously decays, emitting radiation [57]. This can occur in aromatic compounds (anthracene, pyrene), some amino acids (tryptophan) as well as many other compounds. The intensity of fluorescent absorbance, and therefore emission, is governed by the Beer-Lambert law (*Equation 12*).

$$A(\lambda) = -logT(\lambda) = log\frac{I_\lambda^0}{I_\lambda} = \varepsilon(\lambda)lc \qquad (\mathbf{12})$$

Where A is absorption, T is transmittance, I^0 and I the intensity of incident and emitted radiation, respectively, ε is the extinction coefficient, l is the pathlength and c concentration. However, inherent to incorporating fluorescent units in a polymer is the breakdown of the Beer-Lambert law. The Beer-Lambert law assumes that fluorescent molecules are evenly dispersed in solution, without aggregation, and are the sole absorbers of photons [57]. Despite this, some have used the intensity of fluorescence emission to detect conformational changes in polymer networks [58]. Similarly, this could be employed with SMALPs to detect possible conformational changes as polymers and lipids form nanodiscs. Other, more sophisticated techniques could assist in this, such as solvatochromism, which provides information on polymer environment, and FRET, used here to demonstrate the potential of fluorescent SMA in the study of proteins.

1.3.3.2 Solvatochromism

Whilst acknowledging that it has come to have multiple meanings in recent year, Bamfield and Hutchings (2010, [59]) define solvatochromism as fundamentally:

> *"the phenomenon whereby a compound changes colour, by a change in either its absorption or emission spectra, when dissolved in different solvents."*

Where, specifically, solvatochromic probes have been used with polymers as either part of the chain [17, 60] or as free dyes able to penetrate a polymer matrix [60]. Here, fluorescent

units will be introduced as comonomers to interrogate the polarity of their changing environment as SMA forms SMALPs.

When a fluorophore is excited, this excited state may be more or less polar than the ground state. Due to the Frank-Condon principle, essentially stating that electronic transitions (10^{-15} s) are comparatively instantaneous compared to molecular translation (10^{-8} s), the solvent cannot rearrange before a photon has been absorbed. Once absorbed, the solvent relaxes around the excited molecule, and may stabilise or destabilise it, causing there to be a different energy gap compared to when it was excited [59]. If this energy gap is smaller, this causes the emission spectra to be shifted to a longer wavelength, described as a bathochromic shift (red shift). The reverse is called a hypsochromic shift (blue shift). This effect can be visualised by *Figure 14*.

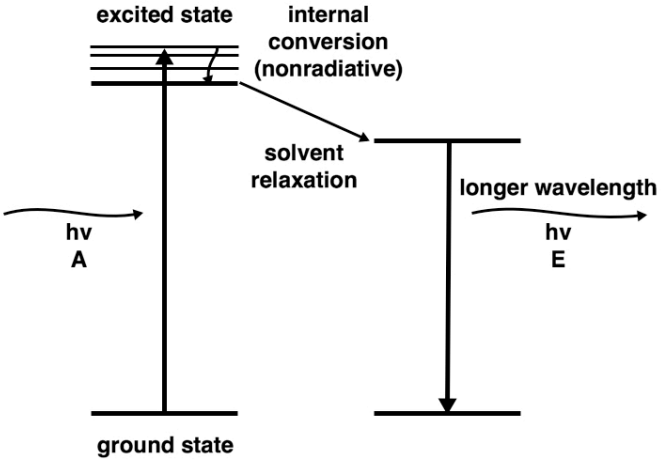

***Figure 14**: Jablonski diagram of bathocrhomic solvatochromism.*

By monitoring the solvatochromic changes of the polymers as SMALPs are formed, it may be possible to ascertain where the polymer arranges itself in the SMALP. Also, if the polymer is behaving dynamically, exchanging between nanodiscs, or changing its conformation, this may also be detected.

1.3.3.3 Förster Resonance Energy Transfer (FRET)

FRET is used to determine the distances, and changes in distance, between donor and acceptor fluorophores. This is a commonly used technique, particularly in the biological study of proteins, used to determine protein conformation and dynamics [65]. It is therefore of specific interest to design FRET-enabled SMA variants, both for the improved downstream analysis of proteins, but also for the benefit of studying SMALPS themselves.

FRET is where a donor fluorophore can be excited and energy is transferred, non-radiatively, to an acceptor fluorophore, which then fluoresces. Certain criteria have to be met for FRET to be possible between two fluorophores, described as follows (Hussain *et al.*, 2009, [61]):

i. There must be spectral overlap between the emission of the donor and excitation of the acceptor fluorophore.

ii. The two fluorophores must be close in space (typically between 1-10 nm).

iii. The fluorescent lifetime of the donor must be long enough for FRET to occur.

iv. The dipoles of the two fluorophores must be roughly parallel as this is how energy is transferred.

The occurrence of FRET is observed in a number of ways, including the decreased fluorescent lifetime of the donor, the decreased emission intensity of the donor, and the increased emission intensity of the acceptor. Here, a proof-of-concept investigation will be conducted between the fluorescent copolymers and the inherently fluorescent protein, gramicidin. Gramicidin is a transmembrane channel protein [62] containing external tryptophan moieties commonly exploited in such investigations [63, 64]. It is hoped that if nanodiscs small enough can also incorporate gramicidin, FRET will be observed. This could prove invaluable, opening research avenues into protein-polymer interactions [17], protein dynamics [65], protein and lipid [18, 19] exchange, aspects all fundamental to SMALP research which have remained elusive thus far.

2.0 Objectives

Ambiguities in the understanding of SMALP technology have thus far restrained research and hindered applications. From reviewing the literature, demand is apparent that controlled polymerisation should be used to allow for the examination of how polymer composition and architecture could afford SMALPs with desirable physiochemical properties. RAFT polymerisation techniques have been recognised as a means of achieving this and further provides an opportunity to functionalise SMA. Fluorescence capabilities have been identified as a meaningful modification that could be made to SMA, allowing for the improved investigation of both the structure and behaviour of SMALPs, as well as their augmented application in downstream protein research.

Therefore, the objectives for this project have been outlined as follows:

1. Synthesise novel, fluorescence-enabled SMA variants with defined molecular weights, compositions and architectures.

2. Compare these polymers to commercial SMA 2000 (*Cray Valley*). Where possible, establish trends between polymeric properties and differences to the structure and behaviour of SMALPs and polymers in solution.

3. Demonstrate and assess the fluorescence capabilities of these polymers and their potential usefulness to both SMALP and protein research:

    i. Solvatochromic effects used to determine polymer conformation and position both in solution and in SMALPs.

    ii. FRET analysis between polymers and the protein, gramicidin, in SMALPs.

4. Exchange the thiocarbonylthio end group of RAFT polymers for a cyanoisopropyl end group and assess how end group identity may affect the structure and behaviour of SMA and SMALPs.

3.0 Experimental

3.1 Monomer & Polymer Synthesis

3.1.1 Materials

Prior to polymerisation, styrene (*Sigma Aldrich*, purity ≥ 99%) was passed through a disposable, pre-packed inhibitor remover column (*Sigma Aldrich*) to remove the stabilising agent 4-tert-butylcatechol. Maleic anhydride (puriss, purity ≥ 99%), the fluorescent species, 9-vinylanthracene (purity ≥ 97%), the initiator , 2,2'-Azobis(2-methylpropionitrile) (AIBN), the RAFT-agent, 2-(dodecylthiocarbonothioylthio)-2-methylpropionic acid (DDMAT) (purity 98%, HPLC grade) and the solvent, 1,4-dioxane were purchased from *Sigma Aldrich* and not purified further before use. Similarly, triethylamine (purity ≥ 99%), acryloyl chloride (purity ≥ 97%, 400 ppm phenothiazine stabiliser), gramicidin (from *Bacillus Aneurinolyticus*), the lipid species, t-2-dimystoyl-glycero-3-phosphocholine (DMPC) (purity ≥ 99%), and all other solvents used, were purchased from *Sigma Aldrich* and were not purified further. Lauroyl peroxide (LPO) was purchased from *BDH Chemicals LTD.*, and mono and dibasic sodium phosphate (purity ≥ 99%) from *Acros Organics*.

3.1.2 Synthesis of 1-Pyrenemethyl Methacrylate (PmMa)

Before pyrene may be copolymerised in a radical polymerisation process, it is necessary to synthetically insert an active C=C bond (*Scheme 4*). As adapted from the work of Lou *et al*. (2004, [66]), 1-pyrenemethanol (0.5 g, 0.0022 mol) and triethylamine (0.1 ml, 0.0065 mol) were dissolved in 25 ml THF (GPC grade) before the dropwise addition of acryloyl chloride (0.6 ml, 0.0065 mol) at 0 °C. This solution was then stirred for 12 hours and allowed to come to room temperature. THF was evaporated under vacuum and the solid residue redissolved in 30 ml dichloromethane. To remove any unreacted triethylamine or acryloyl chloride, the solution was washed with 10 ml 1.0 M HCl using a separator funnel, followed by aqueous sodium hydrogen carbonate and then water. After drying the resulting solution with magnesium sulphate, it was filtered and the solvent removed by rotary evaporation. The resulting yellow solid was then dissolved in 0.5 ml THF and precipitated with 2 ml methanol. This was then left for 20 hours at -20 °C, before being filtered. The precipitation process was repeated before the solid was finally collected. The identity of this compound was confirmed as 1-pyrenemethyl methacrylate by ^{1}H NMR: [($CDCl_3$): δ 7.65-8.24 (9H, m, aromatic), 5.92 (1H, s, H_2C=C), 5.85 (2H, s, CH_2O), 5.50 (1H, s, H_2C=C), 1.94 (3H, s, CH_3)].

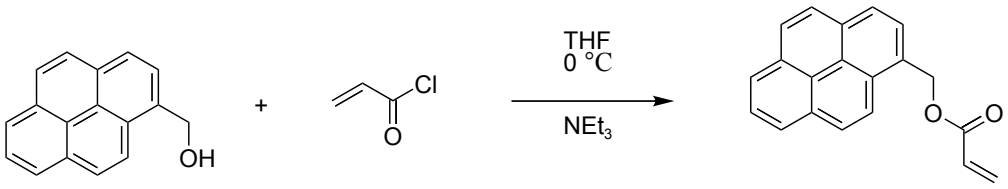

Scheme 4

3.1.3 RAFT Polymerisation of SMAnh & SMAnh Variants

Styrene, maleic anhydride, the initiator, AIBN, and the RAFT agent, DDMAT, were dissolved in 1,4-dioxane in the relative ratios found in *Table 1*. Where appropriate, the fluorescent comonomers 9-vinylanthracene or PmMa were also included in these mixtures.

***Table 1**: Monomer ratios in polymerisation feed.*

Sample / Abbreviation	Reagent	Mass Reagent /g	Mol Reagent	Predicted Molecular Weight / kDa*
SMAnh (R)	Styrene	1.0003	9.60×10^{-3}	6
	Maleic anhydride	0.4039	4.12×10^{-3}	
	AIBN	0.0433	2.64×10^{-4}	
	DDMAT	0.0905	2.48×10^{-4}	
	1,4-dioxane	3.0000	3.40×10^{-2}	
VA SMAnh A	Styrene	1.0003	9.60×10^{-3}	6
	Maleic anhydride	0.4039	4.12×10^{-3}	
	AIBN	0.0433	2.64×10^{-4}	
	DDMAT	0.0905	2.48×10^{-4}	
	1,4-dioxane	3.0000	3.40×10^{-2}	
	9-vinylanthracene	0.0020	9.79×10^{-6}	
VA SMAnh B	Styrene	1.0003	9.60×10^{-3}	53
	Maleic anhydride	0.4039	4.12×10^{-3}	
	AIBN	0.0044	2.68×10^{-5}	
	DDMAT	0.0098	2.69×10^{-5}	
	1,4-dioxane	3.0000	3.40×10^{-2}	
	9-vinylanthracene	0.0020	9.79×10^{-7}	
VA SMAnh C	Styrene	1.0003	9.60×10^{-3}	6
	Maleic anhydride	0.4039	4.12×10^{-3}	
	AIBN	0.0433	2.64×10^{-4}	
	DDMAT	0.0905	2.48×10^{-4}	
	1,4-dioxane	3.0000	3.40×10^{-2}	
	9-vinylanthracene	0.0002	9.79×10^{-7}	
P SMAnh	Styrene	1.0003	9.60×10^{-3}	6
	Maleic anhydride	0.4039	4.12×10^{-3}	
	AIBN	0.0433	2.64×10^{-4}	
	DDMAT	0.0905	2.48×10^{-4}	
	1,4-dioxane	3.0000	3.40×10^{-2}	
	PmMa	0.0001	3.50×10^{-7}	

** As calculated by Equation 13.*

Polymerisation reactions were conducted as described by Harrisson and Wooley (2005, [46]) (*Scheme 5*). Reaction mixtures were transferred to a sealed round bottomed flask before being degassed with nitrogen, followed by three freeze-thaw cycles under vacuum using a Schlenk line. This was to purge any oxygen that could potentially poison the free-radical initiator. The mixture was then covered with aluminium foil to prevent light

from affecting the reaction, before being heated to 60 °C for 22 hours. The polymer solution was then cooled and precipitated in 500 ml diethyl ether at 0 °C.

The number average molecular weights, M_n, of the polymers were predicted as a function of the ratios of monomer to RAFT-agent in the reaction feed (*Equation 13*). A conversion of 100% was assumed.

$$M_{n(Pre)} = \left(\frac{mol_{Sty} \times MW_{Sty} \times conversion}{mol_{RAFT}}\right) + \left(\frac{mol_{MAnh} \times MW_{MAnh} \times conversion}{mol_{RAFT}}\right) + MW_{RAFT} \quad \textbf{(13)}$$

The molar ratio of styrene to maleic anhydride in the polymerisation feed governs the ratio of these components in the polymer product. Hence, all synthesised polymers are expected to have an approximately 2:1 styrene to maleic anhydride ratio.

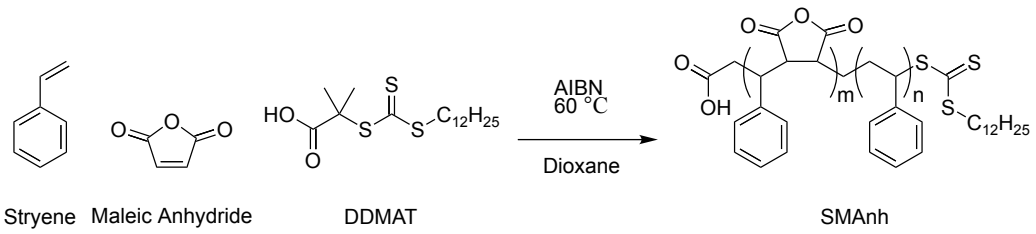

Scheme 5

3.1.4 Hydrolysis of SMAnh to SMA

SMAnh was hydrolysed to SMA according to the procedure described by Hall *et al.* (2018, [33]). A 10% (w/v) solution of the polymer in 1 M aqueous NaOH was first heated for 2 hours at 120 °C under reflux. The polymer was then precipitated by acidifying this solution to pH 3.0 with 4 M aqueous HCl. As the precipitate was too fine for standard filter paper, this mixture was then centrifuged using an *Eppendorf 5804R* centrifuge for 15 minutes at 21 °C and 8000 rpm. The supernatant was drained to collect the pellet which was then washed with water and recentrifuged a further three times. In order to achieve a greater purity, the precipitate was then redissolved in 0.6 M NaOH and again precipitated with HCl, before repeating the washing procedure. Finally, the precipitate was redissolved in a minimal amount of 0.6 M NaOH and adjusted to pH 8.0 before freeze drying (*Virtis SP Scientific*) for at least 24 hours.

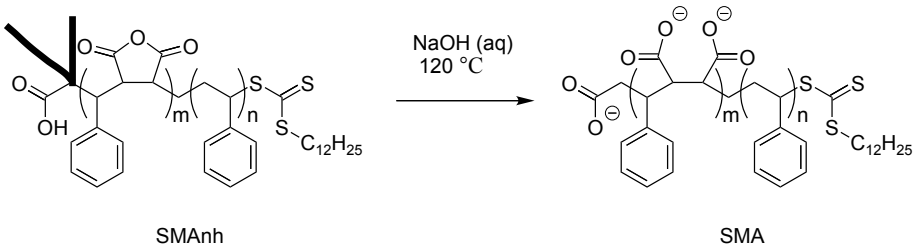

Scheme 6

3.1.5 End Group Modification: Thiocarbonylthio to Cyanoisopropyl

Procedure for the exchange of the RAFT end-group (thiocarbonylthio) follows the work of Chen *et al.* (2009, [54]). As suggested, to achieve a higher success rate, a large excess of AIBN (20 molar equivalents) and LPO (2 molar equivalents) were added to a 3% (w/v) solution of the polymer in toluene (HPC grade). This was then degassed by three freeze-thaw cycles before being heated to 80 °C for 4 hours. The solution was then dried under nitrogen before being hydrolysed without the need for further modification.

3.1.6 Nanodisc Formation

A 50 mM phosphate buffer solution (PBS) was first made by mixing 0.1 M aqueous solutions of monobasic sodium phosphate (2.65 ml, 2.65×10^{-4} mol) and dibasic sodium phosphate (47.35 ml, 4.735×10^{-3} mol), which was then made up to 100 ml with 18.2 ΩM ultra-filtered water. NaCl (1.1688g, 0.02 mol) was then added, resulting in a 0.2 M salt concentration. This produced a PBS stabilised at pH 8.0, within the pH range SMALP nanodiscs have been shown to be stable [33, 41].

The lipid, DMPC (0.005 g, 7.38×10^{-6} mol), was dissolved in 0.679 ml PBS and dispersed by sonication in two 10-second bursts, separated by a 15-second rest period to prevent overheating. 0.015 g of the polymer in 0.231 ml PBS was then added, producing a nanodisc solution containing 1.65% (wt) polymer and 0.55% (wt) lipid. An immediate gauge of successful nanodisc formation can be observed from the loss of turbidity upon the addition of the polymer solution.

The protein, gramicidin, was incorporated into nanodiscs by initially dispersing the protein in DMPC vesicles, as described by Rawat *et al.* (2004, [63]). This was achieved by first dissolving DMPC (0.005 g, 7.38×10^{-6} mol) in a minimum volume of 1:1 chloroform:methanol and gramicidin (0.0004 g, 2.13×10^{-7} mol) in a minimum volume of methanol, before mixing. A few drops of chloroform were then added to this before the solution was dried by rotary evaporation at 40 °C until only a residual film remained. This film was then swelled with 1 ml PBS and agitated until all the lipid had been resuspended. This resulted in a lipid-protein solution at the same concentration used for nanodisc formation as described above. Therefore, this solution can be sonicated and used with polymer solutions without further alteration.

3.2 Polymer & Nanodisc Characterisation

3.2.1 Fourier Transform Infrared Spectroscopy (FTIR)

All FTIR spectroscopy was conducted on a *Perkin Elmer* desktop spectrometer with polymer samples in the solid-state at room temperature. Each data set was collected using 14 runs, measuring percentage transmittance, scanning between the wavenumbers 500 to 4000 cm^{-1}. Spectra were then used to confirm the presence of species incorporated into the polymer by the identification of characteristic bond vibrations, as well as to monitor the success of the hydrolysis of SMAnh to SMA.

3.2.2 UV/vis Spectroscopy

All UV/vis spectra were collected using an *Agilent Cary 60 UV-vis* spectrometer with a quartz cuvette. Specifically, the technique was used to monitor the presence of the DDMAT end group of the polymers, before and after removal. This was possible by observing the absorbance peak at a wavelength of 310 nm, characteristic of its yellow colour [38, 54]. To allow quantitative comparison, spectra were normalised by being indexed to 262 nm, representing the styrene content that theoretically remains unchanged.

3.2.3 ^{1}H NMR & ^{13}C NMR

All ^{1}H NMR spectra were recorded using an *Agilent* 500 MHz NMR spectrometer at room temperature. Polymers were either dissolved in D_6-acetone (anhydride) or D_2O (acid) at concentrations between 30-40 mgml^{-1} to ensure good quality spectra. All spectra were processed in *Mestrelab MNova 11.0* software, where spectra were baseline corrected using Bernstein polynomials to allow for the accurate integration of peak area. Here, this is essential as ^{1}H NMR was primarily used to ascertain the ratio of styrene to maleic anhydride units within polymer samples. Furthermore, as polymers in general express complicated peak patterns due to the range of environments for similar molecular units, line broadening was frequently used to ease analysis of these spectra.

^{13}C NMR was conducted using the same method described above, with the exception that acquisition times were lengthened to improve the signal-to-noise ratio of the spectra.

3.2.4 Diffusion Ordered Spectroscopy (DOSY) ^{1}H NMR

All spectroscopy was conducted on a *Bruker AV* 500 MHz spectrometer at room temperature with anhydride polymer samples dissolved in D_6-acetone (20 mgml^{-1}) At least 8 gradient steps were used to ensure a reliable measurement of the diffusion coefficient (see *Section 1.3.2.1*).

3.2.5 Gel Permeation Chromatography (GPC)

SMAnh polymer solutions in THF (2 mgml^{-1}) were passed through an *Agilent GPC 1260 Infinity* system, along with a blank THF sample, in a run time of 40 minutes per sample. Here, the elution time of solutes is inversely proportional to their molecular weight, which was calibrated using a standard of polystyrene. Whilst it is commonly reported that the use of this standard is acceptable for SMAnh polymers, it is possible that unaccounted for interactions between maleic anhydride units and the stationary phase will cause disparity between the measured molecular weight and the absolute value [38, 47].

Solutes were detected by measuring variation to the refractive index from the blank THF sample, which is directly proportional to concentration. GPC chromatograms were then analysed using *Agilent GPC/SEC* software to obtain the M_n and PDI values for each polymer.

3.2.6 Dynamic Light Scattering (DLS)

DLS was conducted using a *Malvern Zetasizer Nano Series*, at θ = 173° (backscattering, high angle) and λ = 633 nm, using disposable, plastic cuvettes. Measurements were analysed

using *Zetasizer* software and constants such as the refractive index and viscosity were set to values calibrated from *p*(styrene-*alt*-maleic acid) in PBS (50 mM, 0.2 M NaCl). Nanodisc samples were diluted to a concentration of 0.1% (wt) polymer to ensure an infinite dilution regime. Prior to measurement, solutions were also passed through a 0.45 μm *Millex Millipore* membrane syringe driven filter to remove contaminating scatterers such as dust.

The output values from DLS, or particle size distributions (PDS), can either be based on intensity or volume. Intensity PDS highlights larger objects, which dominate the data, whilst volume PDS attempts to correct this and account for smaller objects. Therefore, throughout this report volume PDS was used, allowing for comparison across the data. Due to the assumptions made in DLS experiments (see *Section 1.1.2.1*), in all cases, five sets of measurements were taken and a satisfactory cumulate fit achieved to ensure reasonable reliability before accepting the averaged results. Whilst absolute values for diameter may not have been achievable, comparisons between the DLS data here remains valid.

3.2.7 Small Angle X-ray Scattering (SAXS)

All SAXS data was collect *in vacuo*, with a CuKα X-ray tube source, using nanodisc samples at the concentration of preparation (*Section 3.1.6*) in sealed 1 mm capillary tubes. Experiments were conducted at, and equipment provided by, the *ISIS Neutron and Muon Source* at the *Rutherford Appleton Laboratory* on a *Xenocs NanoInXider* instrument. The raw data was reduced from an image to a plot of *I* vs *q* using *Foxtrot*.

All SAXS data was processed using open-source *SasView* software. Here, data is fitted using the Levenberg-Marquardt method to a '*core shell bicelle'* cylindrical model, assuming dilute solutions (*i.e.* no contribution from *S(q)*), using a combination of best estimates from DLS data and previously found values for scattering length density. As the mean molecular weight, and density, of SMALP particles was unknown, the intensity of the pattern also had to be fitted to a corrected scale.

3.2.8 Surface Tensiometry

A measurement of surface tension was acquired using a *KSV Instruments Attension Sigma* tensiometer using 0.08% (wt/v) polymer solutions (30 ml) in PBS. Here a ring is pulled between the liquid (bulk H_2O: ρ = 0.9986 g/mol, γ = 72.8 mN/m) and air (ρ = 0.0013 g/mol) interface and measures the downward force acting upon the ring. Several measurements are taken while the system takes time to reach an equilibrium surface tension, γ, due to the diffusion of the polymers between the bulk and surface. An example of this measurement can be found in *Figure 15*.

Surface tension is calculated from the downward force (F_{max}) using *Equation 14*, where *r* is the radius of the ring (diameter = 9.58 mm, wire thickness = 0.185 mm). Before each measurement, the solution vessel was washed thoroughly with ethanol and 18.2 ΩM water, and the ring was heated in a flame to purge contaminants.

$$\gamma = \frac{F_{max}}{4\pi r} \quad \textbf{(14)}$$

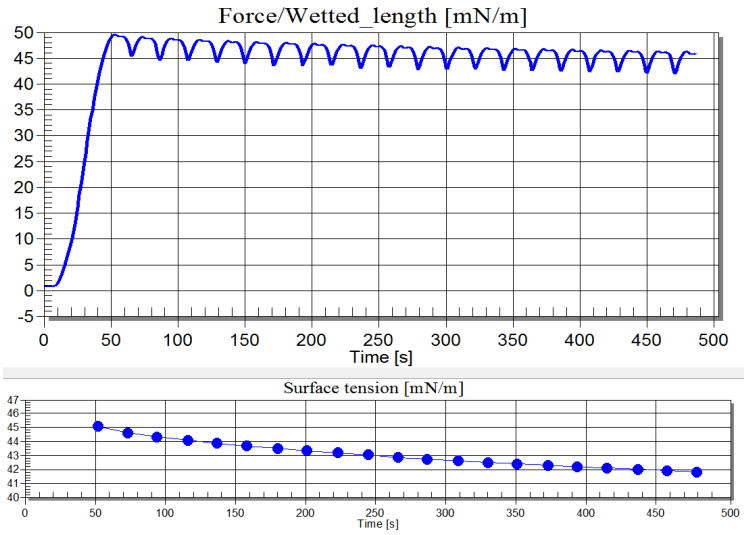

***Figure 15**: Surface tension reaching equilibrium (Attension software).*

3.2.9 Fluorescence Spectroscopy

All measurements were taken on an *Agilent Cary Eclipse Fluorescence Spectrometer* with quartz cuvettes, using *Agilent Scanning, Kinetic and Temperature* applications where appropriate. Due to the Beer Lambert law (*Equation 12*, *Section 1.3.3.1*), where possible, the concentration of samples was maintained at 2.8×10^{-7} M across fluorescence experiments. In cases where spectra were directly compared, it was routine to use 0-1 normalising to mitigate the effects of concentration on spectra intensity. A list of the excitation and emission wavelengths expected from the fluorescent species used is provided in *Table 2*.

***Table 2**: Expected excitation and emission wavelengths of fluorescent species.*

Compound	Spectrum	Wavelength (λ) / nm	Ref.
Gramicidin	Excitation Emission	295 340	[64]
Anthracene	Excitation Emission	320-380 380-480	[67]
Pyrene	Excitation Emission	270-360 360-550	[67] [66]

4.0 Results & Discussion

The main objective of this project was to incorporate fluorescent capabilities into SMA variants, for either the study of SMALPs themselves, or to improve subsequent protein research. Both an anthracene (VA) and pyrene (P) species of the polymer were examined here, as this will clarify if there are any differences in behaviour dependent on the fluorophore identify. To examine how polymer architecture and molecular weight may affect structural or behavioural properties, three different VA SMA variants were synthesised. Further to this, two non-fluorescent, RAFT-made SMA variants were also synthesised, where the end group of one polymer was modified. How this may affect SMALPs has not yet been assessed, but if RAFT polymers are to be routinely used in SMALP research, as discussed in the literature review, it will become imperative that researchers be aware of any implications to behaviour. A summary of these polymers and their primary differences are listed in *Table 3*. The successful synthesis and characterisation of these polymers is detailed in *Section 4.1*.

***Table 3**: Summary of synthesised SMA variants and their differing properties.*

Polymer / Abbreviation	$M_{n(Pre)}$ / kDa	End Group Identity	Content Fluorophore / % (wt)
SMA (R)	6	dodecylthiocarbonothioylthio*	-
SMA (RR)	6	cyanoisopropyl	-
VA SMA A	6	dodecylthiocarbonothioylthio*	0.0010
VA SMA B	53	dodecylthiocarbonothioylthio*	0.0010
VA SMA C	6	dodecylthiocarbonothioylthio*	0.0001
P SMA	6	dodecylthiocarbonothioylthio*	0.0001

**Thiocarbonylthio end group from using DDMAT specifically as the RAFT agent. The remainder of this report uses 'thiocarbonylthio' in place of this to allow discussion of RAFT end groups in general.*

In order to evaluate the success of these novel polymers, it was first necessary to validate them against a commercial standard (SMA 2000, *Cray Valley*). This is to prove that the polymers behave comparably, despite relatively major alteration, and were assessed against both the polymer free in solution and in SMALP nanodiscs (*Section 4.2*).

To discover whether fluorescence capabilities could distinguish the behaviour of different polymer variants, the results of these experiments were then compared to the solvatochromic and FRET responses of the polymers (*Section 4.3*). This serves to demonstrate the potential use of these novel polymers in SMALP and protein research.

4.1 Polymer Synthesis & Characterisation

To ascertain the successful synthesis and hydrolysis of the desired copolymers, a range of techniques, including FTIR, NMR, and GPC were employed. Beyond this, polymeric properties were compared to commercial SMA 2000 to acknowledge whether differences exist that may influence the structure or behaviour of the SMALPs analysed later in the project. The following sections aim to detail these findings with particular emphasis on the comparability between polymer samples, as well as the control that was exercised over their molecular weight and composition.

4.1.1 Polymer Composition & Architecture

Repeatedly, SMALP formation has been seen to be sensitive to changes to the amphiphilic balance of the polymer, namely the ratio of styrene to maleic acid units [3, 33, 37]. Previously, this ratio has been seen to be key in determining whether a polymer may successfully form nanodiscs, and furthermore, some have shown this ratio could be intrinsically linked to the size of nanodiscs produced [38, 41]. Therefore, as part of the routine characterisation of the copolymer, ^{1}H NMR was used to determine this.

From the literature, RAFT polymerisation had been found to induce an *alt-block* gradient to the architecture of the polymer [7, 25, 38, 41, 48]. Here, based on the different carbon environments observed, ^{13}C NMR was used to determine whether this was the case as well as if this was different to the free-radical synthesised, commercial SMA 2000.

4.1.1.1 ^{1}H NMR Spectroscopy

It has been seen that it is important to identify the ratio of styrene to maleic anhydride units within the polymer, as this may influence its ultimate behaviour in SMALPs. As an example, the ^{1}H NMR spectrum of VA SMAnh C is presented in *Figure 16*. Polymers typically express broader peaks due to the increased number of possible environments for any given molecular unit, however, the use of integration techniques to identify the ratio of styrene to maleic anhydride has been widely adopted [33, 68]. The integrals of each peak, representative of the protons labelled in *Figure 16,* are dived by the number of protons responsible for that peak. For example, in *Figure 16*, the value of the integrated styrene peak, 1.00, was divided by 5 hydrogens to give 0.20. Likewise, the integral of the peak representing maleic anhydride, 0.20, was divided by 2 hydrogens to give 0.10. Therefore, the ratio of styrene to maleic anhydride is 2:1, as predicted by the molar ratios of monomers in the polymerisation feed.

Unfortunately, anthracene and pyrene units could not be identified by NMR. This was due to a combination of the low incorporation of these units within the polymer as well as screening by the peak of styrene, which dominated the aromatic range of chemical shift (7.60 - 6.00 ppm). This has meant a quantitative measurement of the percentage weight of the polymer consisting of these units could not be calculated and, as a consequence, it has had to be assumed that all anthracene and pyrene in the polymerisation feed was incorporated in the final product.

In all spectra, including that of SMAnh (RR), but excluding that of the commercial polymer, SMA 2000, the thiocarbonylthio end group, characteristic of the RAFT process,

could be identified by the peak at 0.87-0.90 ppm, representing the end methyl group of DDMAT [69].

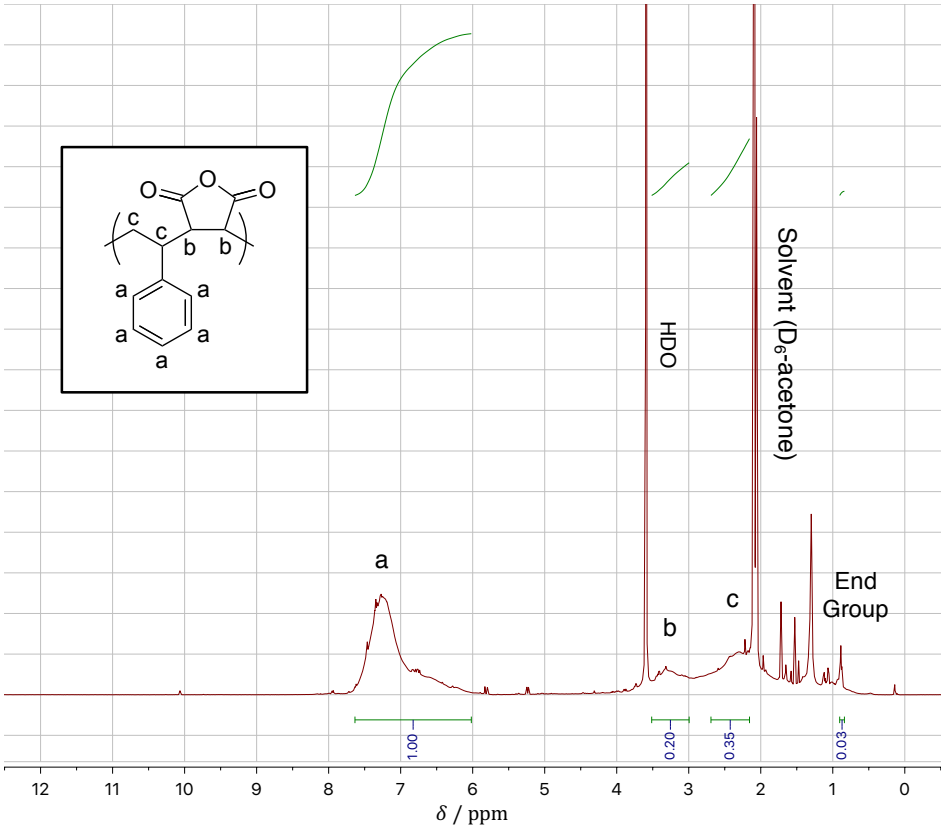

Figure 16: *^{1}H NMR spectrum of VA SMAnh C [(D_6-acetone): δ 7.60-6.05 (5H, broad, H_a), 3.05-3.50 (2H, broad, H_b), 2.15-2.70 (2H, broad, H_c), 0.87-0.90 (3H, t, DDMAT end group)].*

4.1.1.2 ^{13}C NMR Spectroscopy

^{13}C NMR was used as a means of identifying the introduction of the *Sty-alt-MA-block-Sty* architecture of the copolymer. It has been previously shown that peaks at approximately 36.3 and 40.5 ppm refer to the alternating block, and the peaks at 42.0 and 51.8 ppm, the styrene homoblock [70]. *Figure 17* highlights differences between the SMAnh (R) and SMAnh 2000 samples. Although, SMAnh 2000 can be seen to have a similar structure, the peaks are largely broadened, with the 36.3 ppm (*alt*) missing completely, representing a more randomised structure. Furthermore, the lack of any peaks between 37.0-40.0 ppm for SMAnh (R) is indicative of the lack of a semi-alternating structure that can be found in the spectrum of SMAnh 2000. These spectra therefore confirm that RAFT polymerisation was successful in creating the product as expected, allowing for later comparison between samples based on polymer architecture.

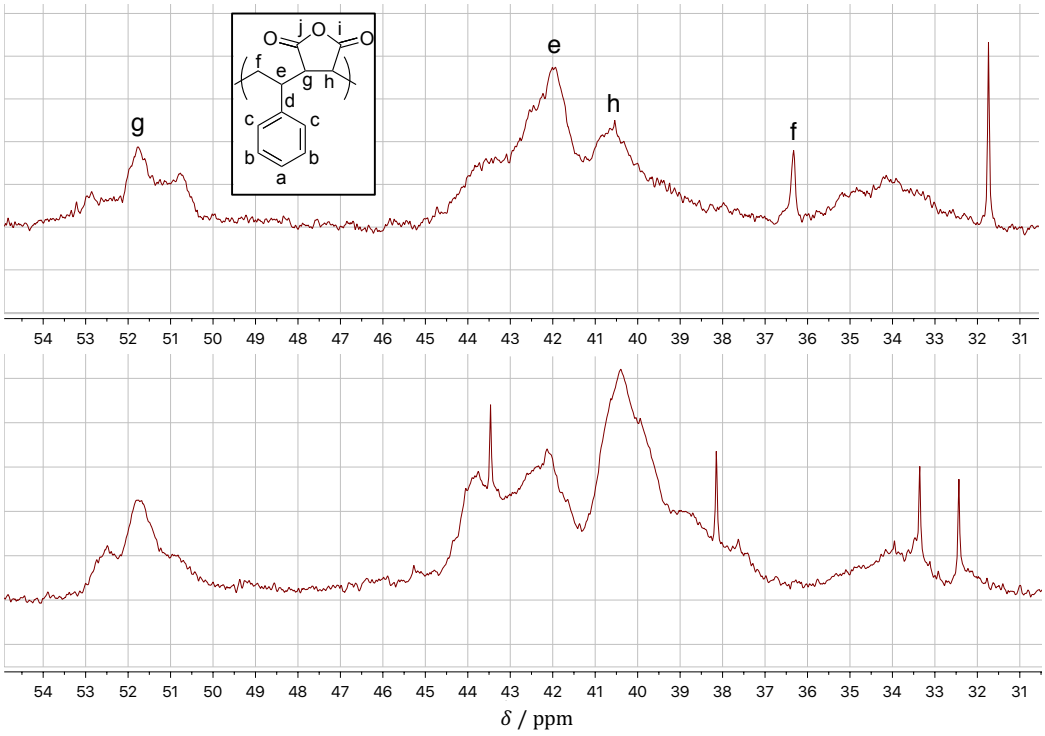

***Figure 17**: ^{13}C NMR spectra of SMAnh (R) (Above) & SMAnh 2000 (Below).*

4.1.2 Molecular Weight & Polydisperisty

GPC was used to find the number average molecular weight of all polymer samples, as well as to provide information on the PDI and the presence of impurities such as monomer residues. *Figure 18*, highlights the narrower molecular weight of the RAFT synthesised polymers in comparison to the commercial polymer, SMAnh 2000. Similar chromatograms were obtained for all in-house synthesised polymers, easing the later interpretation of results as an accurate and narrow distribution of molecular weights can be assumed.

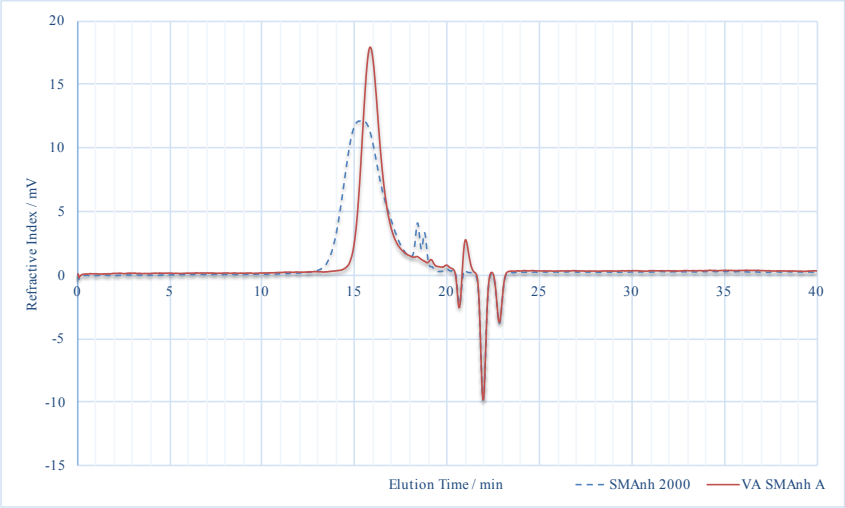

***Figure 18**: Overlaid chromatograms of SMAnh 2000 & VA SMAnh A.*

Table 4 summarises the molecular weights of polymer samples, as well as the values that can be calculated from these. A PDI of 1.20 is generally considered low.

***Table 4**: Molecular weight of polymers (anhydride).*

Sample / Abbreviation	Predicted M_n* / kDa	Conversion / %	M_n / kDa	PDI	DP_n Sty**	DP_n MAnh**	Length Sty Homoblock***
SMAnh (R)	6	64	3.220	1.193	21	11	10
SMAnh (RR)	6	-	3.208	1.270	21	11	10
VA SMAnh A	6	62.9	3.199	1.266	20	11	9
VA SMAnh B	53	74.7	17.176	1.568	113	60	53
VA SMAnh C	6	56.0	3.426	1.240	22	12	10
P SMAnh	6	87.0	5.141	1.160	33	17	16
SMAnh 2000	-	-	4.000	1.796	-	-	-

**Predicted by Equation 13* $^{**} DP = \frac{M_n \times Monomer\ Ratio\ (NMR)}{M_{monomer}}$ $^{***} Length\ Sty\ Homoblock = DP_n Sty - DP_n MAnh$

In all cases the predicted molecular weight was overestimated and not realised in the final products. Whilst using a GPC standard of polystyrene may exacerbate this discrepancy, it is unlikely this is the main cause [38]. Furthermore, as the polymers have low PDI values, and as the predicted value is an underestimation rather than an overestimation, it can also be presumed that oxygen did not poison the initiator. Instead, incomplete polymerisation, as can be seen by comparing the conversion percentages to M_n, should be the primary reason for the reduced molecular weights. Despite this, as desired, all polymers other than VA SMAnh B achieved a relatively similar M_n to the commercial polymer and can therefore be compared.

4.1.3 End Group Modification

Previously, SMALPs have been shown to be highly sensitive to even slight changes to the amphiphilic balance of the copolymer [17, 28, 33]. Therefore, not only is it highly likely that the thiocarbonylthio end group, resulting from RAFT, will affect this system, it is of interest to quantify how exchanging this for a hydrophilic cynaoisopropyl end group affects SMALP behaviour.

It is well known that the end group from DDMAT imparts samples with a pale yellow colour [38], and therefore, its presence can easily be monitored by the absorption peak at

310 nm [33, 54]. *Figure 19*, highlights the loss of this peak, indicating the successful exchange of the thiocarbonylthio end group and its removal during hydrolysis.

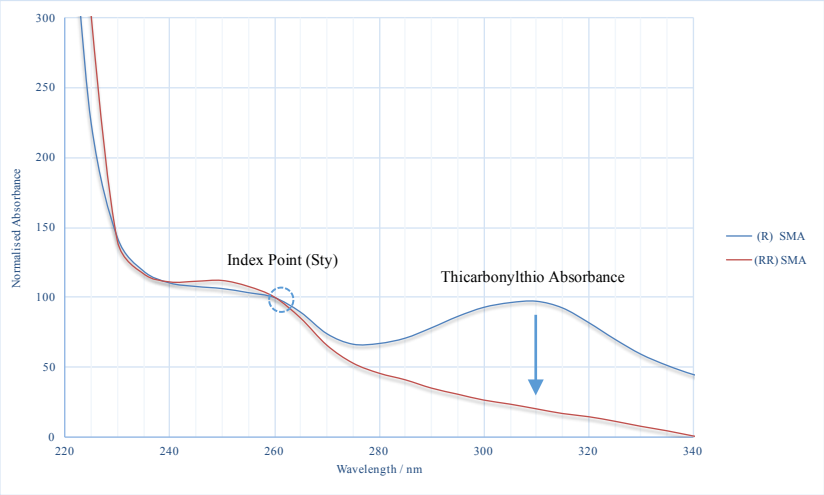

***Figure 19**: Overlaid UV/vis spectra of SMA (R) & SMA (RR) indexed at 262 nm.*

The percentage of the polymer sample with successfully removed thiocarbonylthio end groups can be estimated by comparing the absorbance intensity of the normalised spectra of SMA (R) and SMA (RR). This is possible due to the spectra being indexed at 262 nm, representing the theoretically unchanged styrene content between the two polymers. Here, an estimated removal efficiency of 80% was achieved.

GPC chromatograms were also taken to ensure that chain-combination had not occurred (*see Section 1.3.2*, *Scheme 2*). It is apparent from the overlaid chromatograms in *Figure 20* that a peak at double the original molecular weight did not occur, and so chain-combination can be assumed to have been avoided. It is worth noting however that the PDI increased slightly from 1.19 to 1.27 (*Section 4.1.2*, *Table 4*), further supporting the findings of only 80% end group exchange.

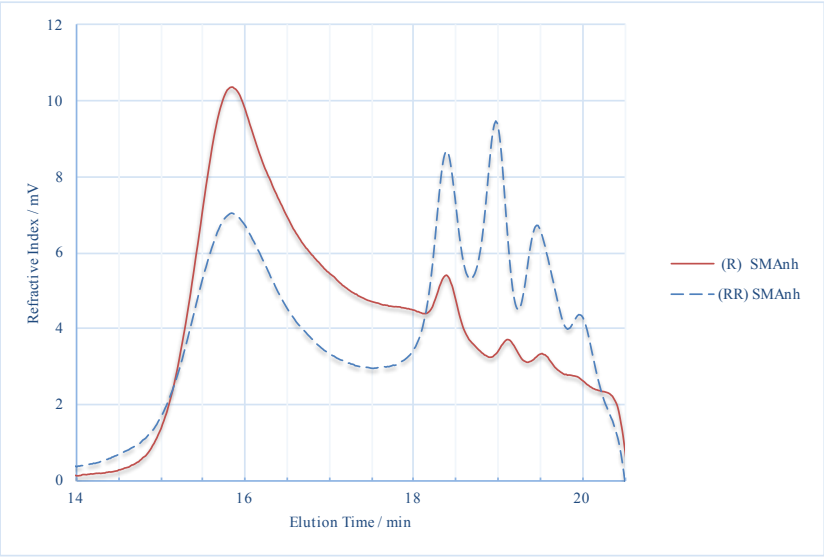

***Figure 20**: Overlaid chromatograms of SMAnh (R) & SMAnh (RR).*

It was believed that the growth of the peak at approximately 18.5 min (476 $gmol^{-1}$) represents the creation of a species containing the combined thiocarbonylthio and LPO radicals (432 $gmol^{-1}$). Whilst this could not be reliably concluded, due to disparity between the calibration standard and analyte, it could be evidenced in future studies by separating this by-product and recording the UV/vis spectra to look for absorbance at 310 nm (as shown in *Figure* 19). Based on suggestions from ^{1}H NMR, whereby additional peaks that occurred upon the removal of the end group did not persist into the SMA spectra, it is assumed that the hydrolysis process was enough to purify out such by-products.

2D DOSY ^{1}H NMR spectra were also recorded for SMAnh (R) and SMAnh (RR) and compared (*Figure 21),* further supporting the the claim that the thiocarbonylthio end group had been successfully detached from polymer chains.

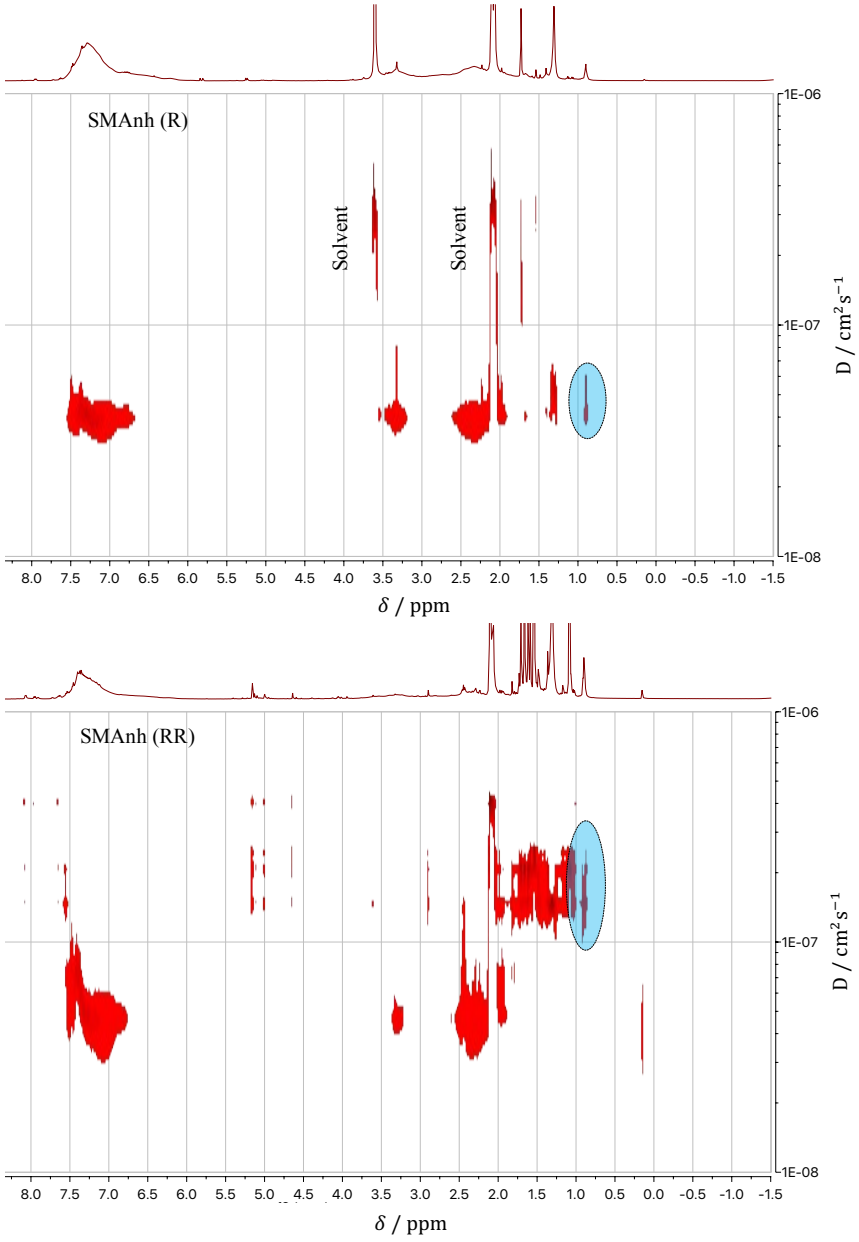

***Figure 21**: ^{1}H DOSY NMR Spectra of SMAnh (R) (Above) & SMAnh (RR) (Below). DDMAT end group highlighted (Blue).*

The peak representing the methyl group on the thiocarbonylthio end group, at a chemical shift of 0.9 ppm, were seen to be diffusing at the same rate as the rest of the bulk polymer in SMAnh (R). The peaks that are not associated with the polymer include solvent peaks (3.6 and 2.1 ppm) as well as unidentified monomer residues. Interestingly, this spectrum confirms that the end group was maintained post hydrolysis. This is significant as the presence of this end group could have implications on the application of these polymers for nanodiscs. Conversely, its presence may also present an opportunity for the simple modification of polymer chains as this is a distinct, reactive group that only appears once in each chain.

In contrast, the spectrum for SMAnh (RR), clearly demonstrates the detachment of the RAFT end group, as the peak at 0.9 ppm has shifted to a diffusion rate equivalent to that of the solvent, rather than that of the polymer chains. Therefore, it can be reliably inferred that the thiocarbonylthio end group has been successfully exchanged for a cyanoisopropyl end group and will be treated as such for the remainder of the discussion.

4.1.4 Hydrolysis

FTIR spectroscopy was primarily used as a method to confirm the transformation of SMAnh to SMA, post hydrolysis. As illustrated in *Figure 22*, the peaks at 1217 and 1075 cm^{-1}, representing the ether bond (C-O-C), present in the spectra of the anhydride form, are lost upon hydrolysis. Furthermore, the asymmetric and symmetric carbonyl (C=O) stretching frequencies at 1854 and 1773 cm^{-1} are shifted to the lower wavenumber of 1563 cm^{-1} [71]. The retention of the aromatic C-H stretching frequencies at 3000, 1493 and 1453 cm^{-1}, associated with styrene, confirms that the hydrolysis only affected the maleic anhydride units in the polymer. Similar spectra were recorded for all polymers to confirm the success of hydrolysis.

Further evidence for the hydrolysis of maleic anhydride could sometimes be seen by the presence of a broad carboxylic acid (COOH) stretching frequency at approximately 3400 cm^{-1}, as shown in *Figure 23*. This peak was only occasionally observed however, due to its dependence on the hydration of the carboxylic acid group. As the polymers are stabilised at pH 8.0 before freeze drying, this peak is unlikely to be present unless samples have been exposed to the atmosphere before having their spectra recorded.

Due to constituting such a low percentage weight of the polymer, similar to the NMR results, the incorporation of anthracene and pyrene units could not be confirmed from FTIR spectroscopy. The thiocarbonylthio end groups of the RAFT agent, DDMAT, however, can be seen from the introduction of the peaks between 2900-2800 cm^{-1} [72] (*Figure 23*). This also suggests that the end group is maintained during the hydrolysis step, corroborating the results from DOSY ^{1}H NMR (*Section 4.1.3*, *Figure 21*).

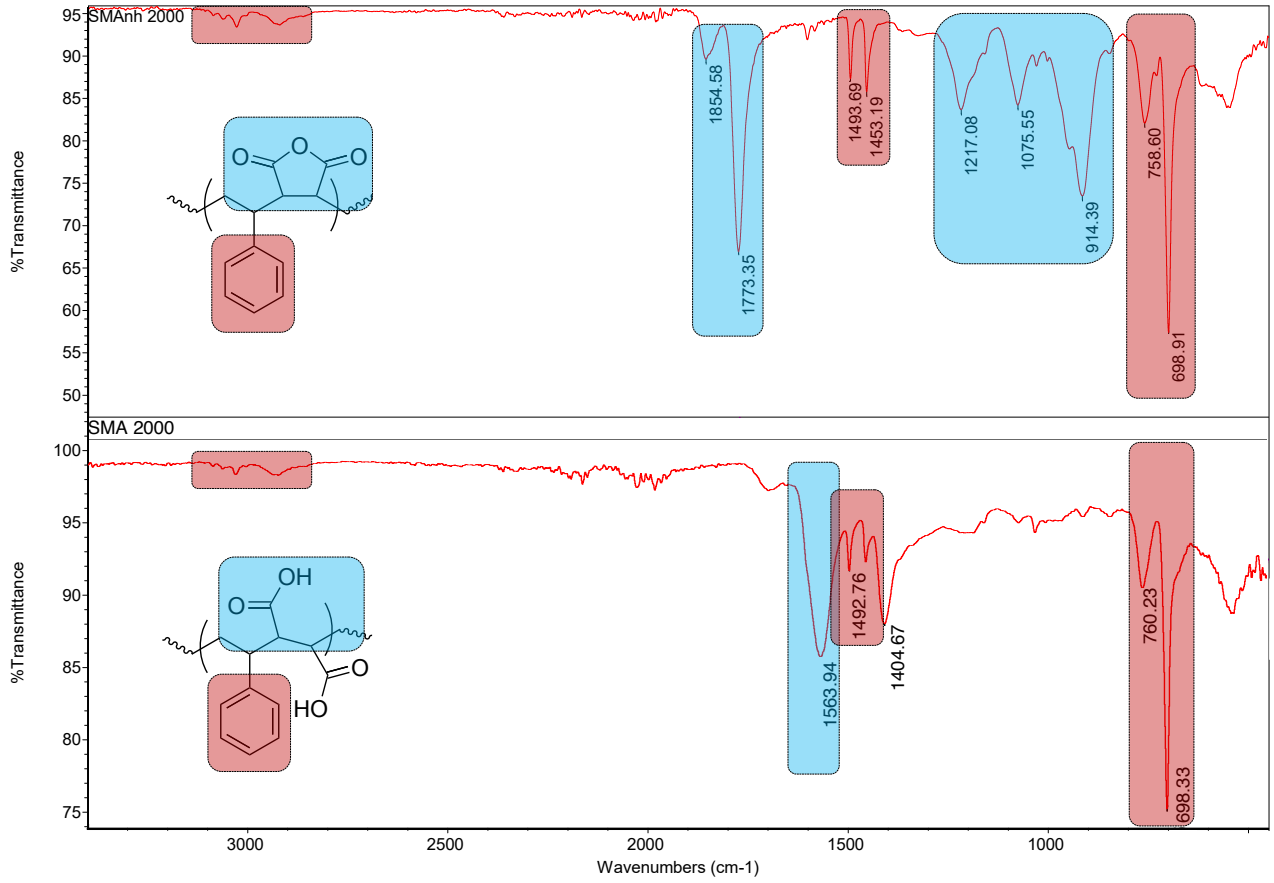

Figure 22: *FTIR Spectra of SMAnh 2000 (Above) & SMA 2000 (Below), highlighting peaks pertaining to styrene (Red) & maleic acid (Blue).*

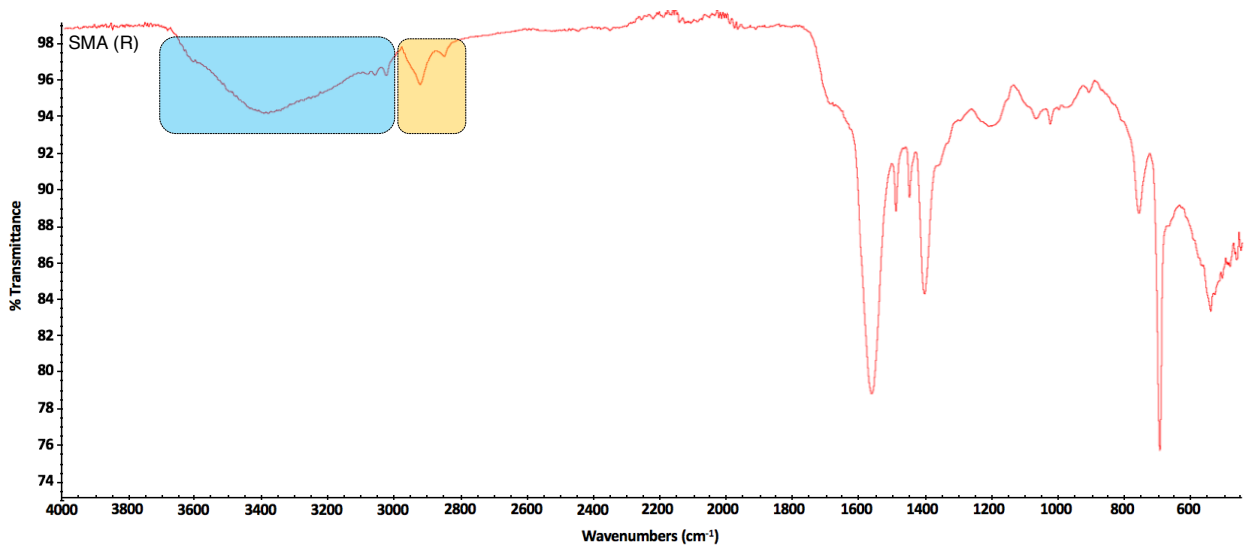

Figure 23: *FTIR Spectrum of SMA (R), highlighting the COOH (Blue) & RAFT (Yellow) end group stretching frequencies.*

4.1.5 Concluding Remarks

All polymers here have been found to have a 2:1 styrene to maleic acid ratio as confirmed by the analysis of ^{1}H NMR spectra. Further to this, ^{13}C NMR has shown that RAFT polymerisation introduced an *alt-block* gradient architecture to the polymers, as expected. This represents a significant difference to SMA 2000 and assessments can therefore be made on how this affects SMA and SMALP behaviour. Whilst the presence of fluorescent units could not be confirmed from the techniques described above, this is evaluated in more detail in *Section 4.3.1*.

The modification of polymer end group in SMA (RR) from thiocarbonylthio to cyanoisopropyl has been confirmed from a combination of UV/vis and DOSY ^{1}H NMR spectroscopy. GPC confirmed that no chain-combination has occurred, and therefore SMA (R) and SMA (RR) can be directly compared to assess the effects of end group identify.

GPC further confirmed the controlled molecular weight of the synthesised polymers, allowing for the interpretation of downstream results without need for considering the effects of broad PDIs. The successful hydrolysis of all polymers to the acid form was confirmed by FTIR, without any effect seen to the polymer end group or styrene units.

It is hoped that such extensive characterisation of these polymer samples will allow for trends to be established between polymeric properties and polymer behaviour. These trends will eventually be compared to the fluorescent response of the polymers later in the report.

4.2 Structural & Behavioural Characterisation of SMA & SMALPs

The following sections aim to analyse the differences, if any, to the structure or behaviour between different polymer samples. How the different polymeric properties, identified in *Section 4.1*, affect the dimensions of SMALPs is of interest to further advance the understanding of SMALP self-assembly as well as improve their application. Furthermore, as the literature has highlighted that SMA aggregates are not well defined, and that this may have implications for SMALP formation, these structures were also examined.

4.2.1 Polymers in Solution

It is likely that SMALP self-assembly is somewhat dependent on the thermodynamics of polymer aggregates in solution. Whether aggregate dissociation is required before SMALPs can form, or if similar interactions favour and govern both aggregation and SMALP self-assembly, it is worth considering how these aggregates behave and how this correlates to polymeric properties.

4.2.1.1 Surface Tension & Polymer Aggregates

Measuring surface tension allows an understanding to be developed of how different polymers may be arranging themselves in solution. This is important to consider as it has been recently found that nanodiscs likely comprise multiple polymer chains [17] and therefore how chains interact could influence the efficiency of nanodisc formation [3].

To allow comparison between polymer samples, PBS at pH 8.0 was used as the solvent throughout. This was necessary as pH dictates the deprotonation of maleic acid units, and hence governs solubility as well as repulsion between individual polymer chains, both of which can affect surface tension [45]. *Table 5* lists the equilibrium surface tensions measured in descending order.

***Table 5**: Equilibrium surface tension of polymer solutions.*

Sample	γ / mNm^{-1} **
P SMA	51.59 ± 0.03
PBS (solvent)	51.45 ± 0.08
SMA (R)*	48.74 ± 0.08
VA SMA A	47.99 ± 0.16
VA SMA C	46.53 ± 0.04
VA SMA B	42.42 ± 0.09
SMA (RR)*	41.91 ± 0.12
SMA 2000	37.99 ± 0.01

** Lower concentration (0.06% (wt/v)) than other samples (0.08% (wt/v)) due to insufficient mass of polymer, SMA (R) and SMA (RR) remain comparable in this respect.*

*** Taken once 5 consecutive measurements did not differ by more then ± 0.2 mNm^{-1}.*

Garnier *et al.* (2000, [45]) previously investigated the effect of pH on surface tension using comparable SMA polymers and solution concentrations. It was observed that at a pH range between 6 – 8, the propensity of the SMA to form multi-chain structures was increased, and hence, at this range, surface tension was maximised. They believed this was due to the forming of 'zips' whereby the styrene between separate chains would interact and align, with the maleic acid unit facing out into solution. If the pH was too high, the higher charge density of the maleic acid units caused interchain repulsion that prevented structure formation. Too low a pH, however, and the polymers were not soluble enough to come away from the interface. Unlike traditional surfactants, where first the surface is saturated before micelle formation, it was found that these 'zips' were preferentially formed until a critical concentration was reached. Whilst in recent years these 'zips' have now been found to be closer to disc-like, 'rosette' structures [46], the theory of how this may affect surface tension stands. *Figure 24* illustrates this concept.

From *Table 5*, it can be seen that the commercial polymer exhibits the lowest surface tension compared to all other polymers. This was expected as, due to the lack of any ordered architecture, a random copolymer is not expected to form well organised structures which

could shield the hydrophobic units from the solvent. In this respect, the novel polymers here, with regular architectures, are expected to deviate from this behaviour significantly, as can be seen by their increased surface tensions.

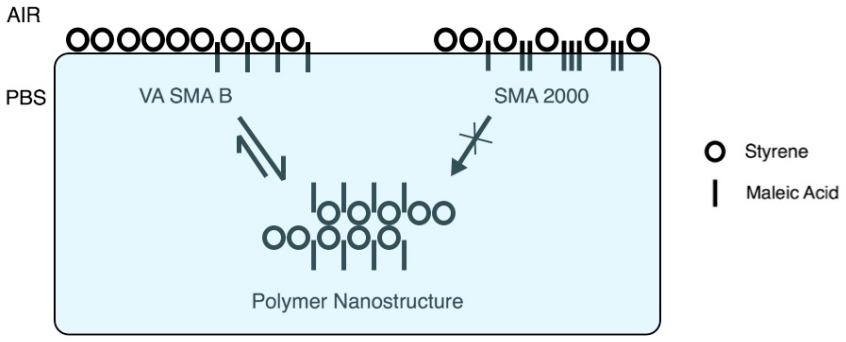

***Figure 24**: Schematic of polymeric structures in solution.*

The incorporation of the large hydrophobic fluorescent units is evidenced by the increased surface tension. This is because there will be a greater propensity for these polymers to shield hydrophobic moieties inside a structure, governed by the entropic gain from the displacement of water. VA SMA A exhibited a higher surface tension compared to VA SMA C due to its higher anthracene content, and P SMA had the highest surface tension, likely due to the increased hydrophobicity of pyrene compared to anthracene. VA SMA B is an exception to this however. As seen previously (*Section 4.1.2*, *Table 4*), this polymer has a significantly larger styrene homoblock but exhibited one of the lowest surface tensions. This long styrene tail is expected to arrange itself at the surface more akin to a hydrocarbon solute, generating an anomalously low surface tension. Furthermore, it is also possible that this tail is too large to effectively insert itself into the structure without disrupting it [36, 37], instead tethering single chains, or structures, to the interface. Large styrene tails have been seen to be detrimental to the formation of SMALPs [25] and the same reasoning here could potentially rationalise this behaviour.

Comparing the SMA (R) and SMA (RR) samples, it can be seen that removing the hydrophobic RAFT end group, and replacing it with a polar cyanoisopropyl group, has produced results similar to the commercial polymer. By reducing the hydrophobicity of the polymer as a whole, the need to protect these groups from the solvent by means of structure formation in solution is reduced. Further to this, as the CN group is capable of forming hydrogen bonds, this may induce enough tension to pull any structures apart, allowing columbic effects to dominate. This is the first inherent consequence of the polymer end group identified in this experiment, and could have significant ramifications for SMALP formation.

Although the structures of the aggregates discussed here were not elucidated in this experiment, their formation is corroborated by the DLS results in *Section 4.2.1.2*.

4.2.1.2 DLS & Polymer Aggregates

To provide insight into the behaviour of the polymer structures found during surface tension measurements, polymer solutions (< 0.1% (wt/v)) were tested at two temperatures: 25 °C

and 55 °C. *Table 6* lists the average diameter and PDI of the polymers in solution, as found by DLS.

Firstly, these measurements corroborate the existence of polymer structures in solution, hypothesised from surface tension measurements (*Section 4.2.1)*. Interestingly, whereas most polymers can be seen to have formed structures of similar sizes, SMA (RR) and SMA 2000 appear to be significantly smaller, indicating single polymer strands or coils. This can be reconciled by calculating the estimated diameter of a Gaussian coil of SMA (RR) from *Equations 15-16*. Where R_g is the radius of gyration and N is the number of monomer units in the polymer, set using the degree of polymerisation (*Table 4*):

$$\text{Diameter} = 2R_g = \frac{R^{0.5}}{6} \quad \textbf{(15)}$$

$$R = 1.54 \times N^{0.6} \quad \textbf{(16)}$$

This gives an estimated diameter of an SMA (RR) coil as 0.6 nm and, considering DLS overestimates diameter, this would suggest SMA (RR) exists as single polymer chains that coil in solution. This again aligns with the resulting surface tension, where single strands would collect at the interface, hence lowering surface tension. VA SMA B exhibited the largest structures, as expected, due to having the largest molecular weight.

***Table 6**: DLS measurements of diameter and PDI of polymer structures in solution at 25 °C and 55 °C. 95% C.I. taken from 5 sets of averaged data; each set using at least 17 scans.*

	25 °C		**55** °C	
Sample	**Diameter / nm**	**PDI**	**Diameter / nm**	**PDI**
VA SMA A	15.0 ± 4.4	0.76 ± 0.22	15.7 ± 1.9	0.39 ± 0.06
VA SMA B	18.2 ± 3.5	0.56 ±0.20	20.0 ± 0.5	0.48 ± 0.21
VA SMA C	16.4 ± 1.4	0.66 ± 0.23	11.3 ± 2.9	0.39 ± 0.12
P SMA	14.3 ± 0.2	0.28 ± 0.02	13.0 ± 0.3	0.21 ± 0.05
SMA (R)	16.0 ± 0.6	0.49 ± 0.12	13.4 ± 0.2	0.16 ± 0.02
SMA (RR)	2.6 ± 1.8	0.32 ± 0.15	1.5 ± 0.5	0.33 ± 0.11
SMA 2000	0.8 ± 0.1	0.43 ± 0.16	1.4 ± 1.0	0.50 ± 0.09

It can be seen that in most cases the diameter of the structure either did not significantly change upon heating or was slightly reduced. However, crucially, for all polymers forming structures greater than 10 nm, the PDI is seen to reduce. This effect can be better appreciated from the individual scans depicted in *Figure 25*. Here, the data for VA SMA B was analogous for the plots obtained for VA SMA A, VA SMA C, and SMA (R). Whereas the results for SMA 2000 matched SMA (RR) and P SMA was unique.

For VA SMA B, it appears from *Figure 25* that heating the solution allows for an energy minimised structure to be formed. As this occurs with increasing temperature, it can be assumed that these structures are primary ordered by hydrophobic interactions, governed by the entropy gain from the dissociation of water. This can be understood by *Equation 17*, where ΔG is the change to Gibbs free energy, ΔH is the enthalpy change, ΔS is the entropy change, and T is temperature.

$$\Delta G^{\circ} = \Delta H^{\circ} - T\Delta S^{\circ} \quad (\mathbf{17})$$

For VA SMA B in particular, it must also be noted that the flexibility of the polymer will increase as the glass to liquid transition temperature, T_g, is approached (77 °C, [46]). This may facilitate the insertion of the larger styrene homoblock into this structure, and may therefore account for its slight increase in size upon heating. P SMA, however, manages to form monodisperse nanostructures even at room temperature. This would match the surface tension results whereby P SMA achieved the highest surface tension. Again, this is likely due to its increased hydrophobicity and therefore propensity to form such structures.

P SMA, SMA (R) and VA SMA (C) all achieved the smallest structures that were larger than 10 nm. This does not seem to correlate to their relative hydrophobicity, but instead could suggest the influence of steric interactions on the structures. VA SMA A and VA SMA B have a higher percentage of anthracene which could therefore be preventing the formation of energy minimised structures.

SMA 2000 and SMA (RR) appeared to be incapable of forming the same type of structure, although upon heating, the beginnings of aggregation could be seen. It may have been that higher temperatures still were required to induce aggregation fully, but unfortunately, this was not measured due to time restrictions of the project. It is worth noting that despite constituting such a small portion of the polymer chain, end group identify has previously been seen to affect aggregation. Du *et al*. (2011, [73]) have previously shown that by replacing the hydrophobic DDMAT end group of RAFT polymers with a hydrophilic one, this was enough to disrupt their aggregation. This therefore, is a clear distinction between commercial and RAFT-made SMA and it is of interest to observe how this may affect SMALP formation.

The propensity of SMA polymers to form these structures may have ramifications on the forces at work when forming SMALP nanodiscs. Whilst more work is needed to fully understand these structures, their presence suggests a significant difference in behaviour to commercial SMA 2000 which does not yet appear to be acknowledged in the literature.

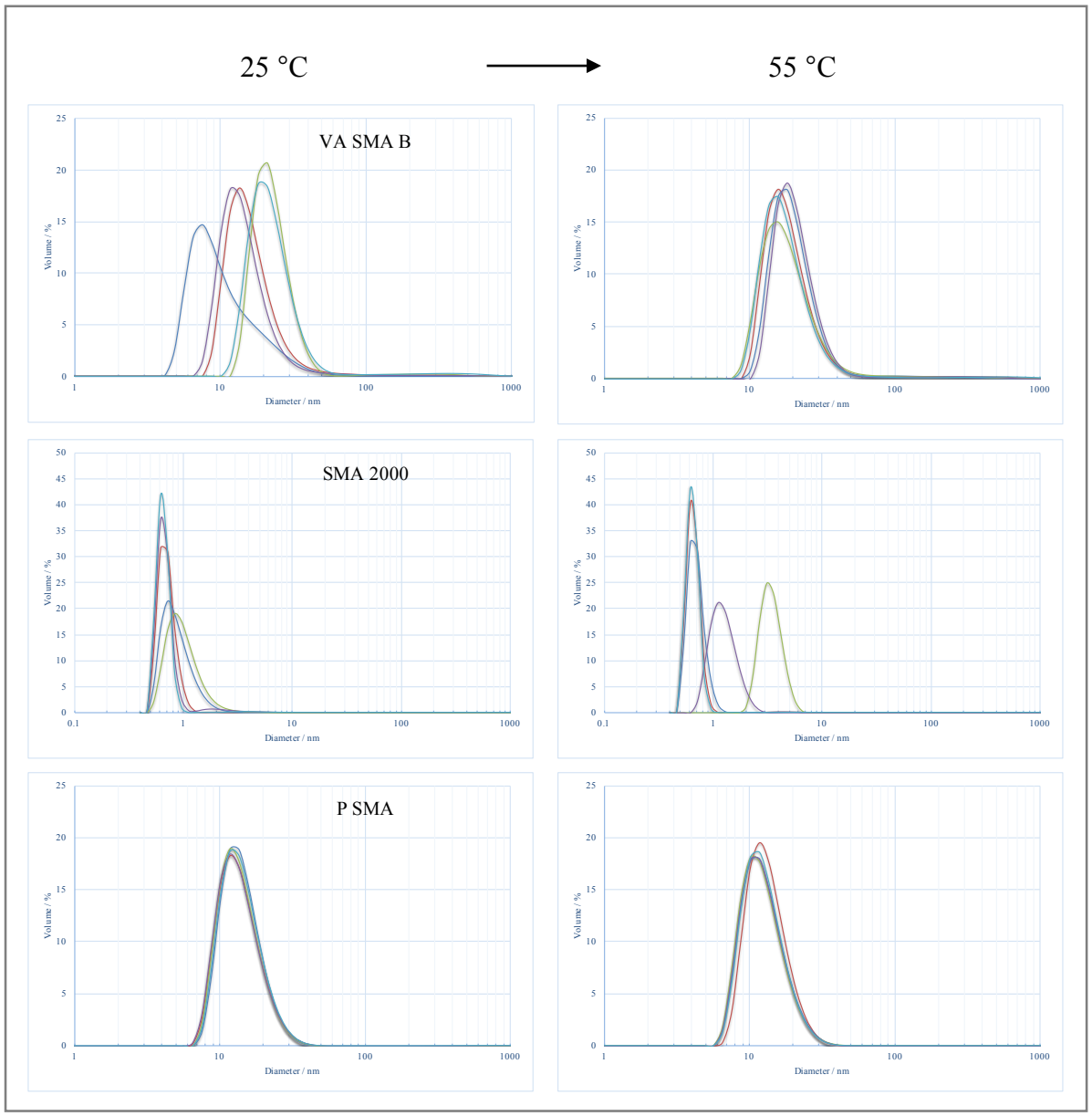

***Figure 25**: DLS scans for VA SMA B (Top), SMA 2000 (Middle) & P SMA (Bottom) at 25 °C and 55 °C.*

4.2.2 SMALP Nanodiscs

Relating polymeric properties to the dimensions of SMALPs will allow for a better understanding of the factors that govern their assembly. Here, DLS allows for rudimentary assessment of SMALP diameter, whilst SAXS provides a more detailed picture of the SMALP morphology.

4.2.2.1 DLS & SMALPs

SMALP nanodiscs both with and without the protein, gramicidin, were prepared in PBS. The incorporation of gramicidin within the nanodiscs, whilst primarily confirmed by fluorescence (*Section 4.3.2.2)*, can be also be deduced from the lack of multiple peaks in the DLS data. All nanodiscs, apart from P SMA and VA SMA B, grew slightly upon protein incorporation (*Figure 26*). Although not significant, this growth plausibly represents the diameter of the protein channel (previously measured as 0.42 nm [62]), measured here by DLS as 0.90 nm ± 0.25 nm. It is also worth noting that gramicidin commonly forms dimers in the lipid bilayer, and this, as well as the overestimation in DLS results, could account for the increased diameter in averaged DLS measurements versus the literature [62]. P SMA and VA SMA B can be theorised to have decreased in size due to the increased hydrophobicity of pyrene compared to anthracene, and a long styrene tail, respectively. The hydrophobic exterior of gramicidin, coupled with these differences, may have cooperatively tightened the SMALP diameter. Interestingly, this would indicate that the styrene tail is in close proximity to the protein, corroborating recent suggestions that the tail is inserted into the nanodisc [33].

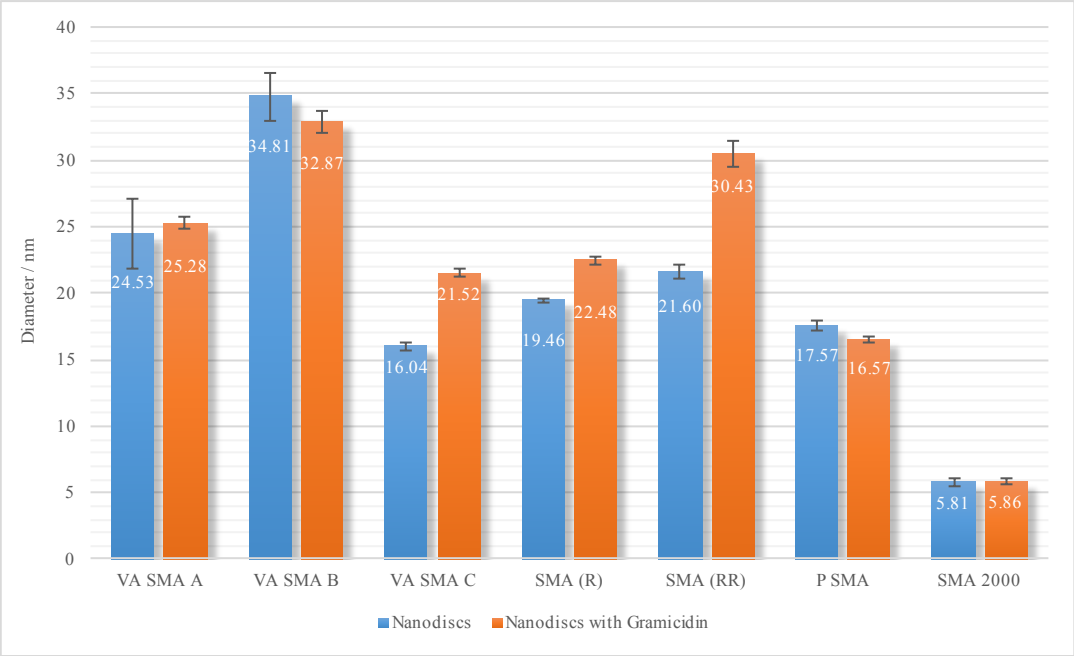

***Figure 26**: DLS measurements of SMALP nanodiscs with and without gramicidin. 95% C.I. taken from 5 sets of averaged data from at least 17 scans.*

In general, two key factors have been attributed to governing the size of SMALP nanodiscs. Firstly, the ratio of hydrophilic and hydrophobic moieties within the polymer, expressly, the ratio of maleic acid to styrene units [38]. Whilst here all polymers have a 2:1 ratio, the general understanding of nanodisc size being minimised when surface tension between the structure and solvent is minimised, can still be employed. Secondly, the M_n of the polymer has been found to contribute towards the size of nanodisc formed [25, 41], explaining the observation that VA SMA B consistently produced the largest structures. Other factors have been identified, such as lipid to polymer ratios and lipid identity [22, 37, 39-42], but these factors are constant across all nanodisc preparations here.

Previous attempts to introduce fluorescent groups have increased the size of nanodiscs, attributed to their increased hydrophobicity [17]. Here, that can be seen to be true for the anthracene polymers, where the overall decreased size of VA SMA C compared to VA SMA A may be assigned to the decreased percentage of VA incorporation. P SMA, however, did not behave in this way, possibly due to the decreased size of pyrene compared to anthracene [36, 37], and therefore may be a preferential candidate for future work.

The increased size of SMA (RR) compared to SMA (R) however, was unexpected, as was its significantly larger growth upon gramicidin incorporation. Both of these observations may be due to the increased polarity of the polymer when replacing the thiocarbonylthio end group with a cyanoisopropyl group. Explicitly, as the styrene homoblock of SMA (RR) instead terminates in a CN group, this may be too hydrophilic to insert itself into, and stabilise, the lipid nanodiscs [33]. This signifies a large difference in SMALP behaviour, perhaps not expected from modifying only one molecular unit in the polymer chain, thus highlighting the overlooked importance of end group identity which would be a good target for future research.

4.2.2.2 SAXS & SMALPs

SAXS was employed in this experiment to confirm that nanodiscs, and not just aggregates, were formed, which is not possible from DLS results. DLS is well known to overestimate the size of particles, due to averaging the hydrodynamic radius. But, further to this, DLS also assumes perfectly spherical samples which is unrealistic for SMALPs. Fluorescent properties are a further cause of interference and again reduces the reliability of DLS results despite satisfactory cumulant fits. SAXS measurements circumvent these difficulties, and were therefore conducted on VA SMA A, VA SMA B and SMA 2000 nanodiscs to provide better insight into the dimensions of the structures observed. *Table 7* identifies the parameters assumed and kept constant for all nanodiscs, as they relate to known quantities, independent of the polymer used.

***Table 7**: Properties held constant for all SMALP samples.*

Fixed Property	Value
SLD solvent	9.46×10^{-6} Å^{-2}
SLD face*	10.30×10^{-6} Å^{-2}
Face thickness**	8.00 Å
Length**	28.00 Å

* Based on 57% hydration of lipid head groups [74].
** Set values from literature [74].

The "*core shell bicelle*" cylindrical model used to fit SAXS data is presented in *Figure 27*.

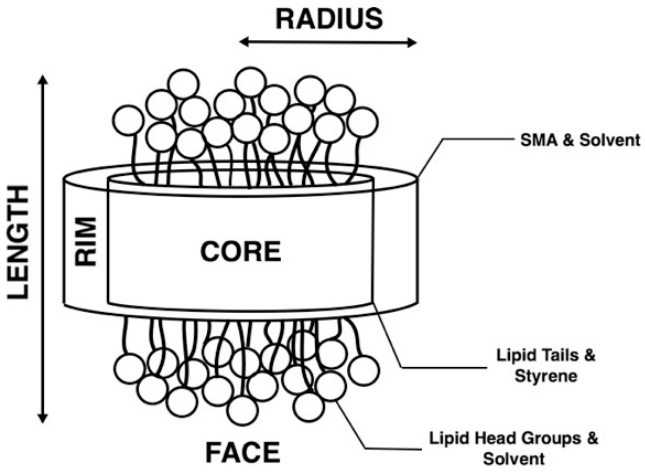

***Figure 27**: Schematic of a SMALP represented by the geometry of a 'core shell bicelle' model.*

The fitted SAXS data is presented in *Figure 28*. VA SMA A and VA SMA B further required that this model be combined with a secondary cylindrical aggregate model to account for signs of aggregation; the steeper gradients at low *q* values are indicative of this. It must be noted that these aggregates were only present in the specific nanodisc samples submitted to SAXS, later confirmed by DLS, and was likely due to the length of time between nanodisc formation and experiments.

The SAXS data for SMA 2000 illustrates the characteristic 'double hump' curvature expected for SMALP nanodiscs. Whilst this was less apparent in the other samples, combination with the secondary model allowed for good agreement between data and fit, suggesting that SMALP nanodiscs were present irrespective of this. Properties obtained from these fits are given in *Table 8*.

Discrepancies were identified between the DLS and SAXS measurements where VA SMA B and SMA 2000 nanodiscs were measured at a diameter reduced by 2 nm compared to DLS, and a greater than 8 nm reduction was seen for VA SMA A. Good agreement in aggregate diameter for VA SMA A was observed between the cylindrical model used to fit SAXS data (32$\pm$ 2 nm, *Table 8*) and the DLS data (30-40 nm, *Figure 29*). Although the data is not shown here, the same was observed for VA SMA B. For VA SMA A, it is plausible that these aggregates could be either between individual nanodiscs, or between the polymer structures seen in *Section 4.2.2.1*. For VA SMA B, however, due to the similarity in size between the aggregates and nanodiscs, these aggregates are more likely composed of polymer alone. Both the acquisition of SAXS data for the polymer structures found in *Section 4.2.2.1*, and the establishment of a temperature-structure trend for these samples, could be used to determine the cause of this behaviour. SANS experiments using deuterated lipids could also be conducted to conclude if lipids were present in these aggregates.

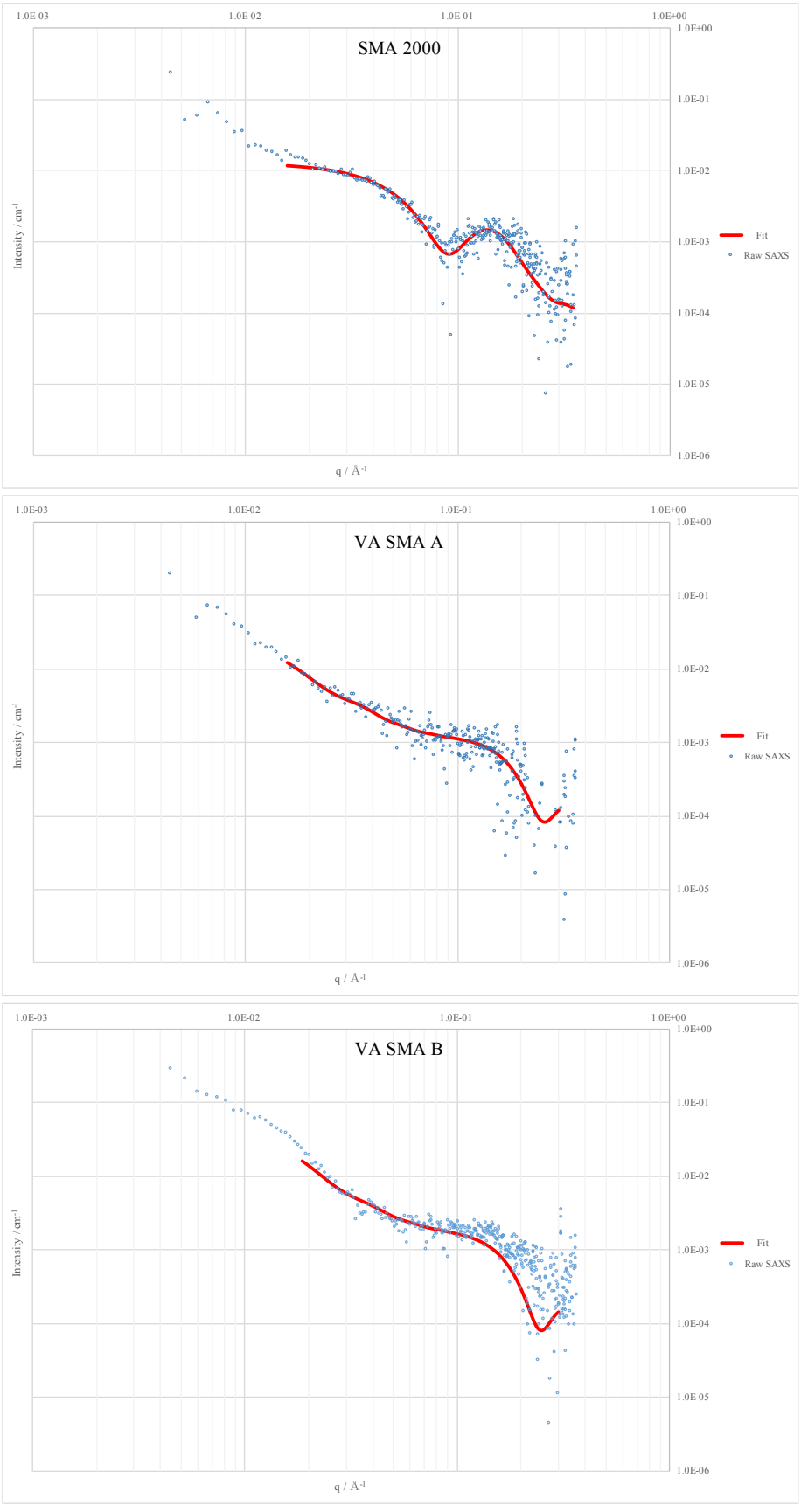

Figure 28: *Fitted SAXS data for SMA 2000 (Top), VA SMA A (Middle) & VA SMA B (Bottom).*

***Table 8**: Properties for SMALPs as obtained from SAXS measurements.*[*]

Polymer in Nanodisc	Property	Value	χ^{2}[**]
SMA 2000	Radius$_{\emptyset}$	18.8 ± 0.8 Å	2.12
	Rim Thickness$_{\emptyset}$	13 ± 1 Å	
	SLD Core	$7.8 \pm 0.1 \times 10^{-6}$ Å^{-2}	
	SLD Rim	$11.1 \pm 0.1 \times 10^{-6}$ Å^{-2}	
	PDI[***]	0.245	
	Total Disc Diameter[****]	63.6 ± 3.6 Å	
VA SMA A	**Nanodisc**		2.97
	Radius$_{\emptyset}$	79 ± 1 Å	
	Rim Thickness	10 ± 1 Å	
	SLD Core	$8.20 \pm 0.01 \times 10^{-6}$ Å^{-2}	
	SLD Rim	$10.0 \pm 0.6 \times 10^{-6}$ Å^{-2}	
	PDI[***]	0.240	
	Total Disc Diameter[****]	178 ± 4 Å	
	Cylindrical Aggregate		
	Radius	160 ± 10 Å	
	Length	30 ± 4 Å	
	SLD	$11.5 \pm 0.1 \times 10^{-6}$ Å^{-2}	
VA SMA B	**Nanodisc**		3.16
	Radius$_{\emptyset}$	161.00 ± 0.04 Å	
	Rim Thickness	10 ± 2 Å	
	SLD Core	$8.0 \pm 0.3 \times 10^{-6}$ Å^{-2}	
	SLD Rim	$10 \pm 1 \times 10^{-6}$ Å^{-2}	
	PDI[***]	0.160	
	Total Disc Diameter[****]	342.0 ± 4.1 Å	
	Cylindrical Aggregate		
	Radius	140 ± 10 Å	
	Length	40 ± 1 Å	
	SLD	$11.5 \pm 0.1 \times 10^{-6}$ Å^{-2}	

[*] *$\emptyset$ indicates that values and error were fitted by sasview software.*

All other values were fitted by trial and error; error taken as change in value to increase χ^2 by 0.1.

[**] *Relates to fit accuracy (lower value; better fit).*

[***] *Obtained from DLS data and fixed.*

[****] *Total Diameter = 2 × (Radius + Rim Thickness)*

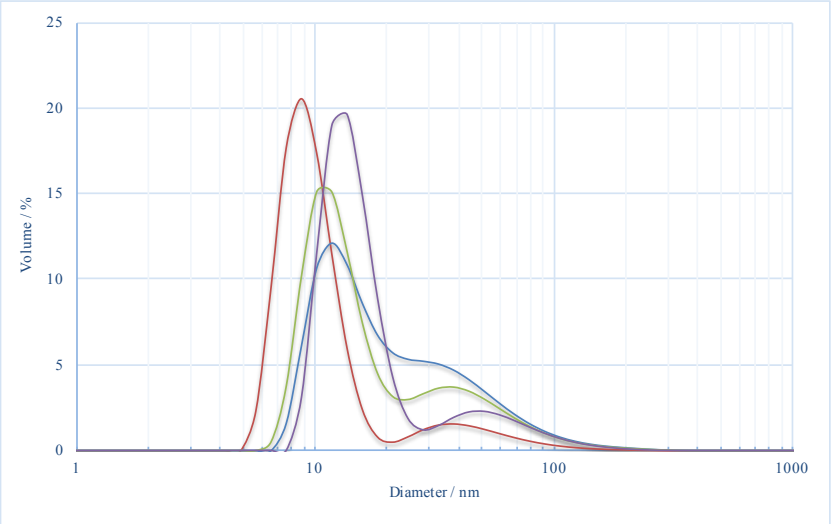

***Figure 29**: DLS scans for VA SMA A nanodiscs with apparent aggregation.*

The scattering length density (SLD) is a measure of how intensely a material interacts with, and therefore scatters, X-rays. As this is proportional to electron density, it is a linear property and therefore the SLD of mixtures can be extrapolated. For example, the SLD of the face is calculated from the known 57% hydration of the lipid head groups [74]: *i.e.* $(0.57\times9.46)+(0.43\times11.5)=10.3$. Therefore, employing the same concept, the closer the SLD of the rim to that of the solvent (9.46×10^{-6} Å^{-2}), the more hydrated it is. Similarly, a higher SLD of the core indicates increased penetration of the polymer. In comparison to SMA 2000, the VA SMA polymers can be seen to both have an increased hydration of the rim, and a greater level of polymer content in the core. It has been recently suggested that the styrene homoblock inserts itself into the lipid core [33], and this would explain the results here. It is interesting that VA SMA B did not give a higher value considering the length of the styrene homoblock, however more data is needed to clarify this. The increased hydration of the rim was also unexpected, although this is in line with a greater percentage of polymer burying itself in the core and a thinner rim. Overall these results can be explained by the general increase in hydrophobicity of these polymers causing more of the polymer to shield itself from solvent in the lipid bilayer fragment.

4.2.3 Concluding Remarks

Several structural and behavioural differences have been identified between the various copolymers. It was found that the propensity of SMA polymers to form aggregates in solution was primarily governed by hydrophobic interactions, where an increase in hydrophobicity, or an increased temperature, increased the likelihood aggregates were observed. The large styrene homoblock of VA SMA B was found to disrupt these aggregates, which may explain why this has previously been found to hinder SMALP formation [25]. The hydrophilic end group of SMA (RR) also prevented aggregation, in agreement with the literature [73].

The incorporation of fluorescent units, in all cases, caused nanodiscs to be larger in diameter in comparison to SMA 2000. This could be attributed to the increased

hydrophobicity of the polymers, corroborating the findings of others who have attempted this [17]. Further suggesting this, SAXS results found that a greater portion of the core consisted of the polymer, and therefore the SMALP rim was also more hydrated.

Exchanging the hydrophobic RAFT end group for a hydrophilic one caused SMA (RR) in solution to behave in a manner similar to SMA 2000. Aggregation was not observed for either of these polymers, where instead chains of individual polymer existed in solution. SMA 2000 and SMA (RR) nanodiscs, however, deviated in behaviour. When incorporating gramicidin, SMA (RR) nanodiscs grew significantly in diameter, opposed to SMA 2000 nanodiscs which did not. Whilst a rationale to describe these differences was not devised here, this work does show that considerations of polymer end group would be a good target for future research.

4.3 Fluorescence

A foundation of biochemical research, fluorescence disciplines have long been used to probe the structure and dynamics of proteins. By incorporating such capabilities into SMA for SMALP nanodiscs, both SMALP and protein studies stand to benefit. The following sections aim to outline whether these novel polymers have been successfully modified to exhibit fluorescence, and if so, demonstrate their potential uses.

4.3.1 Fluorescent Polymers

Until this point of the report, it has not yet been seen if the copolymers presented here have been successfully synthesised to incorporate fluorescent monomers. This was mainly due to the chemical similarity between styrene, anthracene and pyrene, and hence the difficulty in distinguishing these units by spectroscopic methods such as FTIR and NMR. Styrene did, however, provide a secondary means of identifying these units. By employing FRET techniques, it was possible to glean indication that styrene and fluorescent units coexisted in the same polymer chain.

In all cases it was possible to observe the emission of anthracene and pyrene by exciting styrene units at a wavelength of 260 nm, outside the excitation range of either of these fluorophores. For example, it can be seen from *Figure 30* that it was possible to excite VA SMA A at both a wavelength of 260 nm, representing styrene, and 370 nm, representing anthracene. If excited at 370 nm, only the emission spectrum of anthracene was present, when excited at 260 nm, however, the emission spectra of both anthracene and styrene could be observed. A prerequisite of FRET is that the spatial distance between acceptor and donor fluorophores must not be much greater than 10 nm (*Section 1.3.3.3,* [61]). As this was achieved at a highly dilute concentration ($\sim 10^{-7}$ M), it can be presumed that polymers in this regime exist as single chains that do not interact, and that FRET occurred between units on the same polymer chain. It is also likely that the purification process endured during hydrolysis would be enough to remove any unbound comonomers. Therefore, whilst this was not conclusive evidence for the incorporation of these units, it could be reasonably assumed that fluorescent moieties were successfully copolymerised into the product.

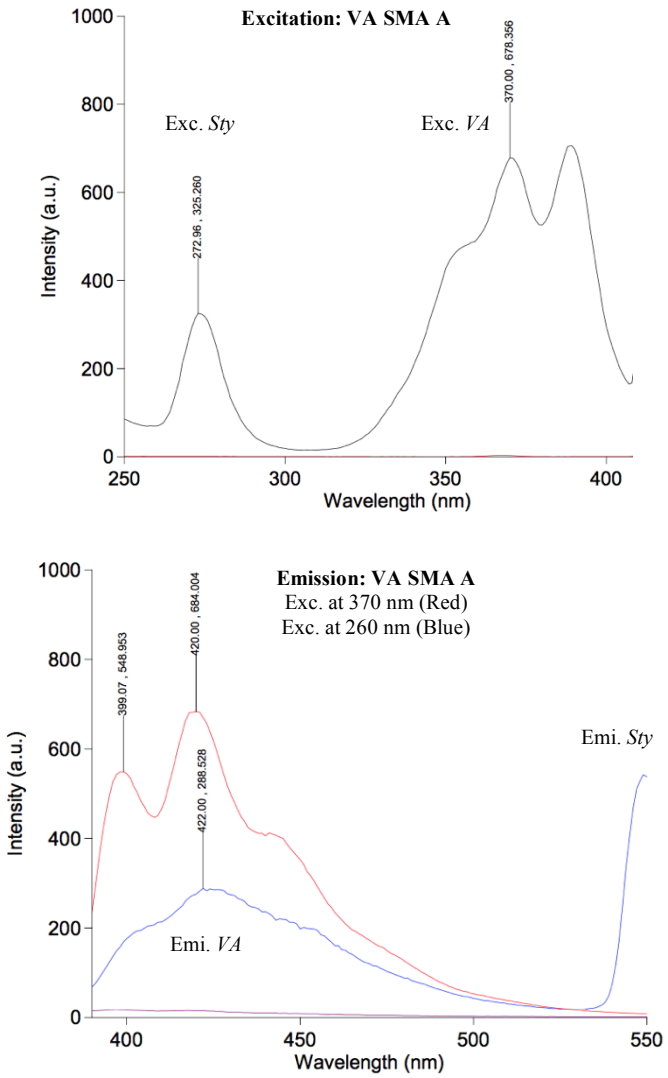

***Figure 30**: Excitation (Above) & Emission (Below) spectra of VA SMA A.*

4.3.2.1 Solvatochromism & Polymers in Solution

Solvatochromism can be used to probe the solvent, or environment type, a fluorophore exists. Both anthracene and pyrene were seen to have a solvatochromic response to changing solvents, as identified in *Figure 31*. Anthracene had the greatest response to being dissolved in toluene and chloroform, which induced a bathochromic shift of the spectra to a longer wavelength. Pyrene however, responded in a different manner, where rather than a shift in wavelength, instead a shift to the ratio of peak intensity was observed. Hexane, decane and tert-decane induced a spectrum where peak **1** was reduced in comparison to peaks **2** and **3** of similar intensity. Whereas chloroform, methanol and toluene induced a spectrum where peak **2** was reduced in comparison to peaks **1** and **3** of similar intensity.

When using either of the fluorophores, PBS, water, and water:ethanol mixes produced very low intensity spectra. This was likely due to the reluctance of these hydrophobic compounds to dissolve in polar solvents, hence causing the breakdown of the Beer-Lambert law due to aggregation (*Section 1.3.3.1*, *Equation 12*).

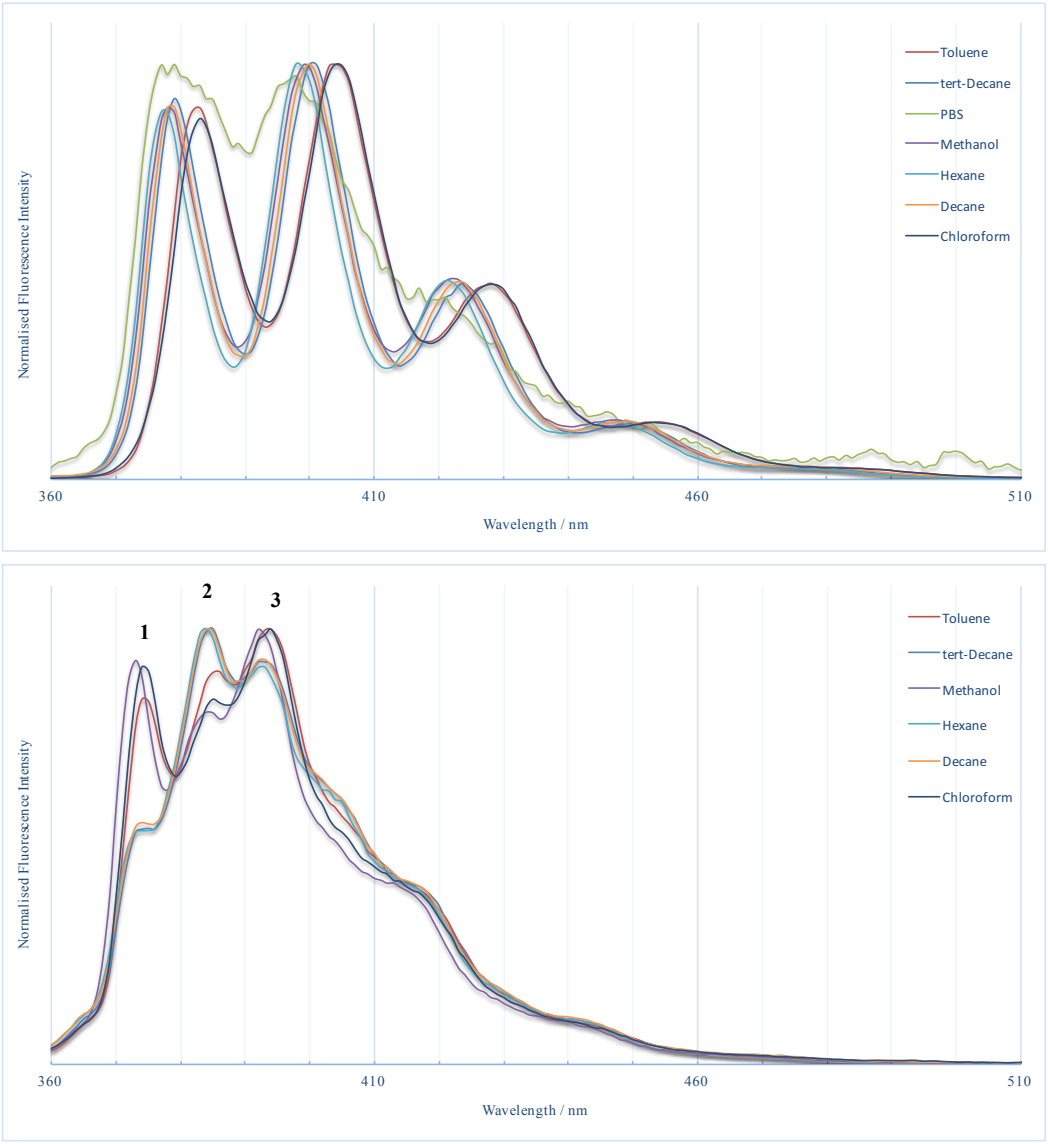

***Figure 31**: Solvatochromic response of anthracene (Top) & pyrene (Bottom) to different solvents.*

The solvatochromic responses of the fluorescent polymers were expected to differ significantly from the spectra above. This is due to a combination of effects, such as the binding of the fluorophore to a greater polymer chain, polymer conformation, the proximity of styrene and maleic acid units, but primarily, the breakdown of the Beer-Lambert law. Inherent to binding a fluorophore to a polymer, fluorophores will not be evenly dispersed in solution. This means that the observed intensities of excitation, and therefore emission, will significantly differ from those of the free fluorophores. In light of this, each polymer was checked for its individual solvatochromic response to PBS, hexane and toluene (*Figure 32*). These solvents were selected as it was believed that they would best represent the possible environments for SMA in later nanodisc studies: the bulk solvent, the lipid acyl chains and the styrene core of polymer aggregates, respectively.

Hexane and toluene were able to dissolve the polymer fully, in line with DLS measurements which did not detect any structures in these solvents. Therefore, in this regime, the Beer-Lambert law can be seen to hold, producing spectra as expected. Hexane and toluene shifted the spectra of all polymers to centralise on 425 and 435 nm, respectively.

Opposed to the spectra in hexane and toluene, polymers in PBS produced very low intensity spectra despite similar concentrations. This was due to the breakdown of the Beer-Lambert law, once again indicating the presence of polymer aggregates in PBS. This means not only was spectra geometry been drastically altered, but that the spectra for each polymer sample was also different. In PBS, individual polymer samples did, however, consistently produce spectra as observed in *Figure 32*, and this could therefore be used as a calibration point when interpreting later results.

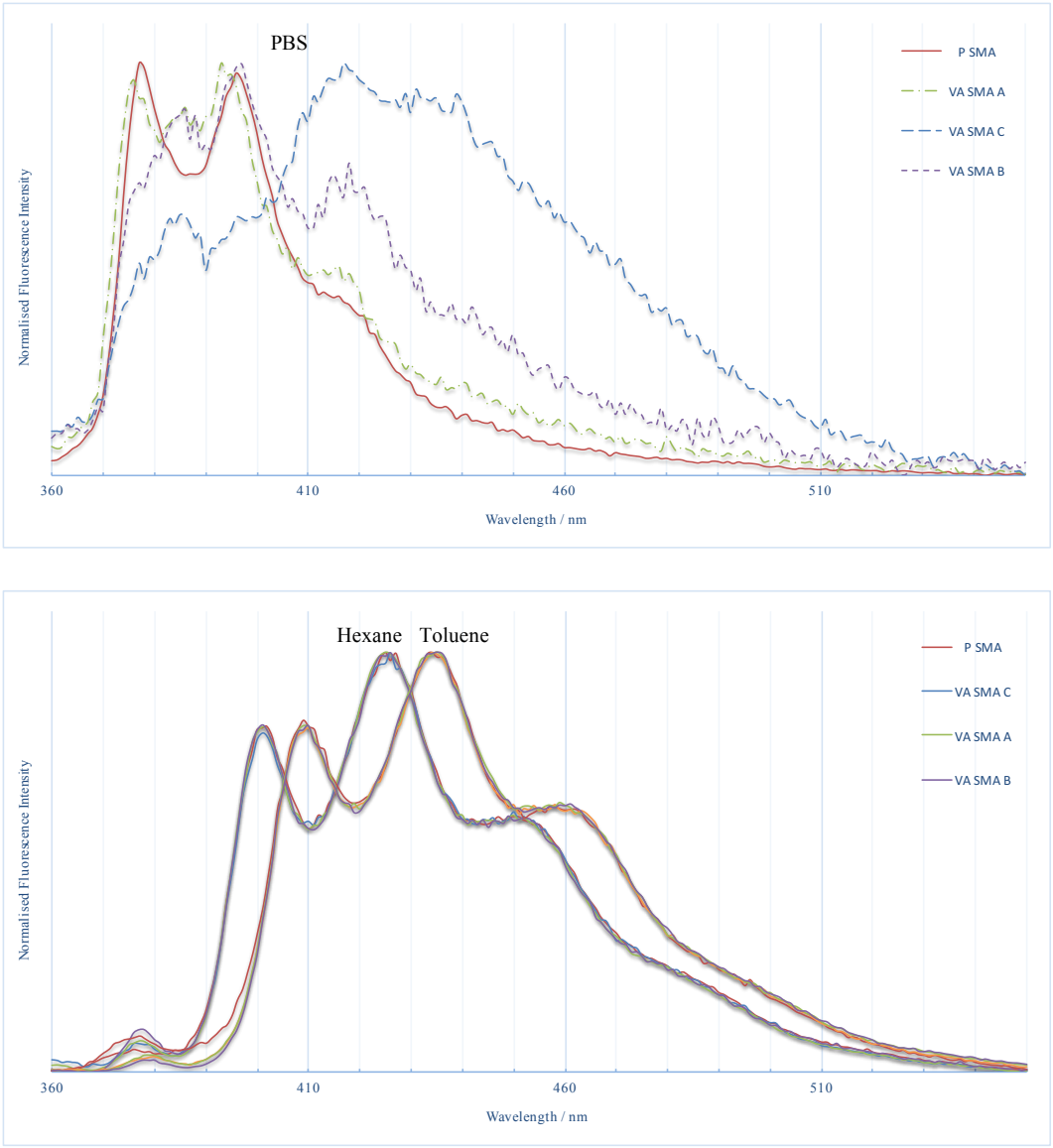

***Figure 32**: Polymer solvatochromic response to PBS (Top), Hexane & Toluene (Bottom).*

4.3.2.2 Fluorescence & Polymer Aggregates

The resulting fluorescence of the polymers so far has further suggested that aggregated polymer structures are indeed formed in PBS. Therefore, temperature trends were established for fluorescence measurements (*Figure 33*), as they were for DLS (*Section 4.2.1.2*). Additional experiments at 77 °C were also conducted, as this has previously been identified to be a T_g for some SMA polymers [46].

Here, VA SMA B responded similarly to VA SMA A, whereas VA SMA C and P SMA were unique. P SMA lacked any temperature related response, corroborating the DLS results whereby P SMA appeared to form monodisperse nanostructures even at 25 °C. VA SMA C may also have formed structures at 25 °C, generating no response until 77 °C, where the peak at 385 nm was reduced. VA SMA B, however, responded in a clear manner which can be rationalised with the same model that explained the surface tension and DLS results (*Section 4.2.1.1-4.2.1.2*).

As VA SMA B approached 55 °C, DLS data suggested structures had formed. During this same temperature change, the peaks at 385 and 395 nm are seen to reduce in comparison to the growth of the peak at 420 nm (*Figure 33*), representing a shift from a PBS-like spectra to a hexane-like spectra (*Figure 32*). Whilst a toluene-like spectra, predicted to represent a styrene core, was not observed, this change is still likely due to the altered environment as the polymer forms aggregates, tucking the hydrophobic fluorescent units into a styrene core. As 77 °C is approached, the spectra can be seen to partly return to a PBS-like spectra, likely indicating the melting of this styrene core, again exposing these units to solvent. This is only a preliminary interpretation, however, that would require further research to confirm.

Further supporting the claim that polymer aggregation occurred in PBS, kinetic measurements of the fluorescence spectra revealed scattering effects, where fluorescent intensity was seen to fluctuate (*Figure 34*). As temperature was increased, and aggregation begins, scattering is seen to increase before dropping off as the sample cooled. This effect primarily occurred in the 420 nm wavelength, but also in the 400 nm wavelength. Whilst it can be easily proven that this fluctuation is due to anisotropy in the solution (*i.e.* caused by the presence of tumbling aggregates) by varying the polarisation of incident radiation [75], unfortunately time-restrictions meant this experiment was not undertaken.

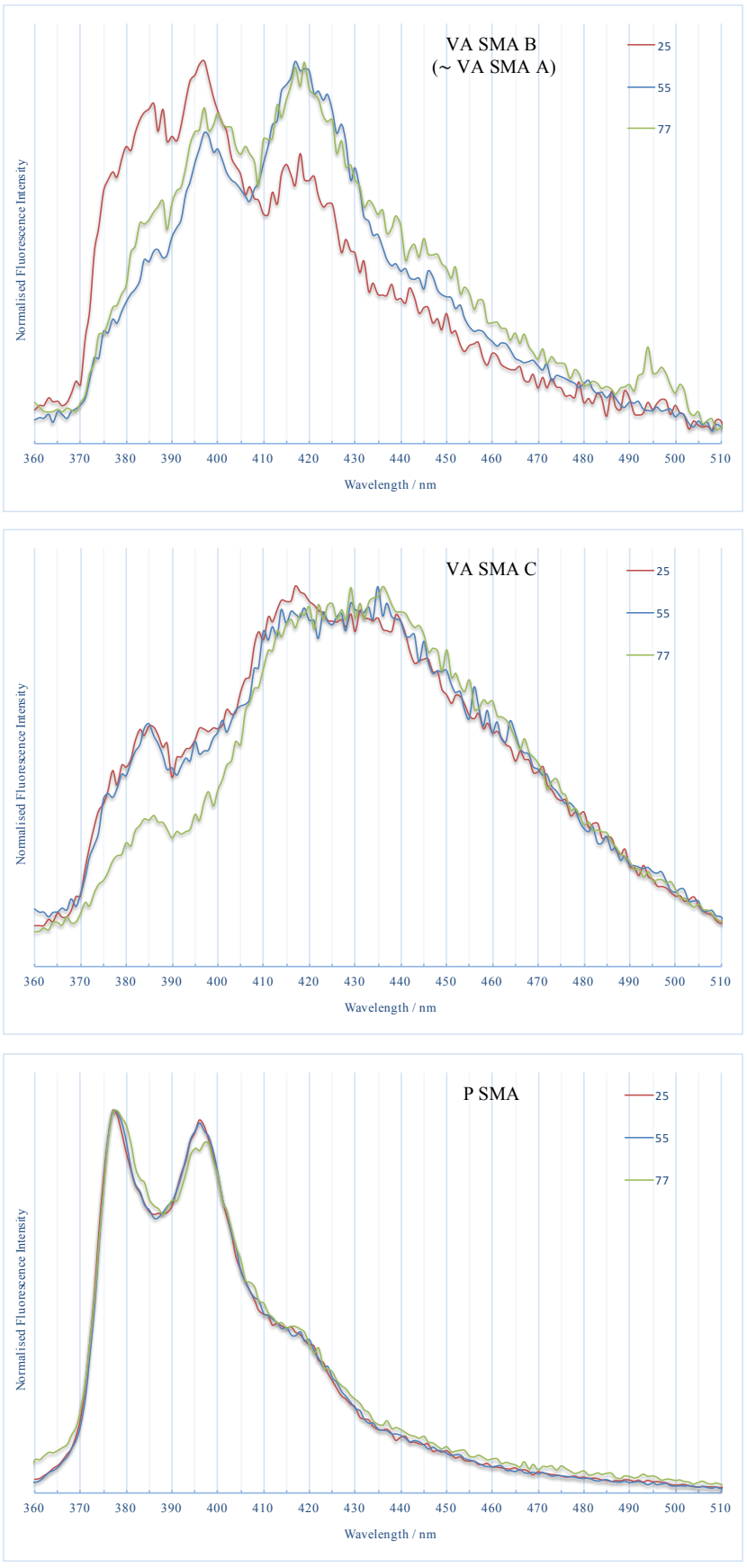

***Figure 33**: Emission spectra for VA SMA B (Top), VA SMA C (Middle) & P SMA (Bottom) at 25 °C, 55 °C & 77 °C.*

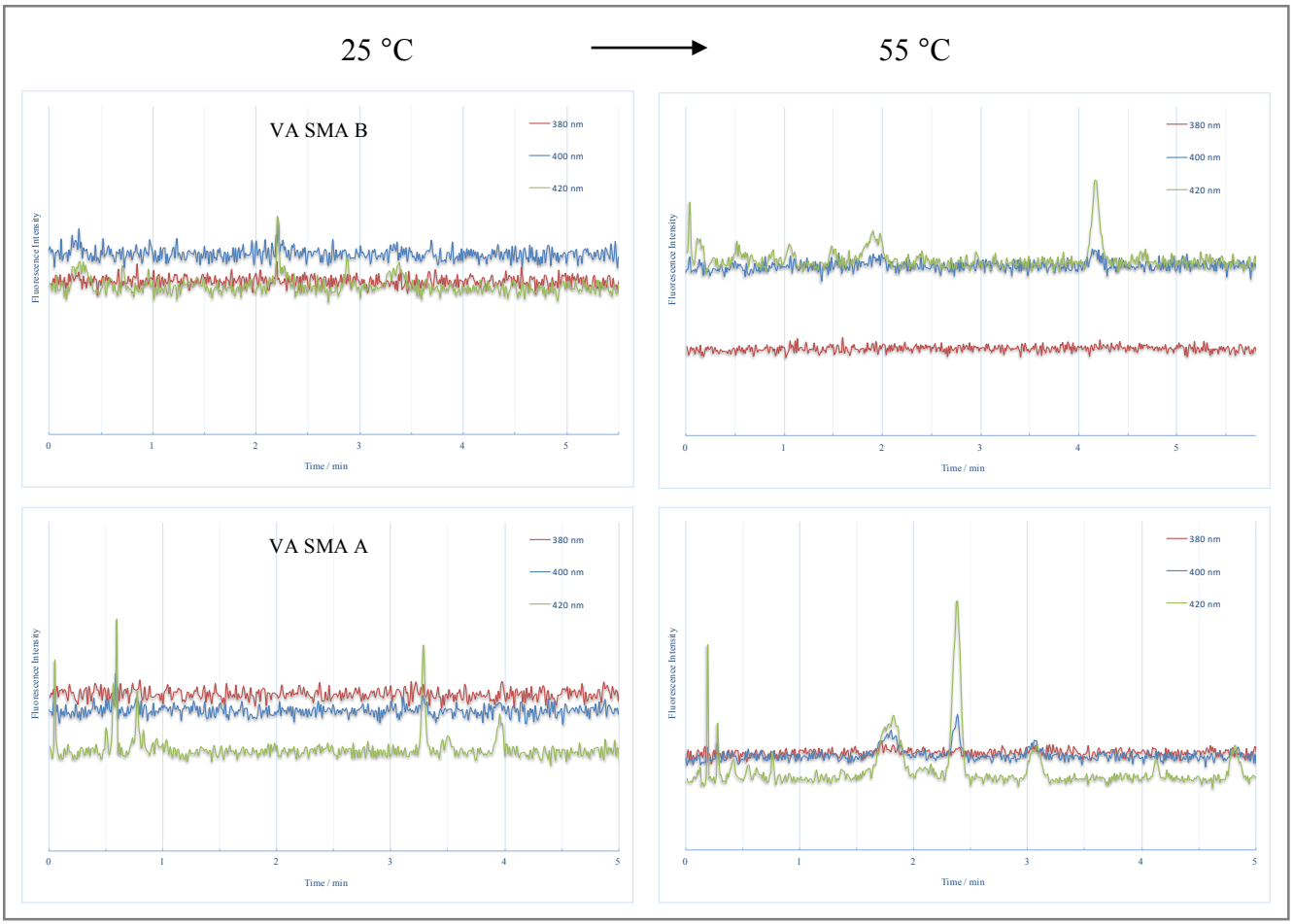

***Figure 34**: Kinetic monitored fluorescence response of VA SMA B (Top) & VA SMA A (Bottom) at 25 °C and 55 °C, highlighting scattering effects in 400 nm & 420 nm.*

4.3.2 Fluorescent SMALPs

It is hoped that by incorporating fluorescent units into SMA that fluorescent techniques may be used to augment both the study of SMALPs and proteins. Therefore, the following sections aim to demonstrate how fluorescent SMA may be used to better understand SMALP formation as well as to monitor polymer-protein interactions.

4.3.2.1 Fluorescence to Monitor SMALP Self-Assembly

It was of interest to monitor changes to fluorescence behaviour as SMALPs self-assembled with the addition of lipids. Due to the break down of the Beer-Lambert law, discussed in the previous section, clear solvatochromic shifts were not apparent. However, the emission spectra of fluorescent SMALPs appear to have somewhat returned to the spectra expected from the free fluorescent units, not incorporated in the polymer (*Figure 31*). This can be particularly appreciated by comparing the spectra for VA SMA C nanodiscs (*Figure 35*), VA SMA C in solution (*Figure 33*) and anthracene in PBS (*Figure 31*). This could be rationalised as the response to the development of a more monodisperse system, with separated fluorescent groups, in agreement with the reduction to PDI seen between polymer

aggregates in solution and SMALPs. This would hence reinstate the Beer-Lambert law, explaining the observation of SMALP spectra coherent with those of the free fluorophores. An alternative explanation is that fluorescent units have transitioned between the styrene core of the polymer aggregates, to a forced conformation in nanodiscs, whereby units are in contact with solvent. Furthermore, as recent findings suggest that polymer chains will exchange between individual SMALPs, the polymer might spend time free in solution, not in the structured form [17]. More experiments, such as FRET between individual polymer chains, would need to be conducted before such distinctions could be made. This does serve, however, to highlight the potential of fluorescence enabled SMA variants in the interrogation of SMALP dynamics.

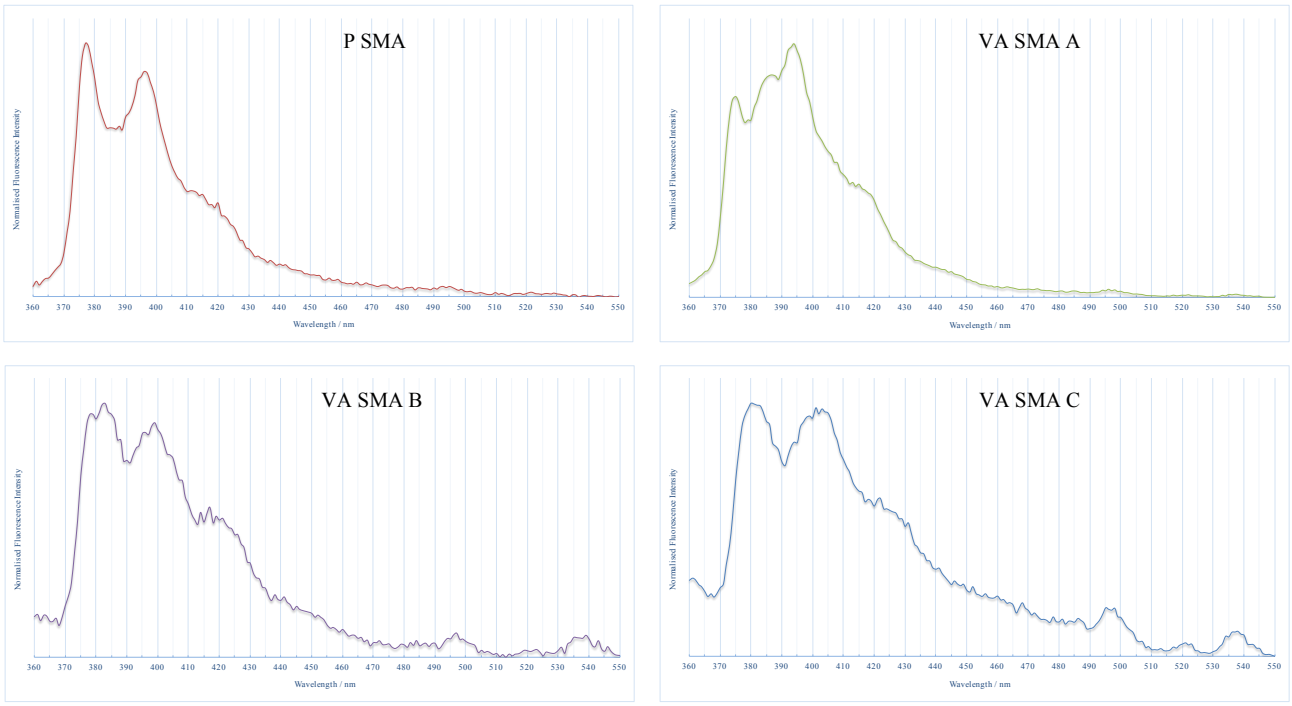

***Figure 35**: Fluorescent emission spectra of P SMA (Top left), VA SMA A (Top right), VA SMA B (Bottom left) & VA SMA C (Bottom right) SMALPs.*

Kinetic measurements of SMALP self-assembly in *Figure 36* more clearly demonstrates the change to the emission spectra as lipids were introduced. The concentration of polymers before and after adding lipids (dashed line) was maintained, meaning the intensity of the spectra are comparable and can be discussed.

For P SMA, VA SMA A and VA SMA C, there is an increase in fluorescence intensity as SMALPs are formed. These growths are proportional to the differences in size between the polymer aggregates in solution, and nanodiscs, as found by DLS results (*Section 4.2.1.2, 4.2.2.1*): VA SMA A increasing the most, then VA SMA C, then P SMA which did not grow in diameter significantly. This therefore suggests that the hydrophobic fluorescent units are indeed protected from solvent inside the styrene core of the polymer structures as previously discussed. As the polymer undoes this structure, and wraps around the circumference of the lipid bilayer, intensity would be expected to increase. Similar changes

to intensity have been used previously to monitor changes to polymer conformation [58] and confidence can be taken in this interpretation.

VA SMA B, however, did not behave in this way. The intensity upon lipid addition, increased slightly, but then reduced, with time, to near its original magnitude. This does not agree with the fact that VA SMA B formed nanodiscs of the largest diameter. However, by considering the significantly larger styrene homoblock, these results can be rationalised. Given the chemical similarity between styrene and anthracene, it is likely the styrene tail contains a high proportion of the anthracene units. As it has been recently found that this tail is likely to insert itself into the core of the SMALP [33], this would account for the temporary increase in intensity, as the polymer structures unfold, and then decrease, as the tail settles inside the SMALP core. Therefore, for future studies fluorescence intensity could be a viable means of monitoring the position of the styrene tail of SMA in SMALPs.

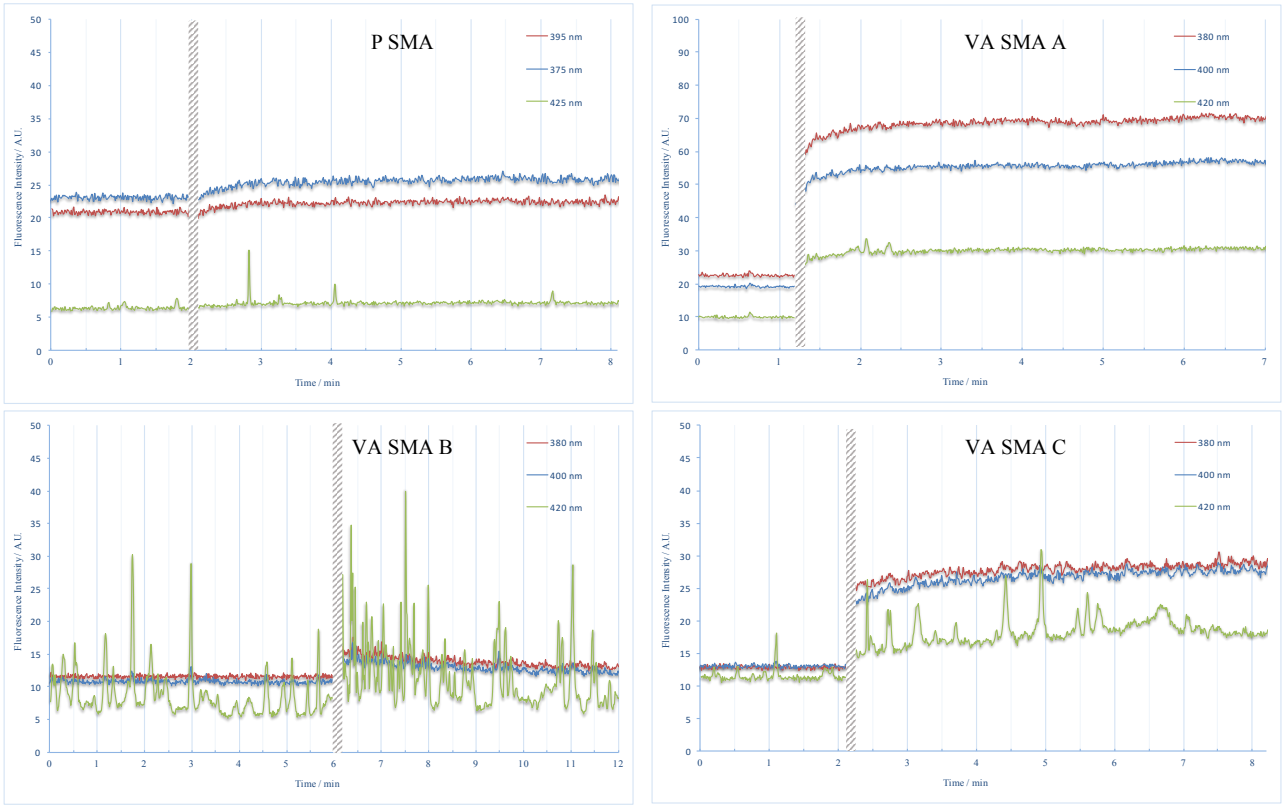

***Figure 36**: Kinetic fluorescence emission of P SMA (Top left), VA SMA A (Top right), VA SMA B (Bottom left) & VA SMA C (Bottom right) during SMALP self-assembly. Spectra before and after dashed line were recorded separately.*

Further to this, the scattering phenomena identified in *Section 4.3.2.2*, can be seen here to have been affected by SMALP formation. In VA SMA B, the fluctuation frequency increases from approximately 3 min^{-1} to 6 min^{-1}. Similarly, VA SMA C, increases from 1 min^{-1} to 2 min^{-1}. The intensity of this scattering also increases upon nanodisc formation, in line with the fact nanodiscs were larger than polymer aggregates. In all cases, the frequency of this phenomenon seems to increase upon lipid addition, before dropping off with time, possibly hinting at the formation of larger structures prior to minimised nanodisc formation.

Although more work is needed to clarify this, this is perhaps a further way SMALP self-assembly could be examined in future.

4.3.2.2 FRET to Monitor Polymer-Protein Interactions

FRET is used to determine the distances, and changes in distance, between donor and acceptor fluorophores. This is a commonly used technique, particularly in the biological study of proteins, used to determine protein conformation and dynamics. It is therefore of specific interest to design FRET-enabled SMA variants, both for the improved downstream analysis of proteins, but for the benefit of studying SMALPS themselves.

In order for FRET to occur, spectral overlap between the emission of the donor, and excitation of the acceptor, is required [61]. *Figure 37* illustrates the spectral overlap (shaded region) between the free gramicidin protein (more specifically the tryptophan residues) and P SMA in PBS solution.

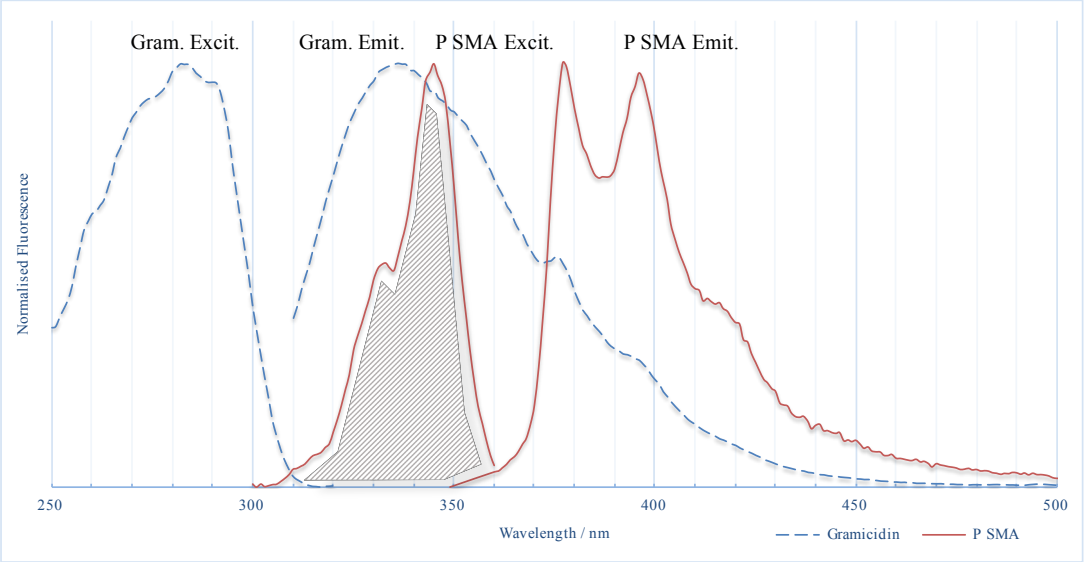

***Figure 37**: Spectral overlap between the emission of gramicidin and excitation of P SMA in PBS.*

Whilst anthracene possess a very similar overlap (excitation λ = 340 nm), FRET was not achieved with any VA polymers. This was likely due to the large size of nanodiscs produced by these polymers, whereas P SMA produced nanodiscs of a reasonable radius for FRET to occur: 8.5 nm (< 10 nm) opposed to 12.5-16.5 nm (>10 nm). *Figure 38* shows the emission spectra of the SMALPs containing gramicidin of P SMA, VA SMA B and SMA (R) (not fluorescence-enabled), excited at 295 nm.

Whilst the emission of pyrene can be seen to have been enhanced, this is insufficient to suggest true FRET has occurred. Certain determiners, such as the decreased fluorescent lifetime of the donor, are routinely used, but unfortunately, time restrictions of the project meant that this was not measured. However, in general, the emission intensity of the donor is expected to decrease, whereas the emission intensity of the acceptor should increase [61]. By comparing the percentage of the absorption intensity of the donor (295 nm) that is

converted to either the emission intensity of the donor (340 nm) or acceptor (375 nm), a comparison can be made. The workings of this are shown in *Table 9*.

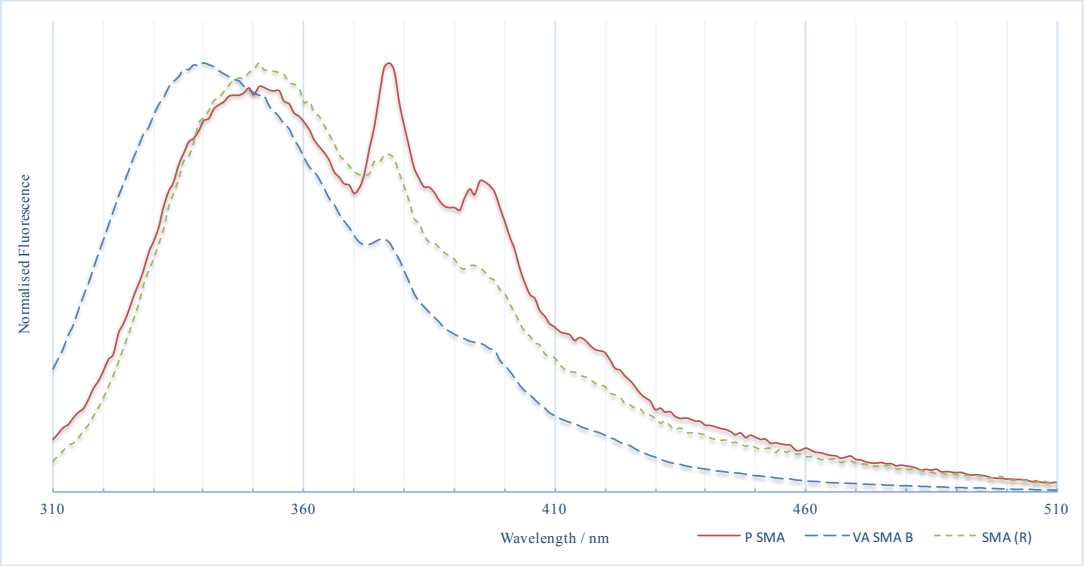

***Figure 31**: Intensified emission spectrum of P SMA when exciting at λ = 295 nm compared to VA SMA B & SMA (R).*

***Table 9**: Calculation of the percentage of absorption intensity converted to emission intensity, and the ratios of this attributed to gramicidin (340 nm) and the polymer (375 nm).*

Sample	Spectrum	Intensity / a.u.	Percentage Intensity Emitted / %	Ratio Percentage Emission (340 nm : 375 nm)
Gramicidin	Excitation (λ = 295 nm)	608	-	**2.0 : 1.1**
	Emission (λ = 340 nm)	469	77	
	Emission (λ = 375 nm)	256	42	
VA SMA B	Excitation (λ = 295 nm)	518	-	**2.0 : 1.2**
	Emission (λ = 340 nm)	349	67	
	Emission (λ = 375 nm)	206	40	
P SMA	Excitation (λ = 295 nm)	137	-	**1.0 : 1.1**
	Emission (λ = 340 nm)	43	31	
	Emission (λ = 375 nm)	46	34	

Therefore, even though gramicidin alone will emit at 375 nm, in P SMA nanodiscs there is a significant shift in the ratio of intensity between 340 and 375 nm, due to the emission of pyrene excited by FRET. Although some intensity differences will exist due to the structure of the nanodisc, this should affect all wavelengths equally, and hence these ratios are a fair measure of successful FRET. Therefore, in comparison to free gramicidin and VA SMA B SMALPs, the increased emission of pyrene and decreased emission of gramicidin, can be used to infer P SMA is within 10 nm of the incorporated protein.

To the author's knowledge this is the first example of a FRET-enabled SMA variant interacting with a protein in a nanodisc. Theoretically, this could allow for the determination of distance between the polymer and protein for variant nanodiscs, opening a new avenue of investigation. Further to this, it is often suggested that the presence of the polymer does not affect the properties, structure or dynamics of a protein in a SMALP. Whilst it still remains unproven if this is the case, FRET could be utilised to determine the presence and extent of these interactions, crucial if subsequent protein studies are to report reliable results.

4.3.3 Concluding Remarks

Fluorescent units were found to be successfully integrated into SMA by FRET between styrene and fluorescent moieties. This therefore represents the first example of SMA achieving such capabilities by the direct incorporation of fluorescent units in the polymer feed.

Whilst solvatochromic responses could be observed for both polymer aggregates in solution and SMALPs, these results were difficult to interpret due to the breakdown of the Beer-Lambert law. Fluorescence emission could, however, indicate the dissociation of polymer aggregates and the formation of SMALP nanodisc due to changes in fluorescence intensity. A secondary effect, fluorescence scattering, was also observed which corroborated the existence of polymer aggregates and SMALP nanodiscs, and could potentially be evaluated further in future studies.

FRET between the inherently fluorescent protein, gramicidin, and P SMA was also observed. VA polymers could not achieve this, likely due to the large diameter of the SMALPs they formed. P SMA, however, demonstrated the first example of FRET between polymers and proteins in SMALPs, representing an opportunity to monitor the extent of protein-polymer interactions as well as polymer and lipid exchange.

5.0 Conclusion

Fluorescence-enabled SMA has been successfully synthesised by its direct copolymerisation with both 9-vinylanthracene and 1-pyrenemethyl methacrylate. Shown to form SMALP nanodiscs, fully capable of incorporating proteins, these novel polymers represent a viable technology to take forward into SMALP and protein research.

RAFT, a controlled polymerisation technique, has been successful in producing polymers with PDIs reduced in comparison to a commercial variant, as well as successfully introducing a controlled *alt-block* gradient architecture. This allowed for the facile interpretation and analysis of SMALPs, where polymer composition and structure was well defined in comparison to the highly polydisperse SMA 2000. Because of this, it could be understood that the incorporation of hydrophobic fluorescent units induced increased nanodisc diameters, in line with previous attempts to similarly functionalise SMALPs in the literature. This was further corroborated by SAXS results which demonstrated that, in comparison to SMA 2000, SMALP rims were more hydrated, and more of the polymer had buried itself inside the hydrophobic lipid core.

As RAFT has been highlighted as a preferential technique for SMA synthesis, it is important that the consequences of this are appreciated. Here, it was found that the polymer architecture induced by RAFT caused significant deviations in behaviour in comparison to the random SMA 2000 copolymer. RAFT-made polymers were prone to aggregation, elucidated here as being governed by hydrophobic interactions by DLS and temperature-structure trends. These aggregates, therefore, likely constituted a styrene core with maleic acid units extended into solution. The results pertaining to VA SMA B, in particular, helped to verify this. This polymer had a significantly larger styrene homoblock which, likely due to steric effects, was found to be detrimental to aggregation and SMALP formation, alike. A similar dependency on the fluorescent unit content was also observed, where, despite a shorter styrene homoblock, the higher VA content in VA SMA A in comparison to VA SMA C, caused the formation of larger SMALPs. It was found that when incorporating pyrene, a moiety more hydrophobic, but smaller than anthracene, smaller aggregates were able to form even at lower temperatures and SMALP diameters were reduced. This serves to highlight that comparison between the behaviour of polymer aggregates in solution and SMALPs is worthy of attention in future, a factor which is only just starting to be recognised by the scientific community.

A further, equally potent consequence of RAFT polymerisation was the intrinsic introduction of the hydrophobic thiocarbonylthio end group. It was found that by exchanging this end group for a polar cyanoisopropyl group the structures and behaviours of the polymer were altered. Even when heated, aggregate formation was prevented and instead polymer chains existed in solution as individual coils, thus behaving analogously to SMA 2000. Interestingly, this behaviour did not seem to be conveyed in nanodisc formation. SMA (RR) produced nanodiscs larger (21.6 nm) than both SMA 2000 (5.8 nm) and SMA (R) (19.5 nm). Distinctly, when incorporating the hydrophobic protein gramicidin, SMA (RR) struggled to stabilise this nanodisc, exhibiting the second largest diameter seen during the experiment (30.4 nm). This was interesting as it suggested that the styrene homoblock could not penetrate and stabilise the SMALP core because of this polar end group.

The fluorescent capabilities of these copolymers were also evaluated to assess if, and to what extent, these polymers might by applied in future research. Whilst the presence of chemically similar styrene meant spectroscopic techniques, such as NMR and FTIR, failed to identify anthracene and pyrene, FRET between styrene and these units confirmed their coexistence in the same polymer chains. Solvatochromic responses, however, proved more difficult to interpret than initially expected. Whilst others have used fluorescent polymers in a similar vein, unfortunately, the inherent behaviour of SMA in aqueous solutions, such as aggregate formation, caused the unanticipated and severe breakdown of the Beer-Lambert law. Consequentially, whilst other, less useful solvents, such as hexane and toluene, could fully dissolve SMA and induce clear spectra, SMALP formation in PBS was difficult to analyse. Secondary fluorescent effects however, such as intensity changes and scattering, provided a means of monitoring SMALP and aggregate formation with time, and may be an interesting phenomenon to examine further in future.

FRET between the inherently fluorescent protein, gramicidin, and the polymer rim of SMALPs was also attempted. This represented a potential method for measuring polymer-protein interactions in SMALPs, an under-examined but primary concern of the technology. P SMA was highly successful in this respect, where the reduced diameters of P SMA nanodiscs, in comparison to those of VA SMA, afforded FRET capabilities with incorporated gramicidin. Whilst only a proof-of-concept study was conducted here, this

functionalised polymer has the potential to augment SMALP investigation. If this polymer was adopted by the SMALP community, research avenues into protein-polymer interactions, the monitoring of protein incorporation, as well as polymer and lipid exchange, are all readily foreseeable.

5.1 Future Work

Primarily due to decreased SMALP diameters and therefore unperturbed SMALP behaviour, this report has identified P SMA as a preferential candidate for future research. Once is has been ascertained if P SMA is capable of extracting MPs not only from lipid vesicles, but from real cells, this copolymer has the potential to benefit both SMALP and protein research. Establishing a calibration between the polymer-protein distance and the FRET response would allow for the unambiguous detection and monitoring of polymer-protein interactions.

As it was identified in this report that the RAFT thiocarbonylthio end group was maintained post-hydrolysis, a more sophisticated means of achieving this could be through end group modification. The thiocarbonylthio end group represents a distinct, reactive bond, which occurs only once in each polymer chain. Therefore, not only could this be used to conjugate fluorescent units with well-established 'click-chemistry' techniques, but also quantitative analysis of fluorescence responses could be made. Furthermore, as this fluorescent unit would therefore be known to exist only on the terminus of the styrene homoblock, this would allow for the determination and tracking of the position of this tail in SMALPs, a matter of controversy that has been highlighted several times both in this report and the literature.

It may also be desirable to correlate fluorescence responses with experiments such as differential scanning calorimetry on polymer aggregates and isothermal titration calorimetry on the injection of polymer solutions into lipid suspensions. This would allow for a complete thermodynamic understanding of the polymer and SMALP behaviour, and would allow fluorescence responses to be better rationalised than was possible during this project. SANS experiments, using deuterated lipids or polymers, could also explicitly elucidate the structures of the polymer aggregates and differing SMALP morphologies explored in this report. It is hoped that by combining such techniques with these novel SMA variants, demonstrated here as fully capable of the formation of viable SMALPs, that this would further advance both the understanding and subsequent application of this state-of-the-art technology.

References

1. E. Wallin and G. V. Heijne, *Protein Sci.,* 1998, **7**, 1029–1038.
2. D. Filmore, *Mod. Drug Discovery*, 2004, **7**, 24–28.
3. Z. Stroud, S. C. L. Hall and T. R. Dafforn, *Methods*, 2018, DOI: 10.1016/j.ymeth.2018.03.011.
4. Nobel Media, https://www.nobelprize.org/nobel_prizes/chemistry/laureates/2012/, (accessed April 2018).
5. Nobel Media, https://www.nobelprize.org/nobel_prizes/chemistry/laureates/2017/, (accessed April 2018).
6. M. Parmar, S. Rawson, C. A. Scarff, A. Goldman, T. R. Dafforn, S. P. Muench and V. L. G. Postis, *Biochimica et Biophysica Acta (BBA)-Biomembranes*, 2018, **1860**, 378–383.
7. J. M. Dörr, S. Scheidelaar, M. C. Koorengevel, J. J. Dominguez, M. Schäfer, C. A. van Walree and

J. A. Killian, *Eur. Biophys. J.*, 2016, **45**, 3–21.
8. D. E. Otzen, *Biophys. J.*, 2002, **83**, 2219–2230.
9. A. M. Seddon, P. Curnow, and P. J. Booth, *Biochimica et Biophysica Acta (BBA)-Biomembranes*, 2004, **1666**, 105–117.
10. S. C. Lee, T. J. Knowles, V. L. G. Postis, M. Jamshad, R. A. Parslow, Y. Lin, A. Goldman, P. Sridhar, M. Overduin, S. P. Muench and T. R. Dafforn, *Nat. Protoc.*, 2016, **11**, 1149–1162.
11. H. X. Zhou and T. A. Cross, *Annu. Rev. Biophys.*, 2013, **42,** 361–392.
12. T. H. Bayburt, Y. V. Grinkova, and S. G. Sligar, *Nano Lett.*, 2002, **2**, 853–856.
13. S. Tonge and B. Tighe, *Adv. Drug Delivery Rev.*, 2001, **53**, 109–122.
14. T. J. Knowles, R. Finka, C. Smith, Y. P. Lin, T. Dafforn and M. Overduin, *J.Am.Chem.Soc.*, 2009, **131**, 7484–7485.
15. M. Orwick-Rydmark, J. E. Lovett, A. Graziadei, L. Lindholm, M. R. Hicks and A.Watts, *NanoLett.*, 2012, **12**, 4687–4692.
16. D. J. Swainsbury, M. S. Proctor, A. Hitchcock, M. L. Cartron, P. Qian, E. C. Martin, P. J. Jackson, J. Madsen, S. P. Armes and C. N Hunter, *Biochimica et Biophysica Acta (BBA)-Bioenergetics*, 2017, **1859**, 215-225.
17. V. Schmidt and J. N. Sturgis, *Biochimica et Biophysica Acta (BBA)-Biomembranes*, 2018, **1860**, 777–783.
18. A. Grethen, D. Glueck and S. Keller, *The Journal of membrane biology*, 2018, DOI: 10.1007/s00232-018-0024-0
19. R. C. Arenas, B. Danielczak, A. Martel, L. Porcar, C. Breyton, C. Ebel and S. Keller, *Sci. Rep.*, 2017, DOI: 10.1038/srep45875.
20. G. Hazell, T. Arnold, R. D. Barker, L. A. Clifton, N. Steinke, C. Tognoloni and K. J. Edler, *Langmuir*, 2016, **32**, 11845–11853.
21. T. Ravula, N. Z. Hardin, S. K. Ramadugu, S. J. Cox and A. Ramamoorthy, *Angew. Chem. Int. Ed.*, 2018, **57**, 1342–1345.
22. D. J. Swainsbury, S. Scheidelaar, N. Foster, R. van Grondelle, J. A. Killian, and M. R. Jones, *Biochimica et Biophysica Acta (BBA)-Biomembranes*, 2017, **1859**, 2133–2143.
23. K. Yasuhara, J. Arakida, T. Ravula, S. K. Ramadugu, B. Sahoo, J. Kikuchi and A. Ramamoorthy, *J. Am. Chem. Soc.*, 2017, **139**,18657–18663.
24. S. Lindhoud, V. Carvalho, J. W. Pronk and M. -E. Aubin-Tam, *Biomacromolecules*, 2016, **17**, 1516-1522.
25. A. A. Smith, H. E. Autzen, T. Larsen, V. Wu, M. Yen, A. Hall, S. D. Hansen, Y. Cheng and T. Xu, *Biomacromolecules*, 2017, **18**, 3706–3713.
26. S. C. Lee, S. Khalid, N. L. Pollock, T. J. Knowles, K. Edler, A. J. Rothnie, O. R. T. Thomas and T. R. Dafforn, *Biochimica et Biophysica Acta (BBA)-Biomembranes*, 2016, **1858**, 2549–2557.
27. M. C. Orwick, P. J. Judge, J. Procek, L. Lindholm, A. Gazidei, A. Engel, G. Gröbner and A. Watts, *Angew. Chem. Int. Ed.*, 2012, **51**, 4653–4657.
28. T. Ravula, S. Ramadugu, G. Di Mauro, and A. Ramamoorthy, *Angew. Chem. Int. Ed.*, 2017, **56**, 11466-11470.
29. M. Jamshad, V. Grimard, I. Idini, T. J. Knowles, M. R. Dowle, N. Schofield, P. Sridhar, Y. Lin, R. Finka, M. Wheatley, O. R. T. Thomas, R. Palmer, M. Overduin, C. Govaerts, J. Ruysschaert, K. J. Edler and T. R. Dafforn, *Nano Res.*, 2015, **8**, 774–789.
30. P. A. Hassan, S. Rana, and G. Verma, *Langmuir*, 2015, **31**, 3–12.
31. H. Schnablegger and Y. Singh, *The SAXS Guide: Getting acquainted with the principles*, Anton Paar GmbH, Austria, 1st edn, 2013, ch. 1-4, pp. 10-71.
32. J. M. Berg, J. L. Tymoczko and L. Stryer, *Biochemistry*, W. H. Freeman, New York, 7th edn., 2012, ch. 12, pp. 367-374.
33. S. C. Hall, C. Tognoloni, G. J. Price, B. Klumperman, K. J. Edler, T. R. Dafforn and T. Arnold, *Biomacromolecules*, 2018, **19**, 761-772.
34. K. Ishihara, H. Nomura, T. Mihara, K. Kurita, Y. Iwasaki and N. Nakabayashi, *J. Biomed. Mater. Res.*, 1998, **39**, 323–330.
35. J. L. Brash and T. A. Horbett, *Proteins at Interfaces II*, American Chemical Society, Washington DC, 1995, vol. 602, ch. 1, pp. 1-23.
36. H. Chen, L. Yuan, W. Song, Z. Wu and D. Li, *Prog. Polym. Sci.*, 2008, **33**, 1059–1087.
37. S. Scheidelaar, M. C. Koorengevel, J. D. Pardo, J. D. Meeldijk, E. Breukink and J. A. Killian, *Biophys. J.*, 2015, **108**, 279–290.
38. A. F. Craig, E. E. Clark, I. D. Sahu, R. Zhang, N. D. Frantz, M. S. Al-Abdul-Wahid, C. Dabney-

Smith, D. Konkolewicz and G. A. Lorigan, *Biochimica et Biophysica Acta (BBA)-Biomembranes*, 2016, **1858**, 2931–2939.
39. J. M. Dörr, M. H. van Coevorden-Hameete, C. C. Hoogenraad, and J. A. Killian, *Biochimica et Biophysica Acta (BBA)-Biomembranes*, 2017, **1859**, 2155–2160.
40. C. Vargas, R. C. Arenas, E. Frotscher and S. Keller, *Nanoscale*, 2015, **7**, 20685–20696.
41. S. Scheidelaar, M. C. Koorengevel, C. A. van Walree, J. J. Dominguez, J. M. Dörr and J. A. Killian, *Biophys. J.*, 2016, **111**, 1974–1986.
42. A. Grethen, A. O. Oluwole, B. Danielczak, C. Vargas and S. Keller, *Sci. Rep.*, 2017, **7**, 11517.
43. H. T. McMahon and J. L. Gallop, *Nature*, 2005, **438**, 590–596.
44. L. J. Pike, *J. Lipid Res.*, 2003, **44**, 655–667.
45. G. Garnier, M. Duskova-Smrckova, R. Vyhnalkova, T. Van de Ven and J.-F. Revol, *Langmuir*, 2000, **16**, 3757–3763.
46. S. Harrisson and K. L. Wooley, *Chem. Commun.*, 2005, **26**, 3259–3261.
47. L. K. Kostanski, D. M. Keller and A. E. Hamielec, *J. Biochem. Biophys. Methods*, 2004, **58**, 159–186.
48. B. Klumperman, *Polym. Chem.*, 2010, **1**, 558–562.
49. E. Chernikova, P. Terpugova, C. Bui and B. Charleux, *Polymer*, 2003, **44**, 4101–4107.
50. H. De Brouwer, M. A. Schellekens, B. Klumperman, M. J. Monteiro and A. L. German, *J. Polym. Sci., Part A: Polym. Chem.*, 2000, **38**, 3596–3603.
51. Z. Hu and Z. Zhang, *Macromolecules*, 2006, **39**, 1384–1390.
52. L. Klumperman, PhD Thesis, Technische Universiteit Eindhoven, 1994.
53. D. J. Lunn E. H. Discekici, J. Read de Alaniz, W. R. Gutekunst and C. J. Hawker, *J. Polym. Sci. Part A: Polym. Chem.*, 2017, **55**, 2903–2914.
54. M. Chen, G. Moad and E. Rizzardo, *J. Polym. Sci. Part A: Polym. Chem.*, 2009, **47**, 6704–6714.
55. J. C. Bart, *Additives in polymers: Industrial analysis and applications*, John Wiley & Sons, Chichester, 1st edn, 2005, ch. 5, pp. 340-341.
56. T. D. Claridge, *High-resolution NMR techniques in organic chemistry*, Elsevier, Oxford, 2nd edn, 2004, ch. 2, pp. 15-19.
57. B. Valeur and M. N. Berberan-Santos, *Molecular Fluorescence: Principles and Applications*, Wiley-VCH, Weinheim, 2nd edn, ch. 1-2, pp. 1-42.
58. C. Pietsch, R. Hoogenboom and U. S. Schubert, *Polym. Chem.*, 2010, **1**, 1005–1008.
59. P. Bamfield and M. G. Hutchings, *Chromic Phenomena: Technological Applications of Colour Chemistry*, The Royal Society of Chemistry, Cambridge, 2nd edn, 2010, ch. 1.7, pp. 96-100.
60. D. Wöll, E. Braeken, A. Deres, F. C. De Schryver, H. Uji-i and J. Hofkens, *Chem. Soc. Rev.*, 2009, **38**, 313–328.
61. S. A. Hussain, D. Dey, S. Chakraborty, J. Saha, A. D. Roy, S. Chakraborty, P. Debnath and D. Bhattacharjee, *J. Spectrosc. Dyn.*, 2015, **5:** 7.
62. D. A. Kelkar and A. Chattopadhyay, *Biochimica et Biophysica Acta (BBA)-Biomembranes*, 2007, **1768**, 2011–2025.
63. S. S. Rawat, D. A. Kelkar and A. Chattopadhyay, *Biophys. J.*, 2004, **87**, 831–843.
64. A. B. Ghisaidoobe and S. J. Chung, *Int. J. Mol. Sci.*, 2014, **15**, 22518–22538.
65. G. S. Loving, M. Sainlos and B. Imperiali, *Trends Biotechnol.*, 2010, **28**, 73–83.
66. X. Lou, R. Daussin, S. Cuenot, A. Duwez, C. Pagnoulle, C. Detrembleur, C. Bailly and R. Jérôme, *Chem. Mater.*, 2004, **16**, 4005–4011.
67. A. Nakajima, *J. Lumin.*, 1977, **15**, 277–282.
68. X. Duan, J. Xiao, Q. Yin, Z. Zhang, S. Mao and Y. Li, *Int. J. Nanomed.*, 2012, **7**, 4961.
69. O. O. Oyeneye, W. Z. Xu and P. A. Charpentier, *RSC Adv.*, 2015, **5**, 76919–76926.
70. P. F. Barron, D. J. T. Hill, J. H. O'Donnell and P. W. O'Sullivan, *Macromolecules*, 1984, **17**, 1967-1972.
71. J. Bonilla-Cruz, B. Hernández-Mireles, R. Mendoza-Carrizales, L. A. Ramírez-Leal, R. Torres-Lubián, L. F. RamosdeValle, D. R. Paul and E. Saldívar-Guerra, *Polymers*, 2017, **9**, 63.
72. L. Tian, X. Li, D. Wan, Z. Ali and Q. Zhang, *Polym. Chem.*, 2017, **8**, 3774–3777.
73. J. Du, H. Willcock, J. P. Patterson, I. Portman and R. K. O'Reilly, *Small*, 2011, **7**, 2070–2080.
74. M. B. Smith, D. J. McGillivray, J. Genzer, M. Lösche and P. K. Kilpatrick, *Soft Matter*, 2010, **6**, 862–865.
75. J. R. Lakowicz, *Principles of Fluorescent Spectroscopy*, Springer, Boston, 3rd edn, 2006, ch. 10, pp. 353-382.